Exploring Arctic-midlatitude teleconnections using observations and numerical models

Peter Yu Feng Siew

Thesis for the degree of Philosophiae Doctor (PhD)
University of Bergen, Norway
2021

UNIVERSITY OF BERGEN

Exploring Arctic-midlatitude teleconnections using observations and numerical models

Peter Yu Feng Siew

Thesis for the degree of Philosophiae Doctor (PhD)
at the University of Bergen

Date of defense: 27.05.2021

Year: 2021

Title: Exploring Arctic-midlatitude teleconnections using observations and numerical models

Name: Peter Yu Feng Siew

Print: Skipnes Kommunikasjon / University of Bergen

Scientific environment

I carried out this work at the Geophysical Institute, University of Bergen and the Bjerknes Centre for Climate Research. I have belonged to the Bjerknes storm tracks research group. I have attended courses provided by Research School on Changing Climates in the Coupled Earth System (CHESS), Advanced Climate Dynamics Courses (ACDC) summer school, the Geophysical Institute and the university. I have attended many scientific meetings organized by CHESS and the Bjerknes Centre. I have attended some international conferences, including the Polar 2018 (Davos, Switzerland), European Meteorological Society (EMS) 2019 annual meeting (Copenhagen, Denmark) and European Geosciences Union (EGU) 2020 annual meeting (online). Finally, I had spent one semester at the Lamont-Doherty Earth Observatory of Columbia University in spring 2019 as a visiting PhD student.

This work has been supported by the Research Council of Norway projects Dynamics of Arctic-Midlatitude Teleconnections: mechanisms, robustness and tropical modulation (DynAMiTe, grant no. 255027) and Nansen Legacy (grant no. 276730), and contributed to a strategic project funded by the Bjerknes Centre for Climate Research.

The Research Council of Norway

CHESS
Research school on changing climates in the coupled earth system

UNIVERSITAS BERGENSIS

BJERKNES CENTRE for Climate Research

Acknowledgements

I would like to take the opportunity here to thank everyone who has helped me during my doctoral study. Without your help, I do not think I can make this thesis possible!

First of all, I would like to thank my supervisors, Camille Li and Stefan Sobolowski, for their support and guidance. I would like to acknowledge colleagues in the Bjerknes stormtrack group, in particular Martin King, Erica Madonna, Clio Michel, Etienne Dunn-Sigouin and Shengping He for the scientific discussion and checking my writing when I needed help. I would like to express my gratitude to Mingfang Ting for taking me as a visiting PhD student at Lamont in New York back to 2019 spring. I also thank XiaoDan Chen who took me around New York City and spent time together to look for good restaurants. I would like to thank my officemates, including Shengping, Stina, Elina, and Leilane for creating a comfortable working environment, food sharing and the casual talks when we are tired from our work. I also want to thank Fabio Mangini and Artem Moiseev who took ski trips with me. I would like to thank Yongbiao Weng, who showed me around the GFI and Bergen when I first arrived. Also I thank him for the generous "too good to go". Lastly, I want to thank my family, who encouraged me to pursue the doctoral degree.

It has been a great journey because of all of you. Thank you!

Abstract

The Arctic is warming at a much faster rate than the rest of the globe, with large declines in sea ice, snow cover and permafrost over the last decades. These profound changes have been proposed to influence the midlatitude atmospheric circulation in ways that lead to midlatitude extreme weather events that impact millions of people. Observational studies to date mostly support the existence of linkages from the Arctic to midlatitudes, but whether these linkages represent causal relationships is uncertain. Some modelling studies show that changes within the Arctic can influence regions outside the Arctic, but it is not clear how applicable these results are for understanding recent variability and trends in the midlatitudes. This thesis asks whether Arctic change has already had a noticeable effect on midlatitude circulation, and investigates the robustness of the proposed underlying mechanisms. It consists of four papers that employ a variety of tools including causal inference algorithms, comprehensive climate models and idealized general circulation models to address these research questions.

We used the Causal Effect Networks approach to test the robustness of a proposed pathway from autumn Barents-Kara sea ice to the winter North Atlantic Oscillation (NAO) via the stratospheric polar vortex (Paper I). Results show that the pathway is highly intermittent and less robust than previously thought. Given the possibility of an intermittent ice-NAO pathway in the real world, we investigated whether such a pathway also exists in state-of-the-art climate models (Paper II). Among bootstrapped samples of long climate simulations, a small number reproduce the observed relationship, but we find no evidence of a causal pathway. These results suggest that even an intermittent causal pathway is unlikely, and that the observed relationship is largely the result of internal variability. Taking one step back, the proposed ice-NAO causal linkage stems from the question of how the atmosphere adjusts to anomalous surface heating (associated with sea ice loss) in high latitudes. We performed idealized experiments with imposed surface heating over a range of latitudes (Paper III). Results show that midlatitude heating tends to generate circulation responses that act to offset the heating perturbation by horizontal advection,

but high latitude heating does not. Finally, returning to sea ice itself, we investigate a proposed mechanism where Barents Sea ice retreat is hypothesized to influence cyclones tracks (Paper IV). The results show that the cyclone tracks are governed by the large-scale atmospheric flow rather than local sea ice conditions.

Overall, the findings in this thesis clarify the subtle effect of recent changes in the Arctic on the midlatitude circulation, and highlight the role of strong internal climate variability in modulating both the observed and simulated linkages.

List of publications

1. P. Y. F. Siew, C. Li, S. P. Sobolowski, M. P. King, Intermittency of Arctic–mid-latitude teleconnections: stratospheric pathway between autumn sea ice and the winter North Atlantic Oscillation. *Weather and Climate Dynamics*, **1**, 261-275 (2020). https://doi.org/10.5194/wcd-1-261-2020.

2. P. Y. F. Siew, C. Li, M. Ting, S. P. Sobolowski, Y. Wu, X. Chen, North Atlantic Oscillation in winter is largely insensitive to autumn Barents-Kara sea ice variability, *Science Advances (in revision).*

3. P. Y. F. Siew, C. Li, S. P. Sobolowski, E. Dunn-Sigouin, Atmospheric response to midlatitude and high-latitude surface heating in an idealized moist general circulation model, *Manuscript in preparation*.

4. E. Madonna, G. Hes, C. Li, C. Michel, P. Y. F. Siew, Control of Barents Sea Wintertime Cyclone Variability by Large-Scale Atmospheric Flow. *Geophysical Research Letters*, **47**, 1–11 (2020). https://doi.org/10.1029/2020GL090322.

Contents

Chapter 1

Preface

The Arctic has experienced profound changes over recent decades, in large part due to anthropogenic climate change. These changes include surface warming rates of more than two times that of the global average, as well as significant loss of sea ice, land ice, snow cover and permafrost. At the same time, the midlatitude continents of the Northern Hemisphere have experienced a number of severe, cold winters (*Cohen et al.*, 2012, 2018a). It has been proposed that these unusually cold winters in the midlatitudes are caused by the shrinking Arctic sea ice via atmospheric teleconnections such as the one pictured in Figure 1. Whether this proposed linkage is causal is a fiercely debated subject among climate scientists. Currently, the literature offers ample evidence arguing both for and against causal Arctic-to-midlatitude linkages (see *Screen*, 2017a; *Cohen et al.*, 2020).

Clarifying the role of Arctic sea ice in influencing atmospheric circulation is important because it can potentially improve our ability to simulate and predict midlatitude weather over a range of timescales, including extreme weather events that have significant social-economic impacts. In seasonal climate forecasts, sea ice conditions in autumn seem to provide predictive skill for temperature and precipitation during winter in the North American and European sectors (*Scaife et al.*, 2014; *Wang et al.*, 2017), which can be useful information for energy or resource management. In the long term, sea ice will continue to decline in the future (*Notz and Community*, 2020), suggesting the counterintuitive possibility of colder midlatitude winters under global warming if the proposed linkages exist.

This thesis investigates Arctic-midlatitude linkages, focusing on whether sea ice influences midlatitude atmospheric circulation and, if so, how to better constrain the robustness of the physical processes responsible for the linkage. The introduction

(chapter 2) provides readers with some background on the relevant climate concepts as well as recent research results. Chapter 3 outlines the scientific questions that this thesis aims to answer. A brief description of the main methods used in my work appears in chapter 4, and a summary of four papers that address the thesis objectives appears in chapter 5. An overall summary and discussion of future research avenues appear in chapter 6.

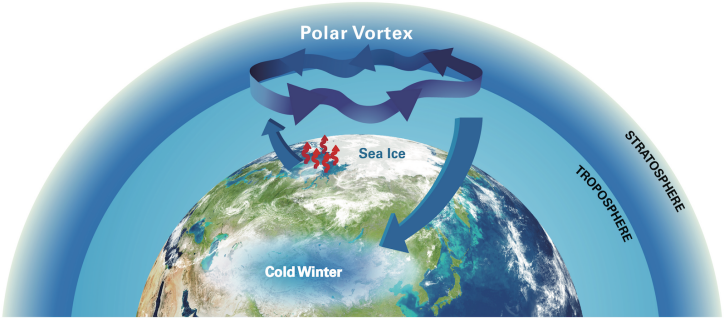

Figure 1: A schematic showing one proposed pathway where sea ice reduction over the Barents-Kara Sea drives cold Eurasian winters via changes in the stratospheric polar vortex. Source: US CLIVAR, https://usclivar.org/research-highlights/loss-arctic-sea-ice-impacts-cold-extreme-events

Chapter 2

Introduction

2.1 Arctic amplification and sea ice reduction

Earth absorbs solar (shortwave) radiation and emits thermal (longwave) radiation back to space. When these two types of radiation are in equilibrium, the result is a stable global average temperature. However, there is currently a disequilibrium. Greenhouse gas concentrations in the atmosphere have increased rapidly due to human activity since the Industrial Revolution. This increase in greenhouse gases traps more thermal radiation around our planet, allowing less to be emitted out to space. This results in a net radiation input at the top of the atmosphere, which forces the global average temperature to rise gradually. However, this warming trend is not uniform over the globe.

The Arctic surface is currently warming at a rate two to three times faster than the rest of the globe. This phenomenon is known as the Arctic amplification of global warming (*Serreze and Francis*, 2006; *Serreze et al.*, 2009; *Cohen et al.*, 2014). Arctic amplification is most evident near the surface during the cold seasons, but the warming is felt throughout the whole of the lower atmosphere, which is known as the troposphere (Figure 2). Alongside the surface warming, Arctic amplification is also manifest in the widespread loss of Arctic sea ice, land ice, snow cover and permafrost in the high latitudes.

Arctic sea ice extent and thickness have shown a decreasing trend in all seasons over the past decades since the late 1970s, and these trends are projected to continue in the future as greenhouse gases continue to increase (*Kwok et al.*, 2009; *Stroeve et al.*, 2012; *Notz and Stroeve*, 2016; *Notz and Community*, 2020). Figure 3 shows that Arctic

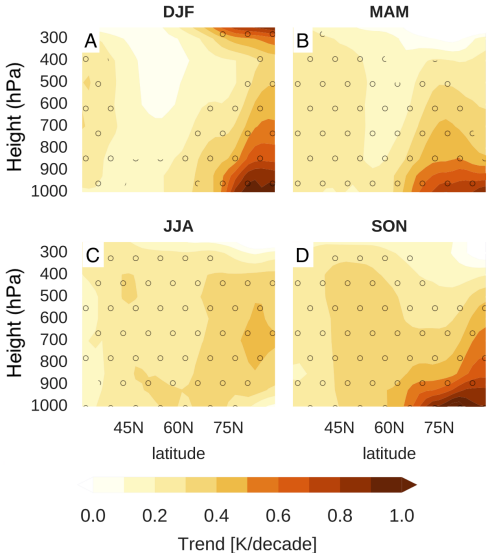

Figure 2: Trends in zonal-mean air temperature (shading) in reanalysis products (the average of MERRA, MERRA-2, ERA-Interim, JRA-55, and CFSR) from 1981 to 2015 in (A) DJF winter, (B) MAM spring, (C) JJA summer and (D) SON autumn. Stippling indicates significant values at the 5% level. Modified from *Cohen et al.* (2020).

sea ice in September has experienced a stronger decreasing trend than in March over the last decades. These two months are always emphasized in sea ice research because the sea ice reaches its minimum extent in September and maximum extent in March, climatologically. This is in response to the seasonal cycle of incoming solar radiation in the Northern Hemisphere (maximum in June, minimum in December) and involves a lag of several months due to the large thermal inertia of the ocean. Earlier onset of ice melt in spring and delayed refreezing in autumn has also been observed (*Markus et al.*, 2009; *Stroeve et al.*, 2014). Geographically, sea ice loss is most prominent in the Greenland, Barents and Kara Seas in March, and in the Chukchi and East Siberian Seas in September (Figures 4A and 4B). On top of this decreasing trend, sea ice also exhibits substantial interannual variability. Regions with the strongest interannual variability in March and September largely coincide with the regions of the strongest trends (Figures 4C and 4D).

A combination of local and remote mechanisms contributes to Arctic amplification and the associated sea ice loss. The warming in the Arctic is amplified by several local feedback mechanisms. These include longwave and lapse rate feedbacks (*Winton*, 2006; *Bintanja et al.*, 2011; *Pithan and Mauritsen*, 2014), cloud and water vapour feedbacks (*Vavrus*, 2004; *Taylor et al.*, 2013), and the sea ice albedo feedback (*Screen and Simmonds*, 2010). Remote mechanisms include the enhanced heat and moisture

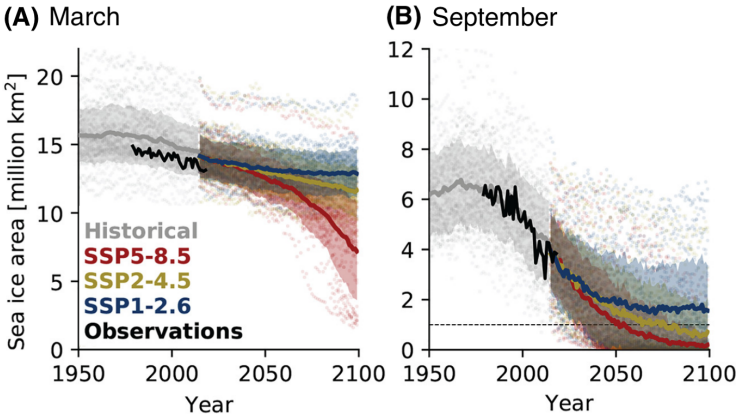

Figure 3: Time Series of Arctic sea ice area from observations (black lines), historical simulations (grey lines), and future projections according to three CMIP6 scenarios (blue for SSP1-2.6; yellow for SSP2-4.5; red for SSP5-8.5) in (A) March and (B) September. Shading indicates one standard deviation around the multi-model mean. Sea ice area is calculated by multiplying the sea ice concentration with the individual grid-cell area and summing over the Northern Hemisphere. Modified from *Notz and Community* (2020).

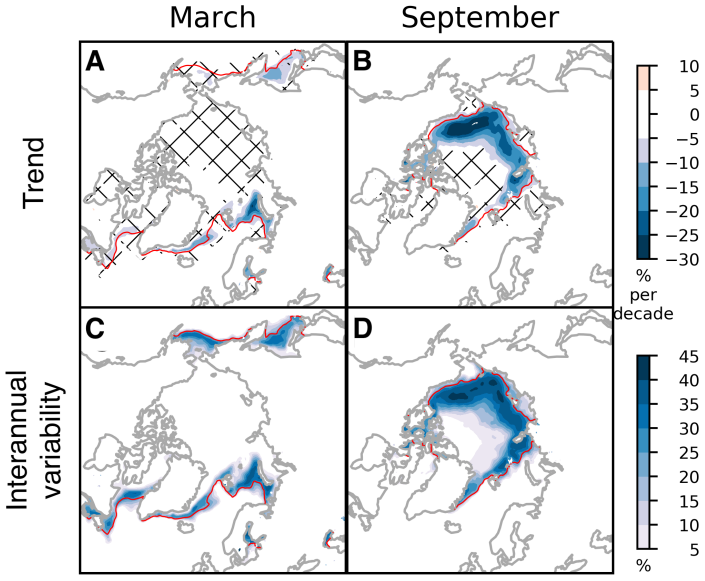

Figure 4: (A, B) Trends and (C, D) standard deviation of sea ice concentration in (A, C) March and (B, D) September from ERA5 during the period 1979–2019. Red contours show the climatological sea ice extent (15% concentration). Hatching indicates non-significant values at the 5% level.

transport by atmospheric (e.g., *Graversen et al.*, 2008; *Lee*, 2014; *Woods and Caballero*, 2016; *Gong et al.*, 2017) and oceanic (e.g., *Holland and Bitz*, 2003; *Smedsrud et al.*, 2013; *Nummelin et al.*, 2017; *Tsubouchi et al.*, 2021) processes. While all of these mechanisms are known to be important, it is not straightforward to ascertain their relative contributions to observed Arctic amplification (e.g., *Pithan and Mauritsen*, 2014; *Graversen et al.*, 2014; *Feldl and Roe*, 2013; *Goosse et al.*, 2018; *Stuecker et al.*, 2018).

2.2 The coupled ocean-ice-atmosphere system

The ocean is a body of water covering the majority of the Earth's surface. Sea ice is the frozen water that forms on the ocean surface in the high latitudes. The atmosphere is a layer of various gases surrounding our planet, in contact with the ice, the ocean surface or land. Before discussing whether and how sea ice influences the midlatitude atmosphere, we need to understand the fundamental physics of how these components communicate with each other.

The first step is to understand the interaction between the ocean surface and the atmosphere when ice is absent. The ocean surface and atmospheric boundary layer exchange energy, moisture and momentum via radiative and turbulent processes and through wind stress. In particular, the surface energy exchange is governed by the surface energy budget, which relates the surface heat content, radiative (solar or shortwave and thermal or longwave) and turbulent (sensible and latent heat) fluxes. The ocean is warmed by incoming solar radiation and downward thermal radiation from the atmosphere, and cools by emitting thermal radiation. In addition, turbulent exchanges of sensible and latent heat occur at the ocean surface. In general, the direction of the turbulent energy fluxes depend on the temperature and moisture gradients between the ocean surface and atmosphere, while the strength of the fluxes is also sensitive to surface roughness and wind speed (see review in *Taylor et al.*, 2018). Upward surface fluxes that cool the ocean are particularly strong in winter, when the temperature gradients between the relatively warm ocean and relatively cold atmosphere are strongest.

These interactions are altered when ice is added to the picture. Sea ice has a high surface reflectivity (high albedo) thus reflects a large portion of incoming solar radiation. Therefore, the Arctic surface cannot be heated up by the sun as efficiently as darker surfaces like the open ocean in summer. Sea ice also acts as an insulating layer that minimizes the exchange of energy between the atmosphere and ocean by inhibiting turbulent processes. In winter, this isolates the cold atmosphere from the

warm ocean during a time of year when there is very little or no incoming solar radiation, depending on the exact location. However, the ocean can still release some heat to the atmosphere through leads and polynyas (i.e., small openings in the sea ice cover), especially in the marginal ice zones (*Boisvert et al.*, 2012). Overall, Arctic sea ice plays an important role in shaping the Arctic climate by modulating the surface energy budget.

Because turbulent surface fluxes are so sensitive to the presence of sea ice, they can offer useful insights into drivers of sea ice variability. For example, enhanced oceanic heat transport can melt the sea ice from below and reduce or remove this insulating layer, promoting upward surface fluxes from the warm ocean surface to the cold atmosphere in winter (Figure 5A). Or else a southerly flow can bring warm and moist air masses into the ice-covered region, reducing or even potentially reversing the temperature and moisture contrasts at the surface. This can result in anomalous downward turbulent fluxes from the atmosphere to the ice, melting the ice from above (Figure 5B). Overall, the direction of surface heat flux anomalies is a good physical indicator that allows us to infer whether the sea ice is driving (Figure 5A) or responding to (Figure 5B) the atmospheric variability in any given situation or at any given point in time (*Sorokina et al.*, 2016; *Blackport et al.*, 2019).

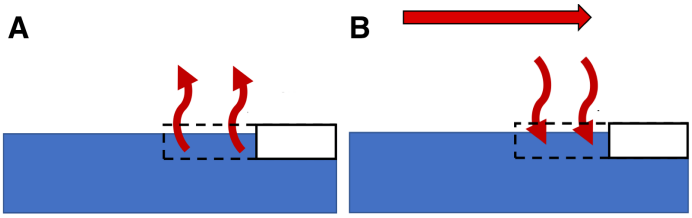

Figure 5: A schematic showing the direction of turbulent heat fluxes (curved red arrows) associated with a retreat of sea ice due to (A) enhanced ocean heat transport and (B) southerly advection of a warm, moist air mass (straight red arrows). Blue is the ocean, white is sea ice. The dotted lines mark the original sea ice extent. Modified from Blackport et al. 2019.

The decline of Arctic sea ice in the last decades has led to a positive trend of upward turbulent heat fluxes in the cold seasons, especially over the Barents-Kara Sea (Figure 6A). These enhanced surface heat fluxes help to warm and moisten the Arctic. It has also been suggested that they have altered the large-scale atmospheric circulation, leading to remote impacts in the midlatitudes (see chapters 2.4 and 2.5). At the same time, a large area over the Arctic shows a strong positive trend of downward longwave radiation (Figure 6B). This seems to indicate that the atmosphere has played a role in driving the sea ice reduction during the last few decades (see *Lee et al.*, 2017; *Gong et al.*, 2017). The flux trends shown in Figure 6 thus indicate that sea ice appears to have both driven and responded to atmospheric changes over the last

decades.

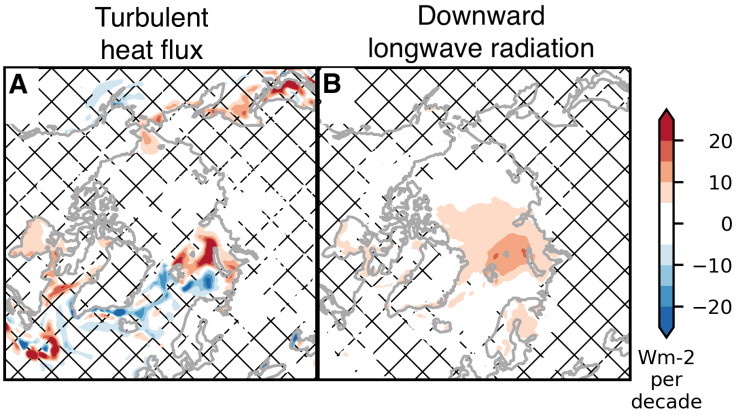

Figure 6: DJF trends (shading) of (A) surface turbulent heat flux (positive indicate upwards) and (B) surface downward longwave radiation (positive indicates downwards) from ERA-Interim 1979–2018. Hatching indicates non-significant values at the 5% level.

2.3 Midlatitude-to-Arctic linkages

Although the aim of this study is to investigate the Arctic-to-midlatitude linkages, it is more natural to start with midlatitude-to-Arctic linkages. Going back to the global energy budget, the top of the atmosphere is nearly in radiative equilibrium, with incoming solar (shortwave) radiation almost balanced by the emitted thermal (longwave) radiation. However, there are large imbalances latitudinally. The equator receives net positive radiation (incoming shortwave is larger than the outgoing longwave) while the poles receive net negative radiation (outgoing longwave is larger than the incoming shortwave), due to the larger solar zenith angle and larger albedo in the higher latitudes. This results in an energy surplus in the low latitudes and a deficit in the high latitudes. As a result, a poleward energy transport from low to high latitudes is triggered in the atmosphere and ocean to offset part of this energy imbalance.

Poleward energy transport by the atmosphere plays a primary role in setting Arctic climate. In midlatitudes and high latitudes, the atmosphere transport does most of the work, transporting approximately 3 PW across 60°N compared to 0.5 PW by the ocean (Figure 7). Part of this is in the form of latent heat transport by atmospheric water vapour. This water vapour, if it accumulates in a certain region, can warm the surface via the greenhouse effect. Heat transport in the midlatitudes and

high latitudes is primarily accomplished by atmospheric eddies. Large-scale stationary eddies are generated by orography and land-sea thermal contrasts, while synoptic-scale transient eddies such as extratropical cyclones are generated by baroclinic instability (an instability arising from the equator-to-pole temperature contrast itself in a rotating fluid). These extratropical cyclones in particular can transport a large amount of heat and moisture if they reach the Arctic, influencing surface temperatures and sea ice conditions (e.g., *Sorteberg and Kvingedal*, 2006; *Sorteberg and Walsh*, 2008; *Graham et al.*, 2019). Together, a variety of types of eddies, from synoptic to planetary scale are responsible for the weather and climate of the midlatitudes and high latitudes.

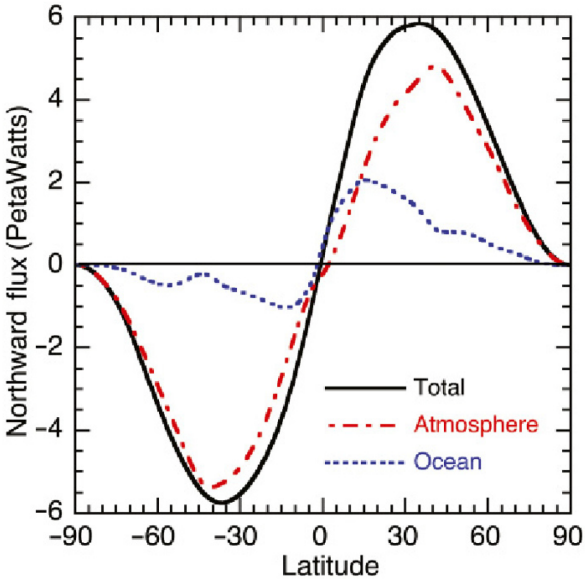

Figure 7: Oceanic and atmospheric poleward heat transport estimated from reanalysis data. Source: Global Physical Climatology, *Hartmann* (2015).

A positive trend in atmospheric poleward energy transport into the Arctic from the midlatitudes in recent decades is now being reported in the literature (*Graversen et al.*, 2008; *Zhang et al.*, 2013). This enhanced transport is associated with an increasing frequency of synoptic moisture intrusions (*Woods and Caballero*, 2016; *Yang and Magnusdottir*, 2017) or intense storms entering the Arctic (*Boisvert et al.*, 2016; *Kim et al.*, 2017), perhaps related to a poleward shift of the storm tracks (*Yin*, 2005; *Tamarin and Kaspi*, 2017). These synoptic systems, which transport both heat and moisture into the Arctic, are favoured by some large-scale circulation patterns such as the positive phase of the North Atlantic Oscillation (Figure 8A, *Deser et al.*, 2000) and blocking over the Urals (*Luo et al.*, 2017). The tropics may also play a role, with convection

over the Pacific warm pool (the region of warmest sea surface temperatures on the planet) suggested to be important for poleward moisture transport to the Arctic via planetary wave propagation (*Lee et al.*, 2011; *Lee*, 2012). The recent increase in moisture content in the Arctic has intensified downward longwave radiation, which is thought to have contributed to a significant amount of Arctic sea ice reduction and local surface warming (*Park et al.*, 2015b,a; *Gong and Luo*, 2017; *Lee et al.*, 2017). While a component of the recent circulation changes might be a response to global warming, some is also due to unforced, chaotic variability intrinsic to the climate system (e.g., *Deser et al.*, 2012; *McKinnon and Deser*, 2018).

2.4 Arctic-to-midlatitude linkages

Sea ice loss in recent decades has already been shown to have impacted Arctic climate, leading to increased warming, more coastal erosion, and an intensification of the hydrological cycle locally (e.g., *Kopec et al.*, 2016; *Moon et al.*, 2019). However, the role of Arctic sea ice in remotely influencing the weather of the midlatitudes is less clear. In the following section, we expand on this question, with a focus on the impact of sea ice loss in particular (i.e. shallow heating that affects the lower troposphere). Arctic amplification (which can include deeper heating of the troposphere) may have different and potentially stronger remote effects (*He et al.*, 2020; *Labe et al.*, 2020).

Many mechanisms have been proposed linking sea ice reduction to midlatitude weather during the cold season (*Cohen et al.*, 2020). These include linkages between autumn/winter Barents-Kara sea ice and the winter North Atlantic Oscillation (NAO); autumn/winter Barents-Kara sea ice and cold Eurasian winters; winter Chukchi sea ice and cold North American winters; and winter Greenland sea ice and cold Northern European winters. This thesis focuses on the Euro-Atlantic sector, and in particular, the proposed causal linkage between autumn/winter Barents-Kara sea ice and the wintertime NAO.

The NAO is the leading mode of circulation variability in the North Atlantic sector (*Hurrell*, 1995). A positive phase of the NAO is associated with warmer and wetter (colder and drier) weather across Northern (Southern) Europe (Figure 8A), while the negative phase of the NAO is associated with the opposite pattern (Figure 8B). The NAO reflects a large portion of the wider hemispheric circulation variability captured by the Arctic Oscillation or Northern Annular Mode (*Thompson and Wallace*, 1998; *Wallace*, 2000). It is also related to the winter temperatures across Eurasia,

which is one of the other ice linkages described above. A "cooling" of Eurasian winters has been observed in recent decades (*Outten and Esau*, 2012; *Cohen et al.*, 2012), with a decreasing trend of wintertime surface temperature that is especially strong in the period 1998-2012. The cooling trend is associated with an anticyclonic anomaly over the Urals and Western Siberian regions which advects colder Arctic air to Eurasia. This Eurasian cooling is somewhat related to the negative phase of the NAO, which is usually associated with cold winters in Northern Europe (Figure 8B).

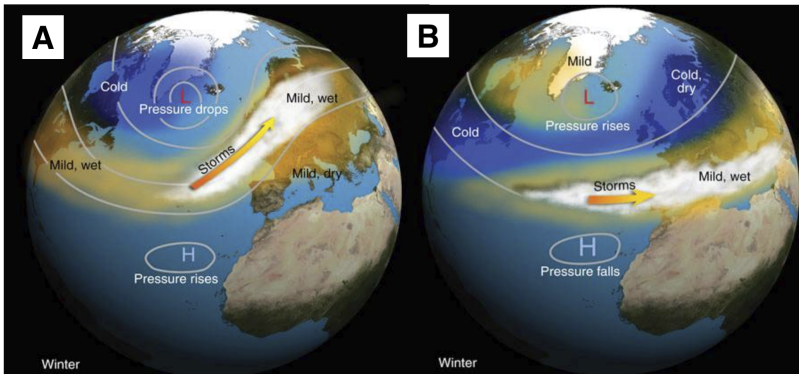

Figure 8: A schematic showing the weather patterns associated with the (A) positive and (B) negative phases of the North Atlantic Oscillation (NAO). Source: https://apollo.nvu.vsc.edu/classes/met130/notes/chapter10/nao.html

A useful conceptual framework introduced by *Barnes and Screen* (2015) to explore the role of sea ice in driving in these linkages is: "Can it? Has it? Will it?". The answer to "Can it?" is most likely yes. Idealized modelling studies with imposed high-latitude heating show clear midlatitude atmospheric responses (*Butler et al.*, 2010; *Wu and Smith*, 2016; *Zhang et al.*, 2018a; *Hell et al.*, 2020), although not always consistent with observed variability. The answer to "Will it?" is also likely to be yes. In the future, sea ice reduction is projected to be more pronounced (Figure 3), which enlarges the midlatitude responses compared to the internal variability. Sea ice removal experiments in realistic model setups using future sea ice conditions generate robust responses, such as the equatorward shift of the midlatitude jet (*Deser et al.*, 2010; *Peings and Magnusdottir*, 2014; *Sun et al.*, 2015; *Deser et al.*, 2015; *Tomas et al.*, 2016; *Screen*, 2017b). However, the effect from greenhouse gas increases in the future seems to partially offset the effect of sea ice loss alone (*Barnes and Polvani*, 2015; *Zappa et al.*, 2018), which complicates the interpretation of such modelling experiments. The answer to "Has it?" – i.e. has Arctic sea ice reduction in recent decades already influenced midlatitudes - is the most controversial.

Almost all observational studies demonstrate a correlation between Arctic sea ice and midlatitude circulation, but correlation does not necessarily indicate a causal

relationship. Figure 9A shows a significant lagged correlation over the satellite era between wintertime circulation (represented by the sea level pressure field) and sea ice conditions during the preceding autumn. Negative NAO conditions tend to follow sea ice reduction in the Barents-Kara Seas, consistent with other studies (*Hopsch et al.*, 2012; *Jaiser et al.*, 2013; *Kim et al.*, 2014; *Kretschmer et al.*, 2016; *García-Serrano et al.*, 2015; *King et al.*, 2016; *Koenigk et al.*, 2016; *Simon et al.*, 2020). However, the autumn ice-winter NAO correlation is found to be non-stationary in historical datasets dating back to the 19th century (*Kolstad and Screen*, 2019), which raises questions about whether the relationship identified in the satellite period is causal or not.

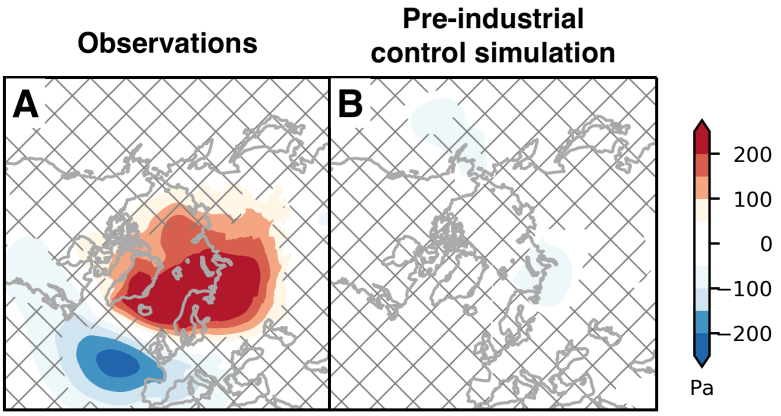

Figure 9: Regressions of December-February sea level pressure on the October-November Barents-Kara sea ice index (standardized and reversed sign) from (A) ERA5 reanalysis 1979/80-2018/19 and (B) a pre-industrial control simulation (499 years) performed using the CESM2-WACCM model. Hatching indicates non-significant values at the 5% level.

Can we turn to modelling experiments to learn more? Perturbation experiments can be performed to identify the impact of Arctic sea ice changes. A perturbation experiment is one where sea ice is removed or forced to melt, and it can be compared to an experiment with normal sea ice or more extensive sea ice to extract the "response" to reduced sea ice. These experiments show a wide spectrum of midlatitude responses to Arctic sea ice loss, casting doubt on the robustness of any specific causal linkages. The NAO/AO responses to sea ice loss range from positive/neutral (*Singarayer et al.*, 2006; *Strey et al.*, 2010; *Orsolini et al.*, 2012; *Porter et al.*, 2012; *Screen et al.*, 2014; *Smith et al.*, 2017; *Warner et al.*, 2020) to negative (*Alexander et al.*, 2004; *Magnusdottir et al.*, 2004; *Deser et al.*, 2004, 2007; *Seierstad and Bader*, 2009; *Deser et al.*, 2010; *Screen et al.*, 2013; *Kim et al.*, 2014; *Nakamura et al.*, 2015; *Deser et al.*, 2015; *Jaiser et al.*, 2016; *Screen*, 2017b; *Blackport and Kushner*, 2017). The negative NAO responses seem to be a more consistent result in sea ice removal experiments using coupled models (*Screen et al.*, 2018), which suggests that ocean feedbacks might be impor-

tant. Despite this, the timing (i.e., autumn ice to late winter NAO) and strength of the linkage do not match with observations (*Smith et al.*, 2017; *Peings*, 2019; *Blackport and Screen*, 2019). Similarly, modelling studies focusing on the linkage between sea ice and Eurasian winter temperatures show disparate results: there are studies arguing that it is mainly causal (*Honda et al.*, 2009; *Petoukhov and Semenov*, 2010; *Mori et al.*, 2014; *Kim et al.*, 2014; *Nakamura et al.*, 2015; *Kug et al.*, 2015; *Zhang et al.*, 2018b; *Hoshi et al.*, 2019; *Mori et al.*, 2019) and others arguing that it is not (*Sun et al.*, 2016; *McCusker et al.*, 2016; *Collow et al.*, 2018; *Ogawa et al.*, 2018; *Blackport et al.*, 2019; *Fyfe*, 2019; *Koenigk et al.*, 2019; *Dai and Song*, 2020; *Blackport and Screen*, 2021). Even when there is a Eurasian cooling response (shown by studies in the first group), it is much weaker than in the observations.

The diversity of results found in perturbation experiments might be explained by the different model and experimental setups used in the various studies. The differences in model setups include whether a model has a well-resolved stratosphere (*Sun et al.*, 2015; *Zhang et al.*, 2018b; *De and Wu*, 2019) and whether it is coupled to a dynamical ocean (*Deser et al.*, 2015; *Screen et al.*, 2018). The differences in experimental setups include: the regions where sea ice reduction is prescribed or forced (*Sun et al.*, 2015; *Pedersen et al.*, 2016; *McKenna et al.*, 2018; *Zhang et al.*, 2018a; *De et al.*, 2020); the magnitude of sea ice loss (*Petoukhov and Semenov*, 2010; *Chen et al.*, 2016; *Ringgaard et al.*, 2020); the timing of sea ice loss (*Zhang et al.*, 2018a; *Blackport and Screen*, 2019; *Peings*, 2019); and how many simulations (ensemble members) are run (*Screen et al.*, 2014; *Chen et al.*, 2016; *Liang et al.*, 2020). The results may also be sensitive to the background climate state, which differs from model to model and can also be adjusted by changing the initial conditions of any given simulation (*Screen and Francis*, 2016; *Smith et al.*, 2017; *Li et al.*, 2018; *Labe et al.*, 2019). Due to the wide range of possible setups, coordinated modelling efforts such as GREENICE (*Ogawa et al.*, 2018) or the Polar Amplification Model Intercomparison Project (PAMIP, *Smith et al.*, 2019) are useful because they allow for better comparisons.

Finally, standard simulations from coupled climate models may also provide some insights into ice-driven linkages to the midlatitudes. These include control experiments or historical experiments that are part of the Coupled Model Intercomparison Project (CMIP, *Taylor et al.*, 2012; *Eyring et al.*, 2016) and "large ensemble" projects where a simulation is run multiple times with slightly different initial conditions to produce a multi-member ensemble (*Kay et al.*, 2015; *Deser et al.*, 2020). Studies using such simulations suggest that atmospheric variability plays an important role in identifying correlations between sea ice and the NAO or Eurasian cooling. Sea ice is not perturbed in these simulations. This, and the fully coupled setup, allows the sea ice to interact with atmospheric variability more realistically. These simula-

tions can successfully reproduce some of the expected covariability expected from Arctic-midlatitude linkages, for example, the covariability between Barents-Kara sea ice and Eurasian cooling seen in observations (*Yang and Christensen*, 2012; *Kug et al.*, 2015; *Kelleher and Screen*, 2018; *Blackport et al.*, 2019; *Blackport and Screen*, 2021). Interestingly, this covariability is mainly associated with anomalous turbulent heat fluxes from the atmosphere to the ocean (*Blackport et al.*, 2019). This implies that it is atmospheric variability that drives both the sea ice reduction and the Eurasian cooling, rather than the sea ice reduction driving an atmospheric response that includes Eurasian cooling. This implication is further supported by the absence of such atmospheric responses in the atmosphere-only models, where observed sea ice is prescribed so that sea ice is not allowed to respond to the atmosphere variability (*Blackport and Screen*, 2021). When studying the autumn ice - winter NAO relationship seen in observations, these types of simulations generally show no such relationship (Figure 9B, *Kelleher and Screen*, 2018; *De and Wu*, 2019). This again suggests that the observed ice-NAO relationship arises from internal variability rather than a causal relationship.

Overall, this body of work tells us that sea ice variability can generate midlatitude circulation responses, especially if the sea ice changes are large and potentially in the right locations. However, it seems quite uncertain whether this is an important mechanism for understanding observed variability or trends in midlatitude circulation. Recent studies emphasize the role of internal variability in shaping the sea ice-midlatitude linkages over the past decades (e.g., *Sorokina et al.*, 2016; *McCusker et al.*, 2016; *Sun et al.*, 2016; *Ogawa et al.*, 2018; *Kolstad and Screen*, 2019; *Koenigk et al.*, 2019; *Peings*, 2019; *Warner et al.*, 2020; *Blackport and Screen*, 2020, 2021)

2.5 Teleconnection mechanisms

To ground our investigation of Arctic-midlatitude linkages, it is useful to briefly describe some of the proposed teleconnection mechanisms in the literature, with a focus on those acting during autumn or winter (also summarized in Figure 10). Readers are referred to the following review articles for a full overview of the mechanisms: *Cohen et al.* (2014); *Walsh* (2014); *Vihma* (2014); *Hoskins and Woollings* (2015); *Barnes and Screen* (2015); *Francis* (2017); *Vavrus* (2018); *Overland and Wang* (2018); *Cohen et al.* (2018b, 2020).

Rossby wave train

Reduced sea ice over the Barents-Kara-Siberian Sea causes an increase in turbulent

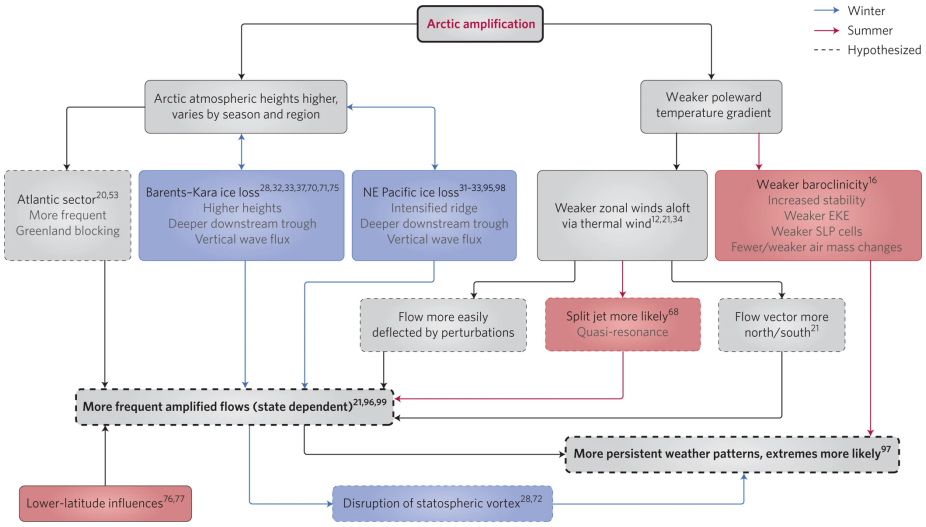

Figure 10: An overview of proposed Arctic-to-midlatitude mechanisms. From *Overland et al.* (2016).

heat fluxes from the ocean to the atmosphere. These fluxes act as a heating perturbation that excites a Rossby wave train with an anomalous ridge over the Urals and an anomalous trough over northeast Asia (*Honda et al.*, 2009; *Kug et al.*, 2015; *Hoshi et al.*, 2017). This pathway is proposed to explain the winter Eurasian cooling response to sea ice loss.

Stratospheric polar vortex

Reduced sea ice over the Barents-Kara Sea causes an increase in turbulent heat fluxes. This excites waves that constructively interfere with the climatological stationary wave in the Northern Hemisphere. This results in an increase in the upward propagation of wave activity from the troposphere to the stratosphere. As these waves reach the stratosphere, they "break" and weaken the stratospheric polar vortex (*Nishii et al.*, 2009; *Smith et al.*, 2010). Downward coupling from the stratosphere to the troposphere subsequently produces circulation anomalies that resemble the negative phase of the NAO or Arctic Oscillation (*Baldwin and Dunkerton*, 1999). This pathway is proposed to explain both the autumn-to-winter delay in the sea ice-NAO and sea ice-Eurasian cooling linkages (*Jaiser et al.*, 2013; *Peings and Magnusdottir*, 2014; *Kim et al.*, 2014; *Sun et al.*, 2015; *Jaiser et al.*, 2016; *King et al.*, 2016; *Nakamura et al.*, 2015, 2016; *Hoshi et al.*, 2017; *Zhang et al.*, 2018b; *Hoshi et al.*, 2019; *De and Wu*, 2019).

Waviness of the midlatitude jet stream

Arctic amplification reduces the meridional temperature gradient, which might be expected to decelerate the jet stream according to a relationship known as thermal

wind balance (the vertical shear of the zonal wind is associated with meridional temperature gradient). It has been proposed that a slower jet could amplify Rossby waves, resulting in more blocking events and thus more persistent weather conditions in the midlatitudes (*Francis and Vavrus*, 2012; *Liu et al.*, 2012; *Tang et al.*, 2013; *Francis and Vavrus*, 2015). However, studies have presented both observational (*Screen and Simmonds*, 2013; *Barnes*, 2013) and modelling (*Hassanzadeh et al.*, 2014; *Screen*, 2014; *Blackport and Screen*, 2020) evidence that opposes this dynamical pathway.

Urals blocking

Atmospheric blocking is a quasi-stationary high-pressure weather pattern that can produce extreme events such as heat waves, wildfires and droughts. Blocking often occurs over the Ural Mountains in winter, and is associated with cold spells. There are multiple factors that can lead to Urals blocking. The anomalous ridge over the Urals in the stationary Rossby wave mechanism (mentioned above) can promote blocking. Alternatively, surface warming over the Barents-Kara Sea weakens the meridional temperature gradient locally, which can weaken the zonal wind and also promote blocking over the Urals (*Luo et al.*, 2016). Finally, sea ice retreat moves the sharp gradients associated with the ice edge out of the Barents-Sea, which may discourage cyclones from tracking through the region and towards the Urals. The absence of low-pressure systems results in an anomalous high over the Urals (*Inoue et al.*, 2012).

While some of these proposed mechanisms are more likely than others to be able to explain Arctic-to-midlatitude linkages, there is, as yet, no definitive answer. Finding the answer continues to be a challenge for several reasons. The various proposed mechanisms are not necessarily independent, and their effects on Eurasian winter temperatures may reinforce or offset each other. For example, the Rossby wave train mechanism is also the initial step in setting up the stratospheric pathway (e.g., *Kim et al.*, 2014; *Hoshi et al.*, 2017). In terms of effects, the warming due to sea ice loss (i.e., surface heating) would oppose any dynamical midlatitude responses that act to cool Eurasia (*Screen et al.*, 2015; *Screen*, 2017b). Finally, internal variability has been shown to play an important role in shaping Arctic-to-midlatitude linkages. Even if a causal mechanism exists, strong internal variability can mask the signal, or inject intermittency into the linkage.

Chapter 3

Objectives

The debate over whether Arctic sea ice decline has had a noticeable effect on mid-latitude weather over the last few decades has yet to be resolved. However, recent studies emphasizing the role of internal climate variability indicate a way forward. (e.g., *Sorokina et al.*, 2016; *Peings*, 2019; *Blackport et al.*, 2019; *Warner et al.*, 2020; *Liang et al.*, 2020; *Blackport and Screen*, 2021). Accounting for the role of internal variability is clearly important, and might help to reconcile the divergence between observational studies, which seem to suggest a noticeable effect, and modelling studies, which mostly show a weak or no causal effect of sea ice.

The work in this thesis considers the role of atmospheric internal variability in investigating and interpreting the linkages from sea ice to the midlatitudes. Sea ice extent and large-scale atmospheric variability have been shown to form a tightly coupled system (e.g., *Deser et al.*, 2000; *Strong et al.*, 2009; *Wu and Zhang*, 2010). Bearing this in mind, we hope to gain insight into the causality of observed relationships.

Papers I and II in this thesis focus on an Arctic-to-midlatitude linkage that has received much attention: from autumn Barents-Kara sea ice to the winter NAO. Previous studies have proposed a pathway from low ice conditions in autumn to a negative NAO in late winter via a weakening of the stratospheric polar vortex (*Kim et al.*, 2014; *King et al.*, 2016; *Kretschmer et al.*, 2016). Perturbation experiments provide mixed answers on the existence or strength of this relationship (e.g., *Kim et al.*, 2014; *Peings*, 2019; *Blackport et al.*, 2019; *Zhang et al.*, 2018b; *Blackport and Screen*, 2021), while coupled climate models largely fail to reproduce it (*Boland et al.*, 2017; *Kelleher and Screen*, 2018). Papers I and II address the questions:

- Given that the sea ice-NAO relationship is non-stationary over the 20th century, how robust are proposed mechanistic pathways during the satellite period of

observations?
- Can climate models simulate the observed sea ice-NAO relationship if the role of internal variability is accounted for?
- If climate models can reproduce the observed relationship, does it arise from the proposed stratospheric pathway?

Part of the reason that it is difficult to identify which of the proposed mechanisms are most important for creating Arctic-midlatitude linkages is an incomplete fundamental understanding of the underlying dynamics (*Wallace et al.*, 2014; *Hoskins and Karoly*, 1981). For example, sea ice loss allows the atmosphere to be heated by the warm ocean during winter. Circulation responses to such a high-latitude thermal forcing are less well understood than responses to lower latitude forcing. For lower latitude forcing, idealized numerical experiments have been analyzed using theoretical frameworks that allow the responses to be qualitatively understood in terms of local circulation signals that attempt to balance the heating perturbation, and remote signals generated as a result (*Hoskins and Karoly*, 1981; *Ting*, 1991). To investigate if the thermal forcing in the high latitudes can be understood in a similar way, we extend the work of *Hoskins and Karoly* (1981) using a general circulation model that is still quite idealized, but includes simplified moisture effects and an interactive slab ocean. Paper III addresses the question:

- How and why are the circulation responses to surface thermal forcing in the high latitudes different from the responses to surface thermal forcing in lower latitudes?

Finally, returning to the theme of internal atmospheric variability, the last study provides a more in-depth synoptic view of how this influences Arctic climate. Extratropical cyclones transport heat and moisture from lower latitudes to high latitudes. Previous studies have shown that cyclones reaching the Arctic can have significant impacts on Arctic climate, causing surface warming and sea ice melt (*Boisvert et al.*, 2016; *Kim et al.*, 2017). Therefore, understanding what factors control the path of cyclones entering the Arctic is important. On one hand, the retreat of the Barents sea ice has been suggested to influence the cyclone tracks by reducing the local baroclinicity in the Barents Sea (*Inoue et al.*, 2012). On the other hand, circulation patterns such as the NAO or blocking are known to be important in steering cyclones (*Simmonds et al.*, 2008; *Luo et al.*, 2017). Paper IV addresses the question:

- What are the primary factors controlling the path and impact of cyclones entering the Arctic from the North Atlantic?

Chapter 4

Methods

This chapter introduces some of the key methods that are used in the three main papers of the thesis. These methods were chosen to help identify and explain the causal linkages that give rise to teleconnection signals in light of the large internal variability of the climate system.

Bootstrap resampling

Bootstrapping is a statistical technique used to assess the characteristics of a population (e.g., mean, spread, standard deviation) based on a limited sampling of that population. One may think of the sample as a dataset of measurements or observations of some unknown population. The procedure of bootstrapping is to resample the dataset many times to create many synthetic samples. These samples build up a bootstrapped distribution that allows us to infer statistics of the unknown population (see *Hesterberg*, 2015, for details). Some of the advantages of bootstrapping are that it is straightforward to use and importantly, it does not make any assumptions about the sampling distribution.

Bootstrapping is used in several different ways in this thesis (Papers I and II). One use is to assess how stable statistical relationships are in the 40-year satellite period of observations. We draw 40 years from the observational record, allowing any given year to be selected any number of times (this is known as bootstrapping with replacement), and calculate the statistic of interest (for example, the mean). Repeating this many times (e.g., 10,000 times, as shown in Figure 11A) produces many synthetic samples. We can then create a bootstrapped distribution of the mean, allowing us to estimate the uncertainty on the "real" mean of the original record from the spread among the synthetic samples. Alternatively, we can use bootstrapping to assess whether a given sample is representative of the population - for example,

whether a short portion of a record is representative of the full record. Here, we can bootstrap the full record without replacement to create a collection of many shorter synthetic records. If the spread of the bootstrapped distribution is large, this can be a sign that the record exhibits a large amount of low frequency variability. This approach can be useful for comparing a long model simulation to a shorter observational record, as shown in Figure 11B. Bootstrapping has been widely used in climate research, for example, to assess the uncertainties of teleconnections in observations and models (e.g., *Cash et al.*, 2017; *Deser et al.*, 2018; *Michel et al.*, 2020).

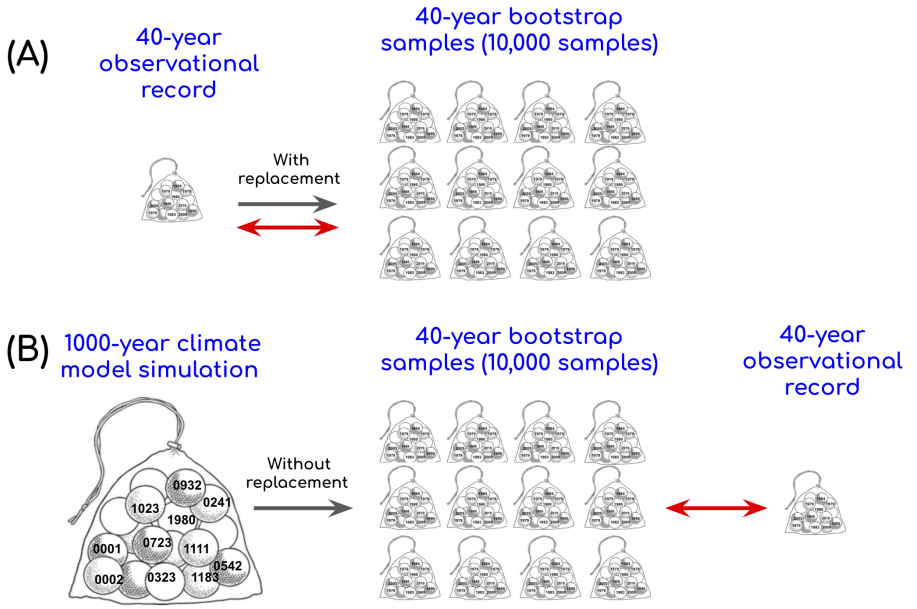

Figure 11: A schematic showing two applications of bootstrap resampling in climate science, as described in the text. Bootstrapping (A) a 40-year observational record with replacement, and (B) a 1000-year climate model simulation without replacement. The red arrow indicates the comparison of interest.

Causal Discovery Algorithms

Identifying causal relationships in the climate system is challenging because of the complex interactions between various components. Many observational studies rely on (lagged) correlations to identify linkages. However, correlation by itself does not imply causation. Figure 12 illustrates three scenarios where a correlation between two variables does not arise from a causal relationship (see figure caption for explanation). Causal inference tools have been developed to infer causality by eliminating such spurious correlations (see *Runge et al.*, 2019a). One such tool, Causal Effect Networks, has been shown to have higher detection power than others, an especially important feature for climate applications (*Runge et al.*, 2019b). Because these are

still statistical tools, albeit quite sophisticated ones, careful interpretation of results is required to arrive at physically meaningful results. Building on previous studies (*Kretschmer et al.*, 2016, 2018), we employ this tool to investigate the robustness of proposed mechanisms behind the ice-NAO linkage (Paper I).

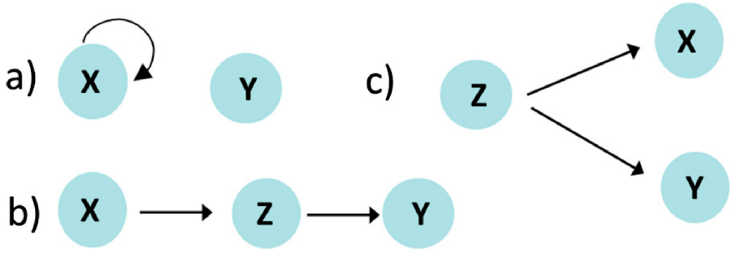

Figure 12: Three scenarios where two variables X and Y are correlated but the relationship is not causal: (A) apparent correlation due to high autocorrelation of X; (B) indirect chain via another variable Z; (C) common driver Z. From *Kretschmer et al.* (2016)

Idealized modelling experiments

Climate models can be broadly classified into two categories: comprehensive and idealized models. Comprehensive models are Earth System Models (ESM) which include all the physical, chemical and biological processes to the best of our knowledge. They aim to simulate our past, current and future climates as realistically as possible. Comprehensive models may not be as valuable as idealized models for understanding specific aspects of the climate system, due to their complexity and expensive running costs (*Polvani et al.*, 2017). Idealized models are simplified models created by leaving out certain components or processes that are included in more comprehensive models. For example, removing landmasses and sea ice and replacing them with still water results in an aquaplanet model. Further removing moisture and the water-covered surface results in a dry model governed by primitive equations, which can be further simplified and linearized to capture just the large-scale atmospheric circulation (i.e., a quasi-geostrophic model). A series of models with complexity ranging from low to high creates the model hierarchy (e.g, *Maher et al.*, 2019). Stripping away components in idealized models allows us to focus on the remaining parts we are interested in examining so that ascertaining physical processes becomes easier. Results from the idealized models can be used to interpret the results from comprehensive models (*Held*, 2005).

In paper III, idealized modelling experiments are carried out to ascertain the dynamical responses to high latitude heating. The results provide insight into the dynamics controlling the atmospheric response to sea ice loss.

Chapter 5

Summary of results

Paper I

P. Y. F. Siew, C. Li, S. P. Sobolowski, M. P. King, Intermittency of Arctic–mid-latitude teleconnections: stratospheric pathway between autumn sea ice and the winter North Atlantic Oscillation. *Weather and Climate Dynamics*, **1**, 261-275 (2020). https://doi.org/10.5194/wcd-1-261-2020.

Autumn Barents-Kara sea ice reduction is hypothesized to lead to a negative NAO in late winter via a pathway that leads from the surface, through the troposphere, into the stratosphere and back down again. However, the robustness of this proposed pathway during the satellite period of observations is unclear. We examined the pathway using a causal discovery tool called Causal Effect Networks (CEN). The CEN detected the full pathway: autumn Barents-Kara sea ice reduction promotes anomalous turbulent heat fluxes into the atmosphere, increasing the frequency of Urals blocking, exciting vertical planetary waves into the stratosphere, weakening the stratospheric polar vortex and eventually influencing the surface weather through a negative NAO in late winter. However, this pathway is less robust than previously thought. We resampled the 39-year observational records to create 10,000 synthetic "historical" realizations. The whole pathway is only detected in 16% of these realizations. The high intermittency is potentially a result of the two-way synoptic interactions between the sea ice and highly variable atmospheric processes, such as the moist intrusions from the midlatitudes.

Paper II

P. Y. F. Siew, C. Li, M. Ting, S. P. Sobolowski, Y. Wu, X. Chen, North Atlantic Oscillation in winter is largely insensitive to autumn Barents-Kara sea ice variability, *Science Advances (in revision)*.

Previous literature has shown that the relationship from autumn Barents-Kara sea ice reduction to the negative NAO in winter is poorly represented in coupled climate models. Some studies have attributed this to model deficiencies in simulating key processes. However, we found that coupled models can reproduce the observed relationship when accounting for the role of internal variability. To show this, we bootstrapped a long pre-industrial control simulation to create 10,000 synthetic realizations equivalent in length to the 40-year observational record. The distribution of the sea ice-NAO relationship across these realizations exhibited large spread. A small number of these realizations captured the observed relationship. The samples that were most consistent with the observed sea ice-NAO relationship did not exhibit features that were consistent with proposed stratospheric mechanisms. Overall, this study suggests that the observed relationship is mostly subject to internal climate variability, and that the observed relationship is unlikely causal.

Paper III

P. Y. F. Siew, C. Li, S. P. Sobolowski, E. Dunn-Sigouin, Atmospheric response to midlatitude and high-latitude surface heating in an idealized moist general circulation model, *Manuscript in preparation*.

Atmospheric circulation responses to surface heating in low and midlatitudes have been previously investigated employing an idealized modelling framework. In this framework, anomalous surface heating at low and mid latitudes generates particular circulation responses that act to restore balance to the atmosphere. Given the ambiguous role of recent Arctic surface heating in influencing atmospheric circulation, it is natural to apply such a framework to study high latitude heating. To investigate this, we performed a set of idealized experiments with prescribed surface heating in the low, mid and high latitudes. Results confirm that midlatitude heating induces circulation responses that act to balance the heating via horizontal temperature advection. When the heating is moved to higher latitudes, the circulation responses that act to balance the heating become weaker, and radiative cooling appears to play a stronger role for removing the excess heat. This study provides insight into how the atmosphere adjusts to Arctic surface heating from sea ice loss.

Paper IV

E. Madonna, G. Hes, C. Li, C. Michel, P. Y. F. Siew, Control of Barents Sea Wintertime Cyclone Variability by Large-Scale Atmospheric Flow. *Geophysical Research Letters*, **47**, 1–11 (2020). https://doi.org/10.1029/2020GL090322.

Previous studies have proposed that Barents-Kara sea ice retreat weakens the local sea surface temperature gradient and thus surface baroclinicity. This is hypothesized

to discourage cyclones from tracking into the Barents and Kara Sea, and instead steers them northwards into the Arctic. This proposed mechanism might result in an increasing frequency of high latitude cyclones and a concomitant increase in the transport of heat and moisture into the Arctic. Results show that sea ice conditions in the Barents Sea exhibit no relationship to cyclone tracks. Rather than sea ice conditions, atmospheric circulation features such as the position of the jet stream and blocking play the main role in guiding the cyclones into the Arctic. Cyclones originating south of 60°N in the North Atlantic carry a significant amount of heat and moisture into the Arctic and lead to strong Arctic surface warming.

Chapter 6

Perspectives and outlook

This thesis investigates Arctic-midlatitude teleconnections, with a focus on whether or not sea ice has influenced midlatitude weather, and the robustness of the physical processes responsible for the linkage. We have used observation-based reanalysis datasets, climate model simulations, and idealized modelling experiments to investigate the effect of sea ice loss and the associated heating anomalies on the midlatitude atmospheric circulation.

The results collectively highlight the subtle role of sea ice in influencing the midlatitudes. Paper I shows that although a causal chain of linkages from Barents-Kara sea ice to midlatitude weather is statistically detectable during the satellite era, the pathway is highly intermittent. Paper II builds from this, using climate model simulations and reanalysis data to argue that the sea ice-NAO pathway is subject to internal climate variability, and that the observed relationship is likely not causal. Paper III is an idealized modelling study which shows that the atmosphere adjusts to midlatitude and high-latitude surface heating via different processes, and outlines a conceptual framework for understanding why. Finally, Paper IV offers a more synoptic viewpoint, showing that Arctic cyclones are steered primarily by the large-scale atmospheric circulation rather than the location of the sea ice edge.

Although our results suggest that sea ice variability itself does not have a systematic influence on midlatitude weather, we cannot rule out a possibility of a highly intermittent pathway connecting them. In other words, a causal linkage may exist, but it can be disrupted by midlatitude variability that arises from processes internal to the atmosphere, such as eddy-mean flow interactions. An extension of this idea is the possibility of preferred background states that allow ice-to-midlatitude pathways to operate. Preferred background states characterized by, for example, a certain phase

of the Quasi-Biennial Oscillation or certain patterns of tropical sea surface temperatures, have been suggested by modelling studies (*Smith et al.*, 2017; *Labe et al.*, 2019), but it is difficult to see if this holds in observations from the relatively short satellite period. One could imagine investigating whether there are preferred background states for sea ice-to-midlatitude teleconnections in longer observational datasets such as the 20th century reanalysis products used in *Kolstad and Screen* (2019).

There is also further insight to be gained from surface heating experiments using models with increasing complexity to better connect the idealized world to reality. Our idealized modelling (Paper III) results show that heating imposed at different latitudes generates different circulation responses, extending results from classical studies (*Hoskins and Karoly*, 1981; *Ting and Held*, 1990; *Ting*, 1991) that focused on tropical to middle latitudes. In the real world, the exact geographic position of the heating source relative to the zonally asymmetric background flow will also matter. To test how this may affect our results, land and topography can be added to the model setup to alter the background flow. It could also be particularly interesting to compare the circulation responses to heating at high latitudes in flows with strong versus weak zonal winds, because this creates very different wave guides that could determine whether Rossby wave trains are generated. More complex moisture schemes could also be interesting to test, as cloud feedbacks have been shown to be important in the Arctic. Step-by-step upgrades in the complexity of the model are possible using the ISCA modelling framework (*Vallis et al.*, 2018), and should be straightforward to implement.

Finally, this thesis highlights that Arctic sea ice loss and the associated surface warming have likely played a minor role in driving midlatitude circulation changes over the last decades. As sea ice decline continues into the future, the impact of sea ice loss on the atmospheric circulation may well change, and even become stronger. Thus, a better understanding of the physical mechanisms connecting sea ice and midlatitude weather will likely remain a priority in the years to come.

Appendices

A Paper I

Intermittency of Arctic–mid-latitude teleconnections: stratospheric pathway between autumn sea ice and the winter North Atlantic Oscillation

Peter Yu Feng Siew[1,2], Camille Li[1,2], Stefan Pieter Sobolowski[3,2], Martin Peter King[3,2]
Weather and Climate Dynamics, **1**, 261-275 (2020)
https://doi.org/10.5194/wcd-1-261-2020

Affiliations:
[1] Geophysical Institute, University of Bergen, Bergen, Norway
[2] Bjerknes Centre for Climate Research, Bergen, Norway
[3] NORCE, Bergen, Norway

Abstract

There is an observed relationship linking Arctic sea ice conditions in autumn to mid-latitude weather the following winter. Of interest in this study is a hypothesized stratospheric pathway whereby reduced sea ice in the Barents-Kara Seas enhances upward wave activity and wave-breaking in the stratosphere, leading to a weakening of the polar vortex and a transition of the North Atlantic Oscillation (NAO) to its negative phase. The Causal Effect Networks (CEN) framework is used to explore the stratospheric pathway between late autumn Barents-Kara sea ice and the February NAO, focusing on its seasonal evolution, timescale-dependence, and robustness. Results indicate that the pathway is statistically detectable and has been relatively active over the 39-year observational period used here, explaining approximately 26% of the interannual variability in the February NAO. However, a bootstrap-based resampling test reveals that the pathway is highly intermittent: the full stratospheric pathway appears in only 16% of the sample populations derived from observations, with individual causal linkages ranging from 46 to 84% in occurrence rates. The pathway's intermittency is consistent with the weak signal-to-noise ratio of the atmospheric response to Arctic sea ice variability in modelling experiments, and suggests that Arctic-midlatitude teleconnections might be favoured in certain background states. On shorter time scales, the CEN detects two-way interactions between Barents-Kara

sea ice and the midlatitude circulation that indicate a role for synoptic variability associated with blocking over the Urals region and moist air intrusions from the Euro-Atlantic sector. This synoptic variability has the potential to interfere with the stratospheric pathway, thereby contributing to its intermittency. This study helps quantify the robustness of causal linkages within the stratospheric pathway, and provides insight into which linkages are most subject to sampling issues within the relatively short observational record. Overall, the results should help guide the analysis and design of ensemble modelling experiments required to improve physical understanding of Arctic-midlatitude teleconnections.

1 Introduction

Autumn sea ice is a potential source of skill in predicting the winter North Atlantic Oscillation (NAO), and hence, European climate (*Wang et al.*, 2017). One proposed mechanism for the relationship focuses on the Barents-Kara Seas, a region with seasonal ice cover that has exhibited strong negative trends during the cold season over the last decades (*Cavalieri and Parkinson*, 2012; *Serreze and Stroeve*, 2015; *Onarheim and Årthun*, 2017). According to this mechanism, reduced Barents-Kara sea ice triggers a wave response that constructively interferes with the climatological stationary wave pattern (*Peings and Magnusdottir*, 2014; *Kim et al.*, 2014; *Sun et al.*, 2015; *Nakamura et al.*, 2016; *Wu and Smith*, 2016; *Hoshi et al.*, 2017; *Zhang et al.*, 2018a; *De and Wu*, 2019), enhancing upward propagation of planetary waves that weakens the stratospheric polar vortex (*Nishii et al.*, 2009; *Garfinkel et al.*, 2010; *Smith et al.*, 2010). Downward coupling from the stratosphere to the troposphere subsequently produces circulation anomalies that resemble the negative phase of the NAO or Arctic Oscillation (AO) (*Baldwin and Dunkerton*, 1999; *Polvani and Waugh*, 2004), along with its attendant climate effects (*Hurrell*, 1995).

A delayed stratospheric pathway linking sea ice and the NAO is suggested by observations, but its exact nature is somewhat unclear. The observational evidence (e.g., *García-Serrano et al.*, 2015; *King et al.*, 2016; *Koenigk et al.*, 2016) hinges on lagged correlations such as the one shown in Fig. 1a (similar to Fig. 10c in *García-Serrano et al.* (2015) and Fig. 6b in *King et al.* (2016)): less Barents-Kara sea ice in November is associated with higher polar cap heights in the stratosphere (i.e., polar vortex weakening), and a subsequent downward propagation of the height anomalies into the troposphere through the winter season, consistent with the appearance of negative NAO conditions several months later. However, the stationarity and statistical significance of this signal has been questioned when using longer records that extend

back before the satellite era (*Hopsch et al.*, 2012; *Kolstad and Screen*, 2019). In fact, the strength and timing of the signal can change when the observational period in Fig. 1a is extended by just several additional winters, showing a statistically insignificant autumn sea ice connection to the winter NAO via the stratosphere (Fig. 1b).

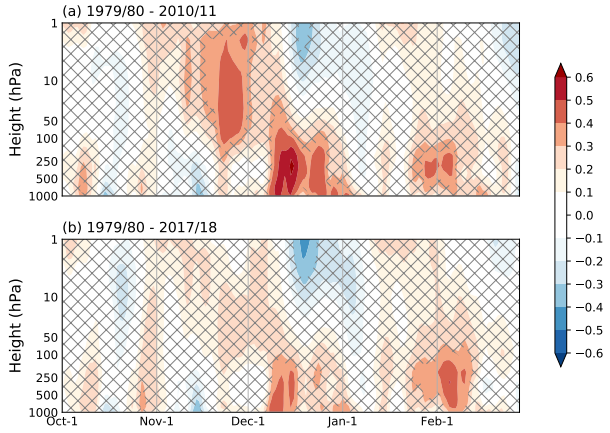

Figure 1: Lead-lag correlations (shading) between November Barents-Kara sea ice index (sign reversed) and polar cap height (70°N poleward) over the October-to-February cold season using ERA-Interim reanalysis for two periods: (a) 1979/80-2010/11 and (b) 1979/80-2017/18. Hatching indicates non-significant values at the 5% level using a two-tailed t-test. Linear trends and the seasonal cycle have been removed.

Evidence from modelling experiments is even more difficult to interpret because the relationship between Barents-Kara sea ice and the NAO is not robust in simulations. Some studies find a clear stratospheric signal after removing sea ice, leading to a weakening of the polar vortex and a negative NAO (*Kim et al.*, 2014; *Nakamura et al.*, 2015; *Sun et al.*, 2015). A negative NAO response to sea ice loss is also possible, although much weaker, if the stratospheric pathway is not well represented or artificially suppressed (*Liptak and Strong*, 2014; *Sun et al.*, 2015; *Wu and Smith*, 2016; *Nakamura et al.*, 2016; *Zhang et al.*, 2018a; *De and Wu*, 2019). However, other modelling studies show a weak or even positive NAO response when sea ice is reduced (*Singarayer et al.*, 2006; *Strey et al.*, 2010; *Orsolini et al.*, 2012; *Cassano et al.*, 2014; *Screen et al.*, 2014), and we lack a comprehensive understanding of why model results are so different (*Screen et al.*, 2018). One reason may be that the atmospheric response depends on where and when sea ice is removed; for example, some studies have shown that sea ice loss in the Pacific sector leads to a strengthening of the polar vortex (*Sun et al.*, 2015; *Screen*, 2017c; *McKenna et al.*, 2018), and that winter ice loss may be more influential than autumn ice loss in weakening and shifting the jet stream (*Blackport and Screen*, 2019). Other possible reasons include nonlinearities with respect to the amplitude of sea ice loss (*Petoukhov and Semenov*, 2010; *Semenov and Latif*, 2015; *Chen*

et al., 2016; *Overland et al.*, 2016), and dependence of the atmospheric response on the background state (*Smith et al.*, 2017, 2019; *Labe et al.*, 2019).

Overall, isolating the sea ice influence on the midlatitudes remains a challenge in part because it is a search for causal drivers in a tightly coupled system with large internal variability (*Shepherd*, 2016). This internal atmospheric variability itself has well-known effects on Arctic climate over a range of time scales. Synoptic weather systems carry heat and moisture poleward from the North Atlantic, and are associated with moist intrusions that have been shown to warm the Arctic and melt sea ice (*Woods et al.*, 2013; *Park et al.*, 2015a,b; *Gong and Luo*, 2017; *Kim et al.*, 2017; *Lee et al.*, 2017). Feedbacks between sea ice and the NAO acting on intraseasonal time scales can yield opposite-signed relationships depending on the time lag considered: anomalously low Barents-Kara sea ice concentrations are favoured by positive NAO conditions (*Fang and Wallace*, 1994; *Deser et al.*, 2000), but are also part of an ice perturbation pattern that has been found to produce negative NAO conditions (*Magnusdottir et al.*, 2004; *Deser et al.*, 2004; *Kvamstø et al.*, 2004; *Strong et al.*, 2009; *Deser et al.*, 2010; *Wu and Zhang*, 2010). The causality problem with respect to sea ice extends beyond the NAO to other midlatitude phenomena such as Eurasian cooling, for which one finds numerous studies arguing both for (*Outten and Esau*, 2012; *Mori et al.*, 2014, 2019) and against (*McCusker et al.*, 2016; *Sorokina et al.*, 2016; *Ogawa et al.*, 2018; *Blackport et al.*, 2019) sea ice loss being responsible for the recent spate of extreme winters.

In the present study, we revisit the observed relationship between autumn Barents-Kara sea ice and the winter NAO with the goal of quantifying the robustness of the stratospheric linkage. In other words, we ask how systematically the stratospheric linkage has appeared during the satellite period. While sampling issues are unavoidable when using a short observational record with large internal variability, our analysis attempts to account for this by exploring the idea that weak but statistically significant signals may arise from a teleconnection pathway that is only intermittently active.

We begin with a description of data and methods (section 2), including a Causal Effect Networks (CEN) approach that provides a statistical framework for assessing causality (applied to climate problems by studies such as *Ebert-Uphoff and Deng*, 2012; *Runge et al.*, 2014; *Kretschmer et al.*, 2016, 2018). Results showing that the pathway is indeed detectable but exhibits a high level of intermittency are presented in section 3, and the implications for understanding present day Arctic-midlatitude teleconnections are discussed in section 4. We end with some concluding remarks in section 5.

2 Data and Methods

2.1 Reanalysis data

The Causal Effect Networks (CEN) approach requires indices (time series) of variables representing key processes in the dynamical mechanism being studied. In our study, we use sea ice area fraction, surface sensible heat flux, surface latent heat flux, sea level pressure, meridional wind, temperature, geopotential height, and downward thermal radiation at the surface. Raw daily data for the period 1979 to 2018 are from the European Center for Medium-Range Weather Forecasts (ECMWF) ERA-Interim reanalysis (*Dee et al.*, 2011). The seasonal cycle is removed at each grid point by subtracting the climatological daily mean to obtain anomalies of each variable, and the data are detrended. The trend is removed through all the days of the year (1 January, 2 January, etc.). The following indices are then calculated from the reanalysis data from September to March:

- Barents-Kara sea ice (ICE): sea ice area fraction averaged over 70°-80° N, 30°-105° E (Fig. 2a)
- Barents-Kara turbulent heat flux (THF): sum of surface sensible and latent heat flux averaged over 70°-80° N, 30°-105° E (Fig. 2b), with positive defined as heat flux from the ocean to the atmosphere
- stratospheric polar vortex strength (SPV): negative of geopotential height poleward of 60° N (Fig. 2c) averaged between 10-100 hPa, as defined by *Kretschmer et al.* (2016), such that positive values of the index indicate a stronger polar vortex
- Urals sea level pressure (URALS): sea level pressure averaged over 45°-70° N, 40°-85° E (Fig. 2d)
- downward longwave radiation (IR): downward thermal radiation at the surface averaged over 70°-90° N (Fig. 2e)
- poleward eddy heat flux (V*T*): product of V* and T* at 100 hPa averaged over 45°-75° N (Fig. 2f), where V and T denote the meridional wind velocity and air temperature respectively, and the superscript * indicates deviations from the zonal mean
- North Atlantic Oscillation index (NAO): from the Climate Prediction Center, based on Rotated Principal Component Analysis of 500 hPa geopotential

height, see details at
https://www.cpc.ncep.noaa.gov/products/precip/CWlink/pna/nao.shtml

Finally, the daily indices are averaged up to monthly, half-monthly and pentad means for the different analyses carried out in this study.

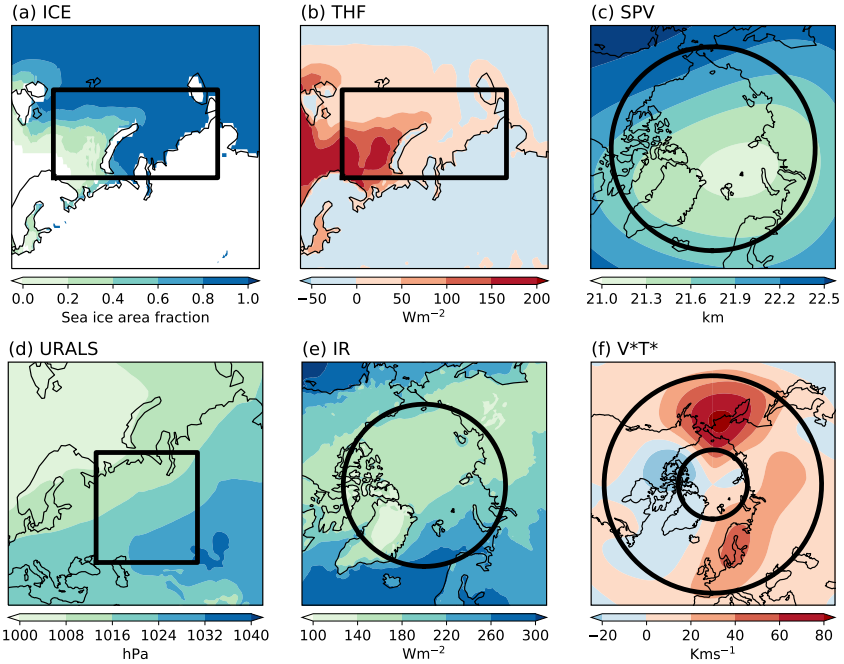

Figure 2: ERA-Interim (1979-2018) DJF climatologies (shading) of key variables and regions (black boxes) for computing area-averaged indices: (a) Sea ice area fraction, 70°-80° N, 30°-105° E, (b) Turbulent heat flux, 70°-80° N, 30°-105° E, (c) Stratospheric polar vortex, which is defined by 10-100 hPa geopotential height, 65°-90° N, (d) Urals sea level pressure, 45°-70° N, 40°-85° E, (e) Downward longwave radiation, 70°-90° N, (f) 100 hPa poleward eddy heat flux, 45°-75° N. For (b), turbulent heat flux from the ocean to the atmosphere is defined as positive.

2.2 Causal Effect Networks (CEN)

The CEN algorithm is a causal inference framework (*Runge et al.*, 2014, 2019b) aimed at identifying causal relationships between variables of interest. It was previously used to study Arctic-midlatitude teleconnections by *Kretschmer et al.* (2016, 2018). Essentially, given a set of indices such as the ones described above, a CEN is constructed following three steps: 1) identify potential causal drivers of each index (condition selection), 2) identify the causal drivers using these potential causal drivers as a "conditioning set", and 3) quantify the strength of the causal relationship. We will

illustrate the algorithm using January stratospheric polar vortex strength (SPV_{Jan}) as an example. Readers are referred to *Kretschmer et al.* (2018) and *Runge et al.* (2019b) for a full description of the CEN algorithm, also known as PCMCI.

In the first step, we find all possible drivers for SPV_{Jan}. A preliminary list of drivers is generated by calculating the Pearson correlation r between SPV_{Jan} and all other indices (including SPV itself) in the preceding months, up to a maximum lag of 2 months (i.e., November and December for this example). Indices with significant correlations are retained, where an optimal significance level is determined using the Akaike information criterion (AIC). The AIC results in the selection of a 20% significance level for the case of SPV_{Jan} (note that the AIC allows for these rather liberal significance levels in the first step, but more stringent levels are used later in the second step). This leaves us with the following possible drivers: $V^*T^*_{Dec}$, $URALS_{Dec}$, SPV_{Dec} and $URALS_{Nov}$. This list is sorted in descending order according to the absolute value of the Pearson correlation coefficient. Next, we test for the conditional independence of all four possible drivers with SPV_{Jan} by calculating partial correlations, controlling for the effect of each driver one at a time starting from the top of the sorted list. If a driver passes the partial correlation test, it is retained in the list of possible drivers; if it does not pass, it is removed from the list, meaning it is no longer in the conditioning set. For example, the partial correlation between $URALS_{Nov}$ and SPV_{Jan} controlling for $V^*T^*_{Dec}$ is, following the notation of *Kretschmer et al.* (2016):

$$\rho(\mathrm{URALS}_{\mathrm{Nov}},\ \mathrm{SPV}_{\mathrm{Jan}} \mid \mathrm{V^*T^*}_{\mathrm{Dec}}) = -0.274, \tag{1}$$

where

$$\rho(x,\ y \mid z) = \frac{r_{xy} - r_{xz} r_{yz}}{\sqrt{1 - r_{xz}^2}\ \sqrt{1 - r_{yz}^2}} \tag{2}$$

The partial correlation is significant at the 20% level (p-value = 0.105), therefore, $URALS_{Nov}$ is retained as a possible driver of SPV_{Jan}. After going through the entire list, SPV_{Dec} is eliminated, leaving us with three possible drivers of SPV_{Jan}: $URALS_{Nov}$, $URALS_{Dec}$ and $V^*T^*_{Dec}$.

In the second step, we retest all possible links (for all indices in the preceding two months, including those rejected in the first step) with SPV_{Jan}, controlling for the *combined effect* of the possible drivers (conditioning set) identified in the first step. This step helps account for false positives when working with highly interdependent time series (as is often the case with climate indices), and enhances detection power (*Runge et al.*, 2019b). Specifically, the test for SPV_{Jan} is:

$$\rho(\mathrm{X},\ \mathrm{SPV}_{\mathrm{Jan}} \mid \mathrm{URALS}_{\mathrm{Nov}},\ \mathrm{URALS}_{\mathrm{Dec}},\ \mathrm{V^*T^*}_{\mathrm{Dec}}), \tag{3}$$

where X represents all indices of ICE, THF, URALS, V*T*, SPV and NAO in both November and December. Any X producing a significant partial correlation in Eq. 3 is regarded as a causal driver of SPV_{Jan}. The conditioning set excludes X when X is being tested, for example:

$$\rho(\text{V*T*}_{\text{Dec}}, \text{SPV}_{\text{Jan}} \mid \text{URALS}_{\text{Nov}}, \text{URALS}_{\text{Dec}}) = -0.453 \tag{4}$$

which is significant at the 5% level (p-value=0.00629). Testing all X leaves us with three causal drivers of SPV_{Jan} : $URALS_{Nov}$, $URALS_{Dec}$ and $V*T*_{Dec}$. Note that these are the same causal drivers identified in the first step, meaning that no new drivers are reintroduced in the second step in this case. As an additional refinement, the Hochberg-Benjamini false discovery rate (FDR) control may be used to account for the multiple testing problem (*Kretschmer et al.*, 2018; *Runge et al.*, 2019b).

In the third step, we use a multiple regression equation to quantify the influence of causal drivers and simultaneous influences on SPV_{Jan}:

$$\text{SPV}^s_{\text{Jan}} = \beta_0 + \beta_1 * \text{URALS}^s_{\text{Nov}} + \beta_2 * \text{URALS}^s_{\text{Dec}} + \beta_3 * \text{V*T*}^s_{\text{Dec}} + \beta_4 * \text{Y}^s_{\text{Jan}} \tag{5}$$

where the β values are regression coefficients for the standardized regressors $URALS^s_{Nov}$, $URALS^s_{Dec}$, $V*T*^s_{Dec}$, Y^s_{Jan}, and the superscript s indicates a standardized index. The inclusion of Y allows us to check for significant simultaneous relationships between all indices. By standardizing, the interpretation is that changing a certain regressor by one standard deviation changes SPV_{Jan} by β standard deviations, provided that all other variables are held fixed.

A two-tailed t-test is used for significance testing. For the AIC in step one, a significance set of (5%, 10%, 20%) is used. There are no substantial changes to the main messages when using other significance sets (Fig. S4). A significance level of 5% is used in the second and third steps.

The above example illustrates how the CEN algorithm identifies and evaluates causal drivers of SPV_{Jan}. In order to construct the complete monthly and half-monthly CENs, we identify causal drivers for all our chosen indices (ICE, THF, URALS, V*T*, SPV and NAO) during the extended winter season (NDJFM). September to December (January to March) indices are taken over the period of 1979 to 2017 (1980 to 2018). All Pearson correlations and partial correlations (first and second steps) and the multiple regressions (third step) are thus based on indices with a sample size of 39 winter seasons. A similar procedure is used for the pentad CEN, but with a maximum lag of two pentads to capture processes occurring on synoptic time scales.

3 Results

This section describes results from our exploration of the ICE-NAO stratospheric pathway using the CEN framework (section 3.1), including an assessment of its strength (section 3.2) and intermittency (section 3.3) in the observational record. We also explore processes occurring on shorter timescales, and discuss how these effects may reinforce or interrupt the stratospheric pathway (section 3.4).

3.1 Seasonally evolving ICE-NAO pathway

We begin by examining pathways from Barents-Kara sea ice to the NAO proposed by previous studies. The CEN analysis follows the approach of *Kretschmer et al.* (2016), but keeps individual months separate rather than considering the DJF period as a whole. This allows us to capture the seasonal evolution of pathways through the cold season.

The CEN (Fig. 3) shows evidence for a stratospheric pathway leading from autumn sea ice perturbations in the Barents-Kara Seas to a late winter NAO response. This pathway appears using both monthly (Fig. 3a) and half-monthly (Fig. 3b) averages as input to the CEN, albeit with slight differences in timing. The half-monthly CEN in Fig. 3b is displayed such that individual half-monthly linkages (shown in Fig. S2) are aggregated into full months to allow for direct comparison to Fig. 3a.

Coloured arrows in the network diagrams highlight the ICE-NAO stratospheric pathway, where red indicates positive relationships and blue indicates negative relationships (the exact values correspond to the beta coefficients in the multiple regression equation, e.g., Eq. 5). Grey arrows show other linkages that are statistically significant, including some tropospheric pathways that also contribute to the ICE-NAO relationship. A figure including all the identified causal linkages and autocorrelations appears in the supplementary material (Fig. S1). For the monthly CEN, the stratospheric pathway is

$$\downarrow \mathrm{ICE}_{\mathrm{Oct}} \Rightarrow \uparrow \mathrm{URALS}_{\mathrm{Dec}} \Rightarrow \uparrow \mathrm{V^*T^*}_{\mathrm{Dec/Jan}} \Rightarrow \downarrow \mathrm{SPV}_{\mathrm{Jan/Feb}} \Rightarrow \downarrow \mathrm{NAO}_{\mathrm{Feb/Mar}}$$

where we use the notation A $\Rightarrow$ B to indicate index A as a "driver" of index B, and $\downarrow$ and $\uparrow$ to represent a decrease or increase, respectively, of the indices. The pathway is described for the case of a negative sea ice perturbation leading to a negative NAO.

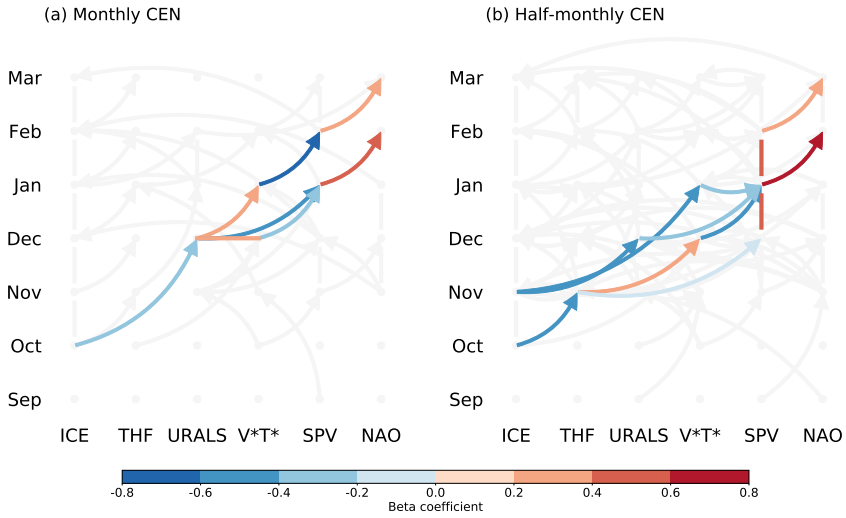

Figure 3: Seasonal evolution of the stratospheric pathway (indicated by coloured arrows) detected by the (a) monthly and (b) half-monthly CENs. Arrows indicate causal linkages; vertical lines indicate auto-correlation; horizontal bars indicate simultaneous relationships; colours show the sign and strength of the linkages as given by the CEN beta coefficients (see section 2.2). The grey background shows other significant linkages (arrows) and autocorrelations (vertical lines), but does not include simultaneous relationships. The half-monthly CEN in (b) has been aggregated into full months for ease of comparison with (a). See Fig. S2 for unaggregated version.

For the half-monthly CEN, the pathway may be summarized as:

$$\downarrow \mathrm{ICE}_{\mathrm{Oct/Nov}} \Rightarrow \uparrow \mathrm{THF}_{\mathrm{Nov}} \Rightarrow \uparrow \mathrm{URALS}_{\mathrm{Dec}} \Rightarrow$$

$$\uparrow \mathrm{V^*T^*}_{\mathrm{Dec/Jan}} \Rightarrow \downarrow \mathrm{SPV}_{\mathrm{Dec/Jan/Feb}} \Rightarrow \downarrow \mathrm{NAO}_{\mathrm{Feb/Mar}}$$

Using the finer half-monthly resolution in the CEN prevents shorter timescale processes (such as linkages through THF) from being averaged out.

The CEN results illustrate how the stratospheric pathway unfolds through the winter season. The timing is in general agreement with previous observational studies, suggesting that the involvement of the stratosphere introduces a few months' delay in the NAO response to Barents-Kara sea ice variability (*Kim et al.*, 2014; *García-Serrano et al.*, 2015; *Jaiser et al.*, 2016; *King et al.*, 2016; *Kretschmer et al.*, 2016; *Yang et al.*, 2016). The causal linkages are consistent with the idea that Arctic sea ice reduction enhances upward wave activity through constructive interference between forced Rossby waves and the climatological stationary waves (*Garfinkel et al.*, 2010; *Smith et al.*, 2010). The resulting increase in wave-breaking in the stratosphere decelerates the polar vortex (*Charney and Drazin*, 1961), which in turn leads to tropospheric circulation anomalies and surface impacts via downward coupling (*Baldwin and Dunkerton*, 1999). Some features of the pathway, such as the relatively long lagged relationship of autumn sea ice to December Urals sea level pressure, are not well understood, an issue that will be further discussed in section 4.

We will focus on the stratospheric pathway from $\mathrm{ICE}_{\mathrm{Oct}}$ to $\mathrm{NAO}_{\mathrm{Feb}}$ in the monthly CEN, as this timing yields the strongest negative ICE-NAO correlation (Fig. S5). The correlation between $\mathrm{ICE}_{\mathrm{Nov}}$ and $\mathrm{NAO}_{\mathrm{Jan}}$ is equally strong, but the causal pathway goes through the troposphere only (Fig. S1b) and is not a focus of this study. Results from the half-monthly CEN yield consistent messages, and will be brought into the discussion where relevant.

3.2 Strength of the pathway

An interesting question is how to assess the strength of the ICE-NAO stratospheric pathway as a whole, and what insights may be gained by such an assessment.

The CEN analysis yields a set of beta coefficients (colours of the arrows in Fig. 3) that describe the strength of individual causal linkages in our network. Following *Runge et al.* (2015), the *total causal effect* of the stratospheric pathway from $\mathrm{ICE}_{\mathrm{Oct}}$ to $\mathrm{NAO}_{\mathrm{Feb}}$ may be calculated by summing over the product of beta coefficients along

Table 1: A summary of the casual effect of all ICE-NAO pathways. The $\downarrow \mathrm{ICE}_{\mathrm{Oct}} \Rightarrow \downarrow \mathrm{NAO}_{\mathrm{Mar}}$ pathway consists of both tropospheric and stratospheric branches.

Pathway	Tropospehric	Stratospheric	Total
$\downarrow \mathrm{ICE}_{\mathrm{Oct}} \Rightarrow \downarrow \mathrm{NAO}_{\mathrm{Feb}}$	N/A	0.0823	0.0823
$\downarrow \mathrm{ICE}_{\mathrm{Oct}} \Rightarrow \downarrow \mathrm{NAO}_{\mathrm{Mar}}$	0.0614 (70%)	0.0258 (30%)	0.0872
$\downarrow \mathrm{ICE}_{\mathrm{Jan}} \Rightarrow \downarrow \mathrm{NAO}_{\mathrm{Mar}}$	0.137	N/A	0.137

the two relevant chains of linkages from Fig. 3a:

$$\downarrow \mathrm{ICE}_{\mathrm{Oct}} \xrightarrow{-0.326} \uparrow \mathrm{URALS}_{\mathrm{Dec}} \xrightarrow{0.390} \uparrow \mathrm{V^*T^*}_{\mathrm{Dec}} \xrightarrow{-0.368} \downarrow \mathrm{SPV}_{\mathrm{Jan}} \xrightarrow{0.426} \downarrow \mathrm{NAO}_{\mathrm{Feb}} \ (0.0199)$$

$$\downarrow \mathrm{ICE}_{\mathrm{Oct}} \xrightarrow{-0.326} \uparrow \mathrm{URALS}_{\mathrm{Dec}} \xrightarrow{-0.449} \downarrow \mathrm{SPV}_{\mathrm{Jan}} \xrightarrow{0.426} \downarrow \mathrm{NAO}_{\mathrm{Feb}} \ (0.0624)$$

The total causal effect (0.0199 + 0.0624 = 0.0823) tells us that a one-standard deviation perturbation in $\mathrm{ICE}_{\mathrm{Oct}}$ yields a like-signed response of 8% of one-standard deviation in February NAO (*Runge et al.*, 2015). One might question the interpretation of the contemporaneous $\uparrow \mathrm{URALS}_{\mathrm{Dec}} \Rightarrow \uparrow \mathrm{V^*T^*}_{\mathrm{Dec}}$ linkage in the first chain as a causal effect, but the fact that it also shows up in the half-monthly CEN as a linkage from the first half of the December to the second half (Fig. S2) supports the point.

A comparison between the stratospheric and tropospheric ICE-NAO pathways shows that the latter are generally stronger in the CEN framework. Table 1 summarizes the causal effect of the three full pathways (Fig. S6). Our main stratospheric pathway of interest from $\mathrm{ICE}_{\mathrm{Oct}}$ to $\mathrm{NAO}_{\mathrm{Feb}}$ is comparable in strength to the pathway from $\mathrm{ICE}_{\mathrm{Oct}}$ to $\mathrm{NAO}_{\mathrm{Mar}}$ (0.0823 and 0.0872). The latter has both stratospheric and tropospheric chains, accounting for 30% (0.0258/(0.0614+0.0258)) and 70% (0.0614/(0.0614+0.0258)) of the total causal effect, respectively. The $\downarrow \mathrm{ICE}_{\mathrm{Jan}} \Rightarrow \downarrow \mathrm{NAO}_{\mathrm{Mar}}$ tropospheric pathway is the strongest in terms of the total causal effect (0.137), primarily because it involves fewer linkages. Overall, the larger causal effect of the tropospheric pathways is perhaps unsurprising, given that the stratospheric pathway may be disrupted by internal variability (noise) from both the troposphere and the stratosphere.

An alternative view of the pathway strength comes from considering the amount of February NAO variance explained by the various linkages along the pathway using a multiple linear regression framework. This gives a sense of the relative importance of each linkage, and how information passes through the pathway. The full pathway can be represented by the following regression equation:

$$\mathrm{NAO}_{\mathrm{Feb}} = \kappa_0 + \kappa_1 \cdot \mathrm{ICE}_{\mathrm{Oct}} + \kappa_2 \cdot \mathrm{URALS}_{\mathrm{Dec}} + \kappa_3 \cdot \mathrm{V^*T^*}_{\mathrm{Dec}} + \kappa_4 \cdot \mathrm{SPV}_{\mathrm{Jan}} \qquad (6)$$

where κ_0 is a constant and κ_1, κ_2, κ_3, κ_4 are the regression coefficients for the standardized regressors $\mathrm{ICE}_{\mathrm{Oct}}$, $\mathrm{URALS}_{\mathrm{Dec}}$, $\mathrm{V^*T^*}_{\mathrm{Dec}}$ and $\mathrm{SPV}_{\mathrm{Jan}}$, respectively. The importance of the regressors may be quantified in different ways, for example:

a) cumulative $\mathrm{NAO}_{\mathrm{Feb}}$ variance explained as regressors are included, calculated by successively adding terms in Eq. 6 from left to right (orange bars in Fig. 4), e.g. for $\mathrm{V^*T^*}_{\mathrm{Dec}}$:

$$\mathrm{NAO}_{\mathrm{Feb}} = \kappa_0^a + \kappa_1^a \cdot \mathrm{ICE}_{\mathrm{Oct}} + \kappa_2^a \cdot \mathrm{URALS}_{\mathrm{Dec}} + \kappa_3^a \cdot \mathrm{V^*T^*}_{\mathrm{Dec}} \tag{7}$$

b) $\mathrm{NAO}_{\mathrm{Feb}}$ variance explained by individual regressors, calculated via a simple bivariate regression between each regressor and $\mathrm{NAO}_{\mathrm{Feb}}$ (blue bars), e.g., for $\mathrm{V^*T^*}_{\mathrm{Dec}}$:

$$\mathrm{NAO}_{\mathrm{Feb}} = \kappa_0^b + \kappa_3^b \cdot \mathrm{V^*T^*}_{\mathrm{Dec}} \tag{8}$$

c) reduction in $\mathrm{NAO}_{\mathrm{Feb}}$ variance explained when individual regressors are removed, calculated by removing the term from the regression equation (green bars), e.g., for $\mathrm{V^*T^*}_{\mathrm{Dec}}$:

$$\mathrm{NAO}_{\mathrm{Feb}} = \kappa_0^c + \kappa_1^c \cdot \mathrm{ICE}_{\mathrm{Oct}} + \kappa_2^c \cdot \mathrm{URALS}_{\mathrm{Dec}} + \kappa_4^c \cdot \mathrm{SPV}_{\mathrm{Jan}} \tag{9}$$

Both the blue and green bars in Fig. 4 provide a measure of the contribution of individual regressors, while comparison of these with the orange bars gives some indication of whether information from a given regressor is redundant.

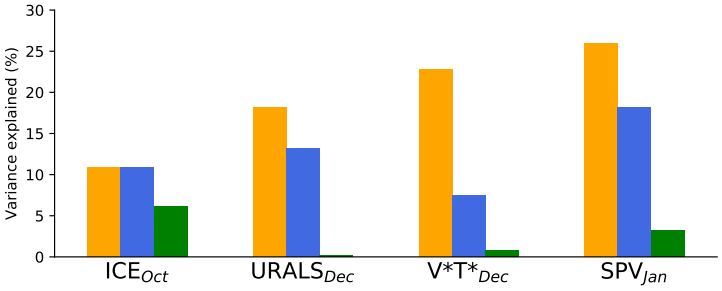

Figure 4: Explanatory power of the stratospheric pathway for the February NAO assessed via multiple linear regression. Orange bars show the cumulative variance explained when including each regressor in succession from left to right; blue bars show variance explained by the individual regressor; green bars show the reduction in total variance explained when removing that regressor

The stratospheric pathway explains 26% of the variance in the February NAO (Fig. 4). The cumulative variance explained (orange bars) increases from 11% to 26%

as regressors are added (moving from left to right), indicating that each linkage in the pathway adds some useful information. This result is consistent with other estimates from observations, but likely represents an upper limit as the Barents-Kara sea ice and NAO relationship is shown to be particularly strong during the current reanalysis period compared to the rest of the twentieth century (*Kolstad and Screen*, 2019).

While successive linkages in the pathway add explanatory power, they are not independent. Comparing the orange and blue bars, we see that the increase of cumulative explained variance moving from left to right is much less than the explained variance from each individual regressor. For example, while SPV_{Jan} explains the most NAO variance of any individual regressor (18%), its removal from the full regression does not have much effect (3% reduction in explained variance), However, we know that variability in upward wave activity and variability in the polar vortex are closely related, so in a sense, it is not physically meaningful to consider one in isolation of the other. Removing both $V^*T^*_{Dec}$ and SPV_{Jan} from the regression equation results in a 8% reduction (not shown) in explained variance, which is perhaps a more representative estimate of the stratosphere's contribution. Sea ice appears to impart information that cannot be explained by the other three regressors (6% reduction in explained NAO variance when removed), but this may also be a result of atmosphere-ice feedbacks explored in section 3.4.

Overall, these analyses show a role for the stratosphere in connecting autumn ICE to late winter NAO, but one that accounts for a modest fraction of the total NAO variance. However, the pathway strength reported here should be considered as an estimate, as there remain uncertainties associated with analysis choices such as the time resolution of the input data and the relevant lags to include. In the next section, we will further explore reasons for this relatively weak ICE-NAO covariability.

3.3 Intermittency of the pathway

The ICE-NAO stratospheric pathway identified by the CEN comprises statistical relationships inferred from a relatively short observational record of only 39 winters. It is meaningful to ask how robust the pathway is, that is, how systematically the relevant statistical relationships occur in the record. To assess the robustness, we perform a bootstrapping test, where bootstrap samples are created by randomly selecting 39 winters with replacement from the entire reanalysis period. The CEN of each sample is then constructed. This procedure is repeated 10,000 times.

The bootstrapping results (Fig. 5) indicate that the stratospheric pathway is intermittent. Percentages show the occurrence rate of individual segments in the pathway within the bootstrap sample population (see Fig. S7 for occurrence rates of other statistically significant linkages). By this measure, it is clear that individual segments have varying levels of intermittency, ranging from 46% for the segment $\downarrow$ SPV_{Jan} $\Rightarrow\downarrow$ NAO_{Feb} to 84% for the segment $\uparrow$ $V^*T^*_{Dec}$ $\Rightarrow\downarrow$ SPV_{Jan}. The full stratospheric pathway (the sequence of all four segments) is detected in only 16% of the samples, suggesting that it does not occur systematically during every winter season. An alternative three-segment pathway $\downarrow$ ICE_{Oct} $\Rightarrow\uparrow$ $URALS_{Dec}$ $\Rightarrow\downarrow$ SPV_{Jan} $\Rightarrow\downarrow$ NAO_{Feb} is slightly less intermittent (22% occurrence rate), but its physical interpretation is unclear given that there is no linkage through V*T* to the polar vortex, as expected from theory. These intermittency results are a likely reason why detection of the pathway is sensitive to the choice of observational period (Fig. 1), and suggests that it may be favoured in certain background states (*Overland et al.*, 2016; *Smith et al.*, 2017).

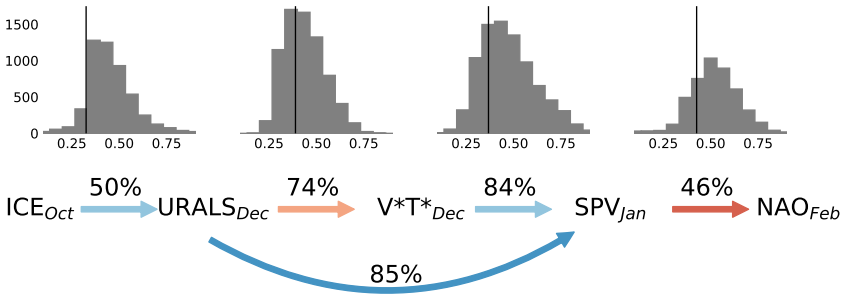

Figure 5: Results of a bootstrapping test to assess the robustness of causal linkages within the stratospheric pathway. Percentages above arrows show the occurrence rate of each linkage out of 10,000 bootstrap samples. Colours of the arrows (identical to Fig. 3) and the black lines show observed beta coefficients for each linkage for the reanalysis period. Histograms above show the corresponding distribution of beta coefficients (absolute value) in the bootstrap samples. The histogram for the $\uparrow$ $URALS_{Dec}$ $\Rightarrow\downarrow$ SPV_{Jan} linkage is not shown. Note that the distributions are composed only of samples in which the linkage is detected.

The existence of intermittency in the stratospheric pathway is consistent with previous suggestions that internal variability modulates the influence of Arctic sea ice on the midlatitude circulation (*Screen et al.*, 2014; *Overland et al.*, 2016; *Shepherd*, 2016). An examination of where in the pathway the intermittency is strongest provides clues to its origins. For example, the upward coupling from sea ice to the stratosphere includes the segments $\downarrow$ ICE_{Oct} $\Rightarrow\uparrow$ $URALS_{Dec}$ and $\uparrow$ $URALS_{Dec}$ $\Rightarrow\uparrow$ $V^*T^*_{Dec}$, whose occurrence rates are 50% and 74%, respectively. The occurrence of these two linkages

together is seen in about 41% out of 10,000 bootstrap samples, meaning that most of the time when the $\downarrow$ ICE_{Oct} $\Rightarrow\uparrow$ $URALS_{Dec}$ linkage is detected, the subsequent linkage to $V^*T^*_{Dec}$ follows. Conversely, when the $\uparrow$ $URALS_{Dec}$ $\Rightarrow\uparrow$ $V^*T^*_{Dec}$ linkage is detected, it is preceded by the $\downarrow$ ICE_{Oct} $\Rightarrow\uparrow$ $URALS_{Dec}$ linkage in only about half the cases. An obvious source of the intermittency in both segments (individually and in terms of their "combined" occurrence rate) is regional SLP variability over the Urals related to atmospheric internal variability. Similarly, the downward coupling from SPV to NAO is vulnerable to both stratospheric and tropospheric internal variability, leading to a relatively low occurrence rate of 46%. This is consistent with the idea that not all polar vortex strengthening and weakening events affect the tropospheric circulation (*Karpechko et al.*, 2017). Most robust is the $\uparrow$ $V^*T^*_{Dec}$ $\Rightarrow\downarrow$ SPV_{Jan} linkage (84%), which arises from well-known physical processes related to upward planetary wave flux and polar vortex weakening. Sea ice variability can also contribute to intermittency in the pathway through higher frequency synoptic processes, a topic we will explore in section 3.4.

The strength of the segments in the pathway also exhibits large variability among the bootstrap samples. This can be seen in histograms of the beta coefficients for all segments in the pathway (Fig. 5). While the beta coefficients exhibit ranges of up to 0.5 for any given segment, the sign is always the same, indicating that the sign of the relationship between variables is robust. The observed beta coefficients (black lines) for the reanalysis period itself fall within the spread of the distributions. Note that the distributions are composed only of samples in which the linkage of interest is detected by the CEN algorithm (i.e., a beta coefficient can be calculated from Eq. 5), which is why some of the distributions appear skewed. This is particularly true for the linkages that are least robust (the first and last segments, for which the observed beta coefficients are towards the weaker end of the distributions). Overall, these results indicate that even when the stratospheric pathway is active, there is substantial interannual variability in how it manifests.

3.4 Synoptic linkages and interactions across times scales

In the monthly CEN analysis, there are simultaneous relationships between Barents-Kara sea ice, Urals sea level pressure and the NAO (Fig. 6) that point to linkages through shorter timescale synoptic processes. For example, the NAO shows significant negative simultaneous relationships with Barents-Kara sea ice (positive NAO with reduced ice) in December and March, reflecting a well-known pattern of atmospheric forcing on sea ice via anomalies in surface heat fluxes driven by wind and

temperature variability (*Fang and Wallace*, 1994; *Deser et al.*, 2000). Additional simultaneous relationships between sea ice, turbulent heat flux, and Urals sea level pressure are consistent with synoptic features related to cyclones (*Boisvert et al.*, 2016; *Wickström et al.*, 2019) and moist intrusions (*Woods et al.*, 2013; *Park et al.*, 2015b) entering the Arctic. Moist intrusions in particular appear to occur preferentially during the positive phase of the NAO (*Luo et al.*, 2017) and have been shown to lead to enhanced downward longwave radiation, surface warming, and sea ice reductions (*Gong and Luo*, 2017; *Chen et al.*, 2018). We explore the possible influences of such events within the CEN framework by using higher frequency data to capture the relevant synoptic processes. The input data are pentad (5-day) means of Barents-Kara sea ice (ICE), Urals sea level pressure (URALS) and downward longwave radiation (IR). The maximum lag is set to two pentads (10 days) to isolate the synoptic timescale. The results are summarized in Fig. 7 by summing the number of times a linkage appears in each month from Fig. S8. The maximum count for a given linkage in a month is 12 (six pentads in a month and up to 2-pentad lag considered). Autocorrelation is strong on these short time scales, and thus is not used to reject causal linkages in the partial correlation tests.

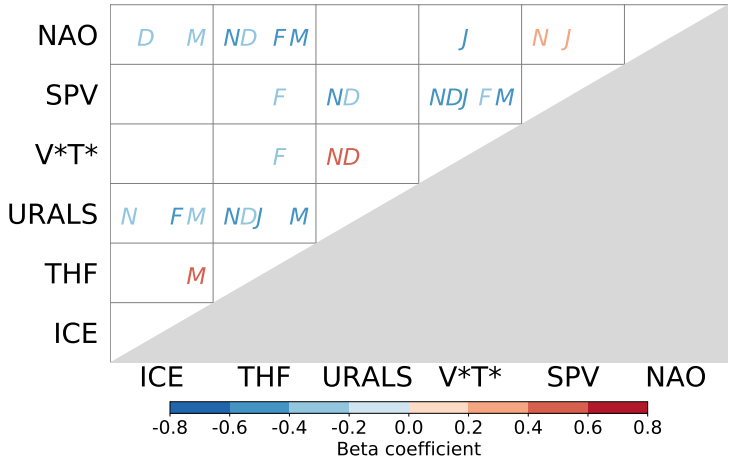

Figure 6: Simultaneous relationships between monthly indices in November (N), December (D), January (J), February (F) and March (M). Colours indicate the sign and strength of the relationship as given by the CEN beta coefficients.

The CEN detects synoptic-scale influences from the Arctic to the midlatitudes that reinforce linkages found in the monthly analysis. A linkage from ICE to URALS appears regularly throughout the winter season (Fig. 7a), both indirectly through IR and as a direct connection, and in the correct sense to contribute to the $\downarrow \mathrm{ICE}_{\mathrm{Oct/Nov}} \Rightarrow \uparrow \mathrm{URALS}_{\mathrm{Dec}}$ linkage shown in the monthly and half-monthly CENs (Fig. 3). The $\downarrow$ ICE $\Rightarrow \uparrow$ IR linkage (blue bars, first histogram in Fig. 7a) follows

from the idea that sea ice retreat exposes open ocean, which is a local evaporative source for water vapour, leading to a moister, optically thicker atmosphere (*Kim and Kim*, 2017; *Zhong et al.*, 2018). The linkage ↑ IR ⇒ ↑ URALS (red bars, second histogram in Fig. 7a) is consistent with a suggested mechanism whereby the resulting surface warming weakens zonal wind locally and promotes blocking over the Urals (*Luo et al.*, 2016). These synoptic processes, if habitually occurring, can imprint onto longer timescales, but may also produce interference effects, as seen by the appearance of opposite-signed causal relationships from those described above from time to time through the winter season.

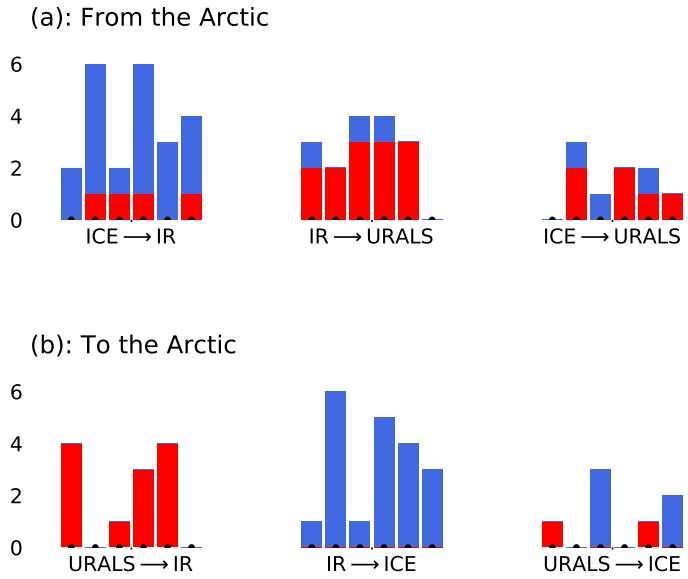

Figure 7: Results of the pentad CEN analysis assessing relationships between downward longwave radiation (IR), Barents-Kara sea ice (ICE) and Urals sea level pressure (URALS) aggregated into months (October, November, December, January, February and March from left to right). The height of each bar is the number of counts. (a) Linkages from the Arctic to the midlatitudes. (b) Linkages from the midlatitudes to the Arctic. Red (blue) colours denote positive (negative) relationships. See Fig. S8 for unaggregated version.

At the same time, causal effects from the midlatitudes to the Arctic are also detected, consistent with an influence from moisture transport by cyclones or synoptic moist intrusions (Fig. 7b). This is represented by the ↑ URALS ⇒↑ IR linkage (most frequently observed in October, January and February) and the ↑ IR ⇒ ↓ ICE linkage (most frequently observed in November, January and February), which reflect the transport of moist air into the dry Arctic atmosphere by the large-scale flow or by cyclones tracking into the Barents. These midlatitude-to-Arctic linkages have a uniform sign (all red bars in first histogram, all blue bars in second histogram),

suggesting that the effect of the relevant processes is rather systematic despite exhibiting month-to-month variability. We also detect a direct linkage from the Urals to Barents-Kara sea ice that can be of either sign. In the slightly more frequent negative sense (↑ URALS ⇒↓ ICE), it can be interpreted as a direct effect of warm air advection and mechanical forcing of the ice cover from enhanced southerlies over the Barents-Kara region (*Sorokina et al.*, 2016; *McCusker et al.*, 2016). Together, these synoptic linkages show how Urals SLP variability, which has a large internally generated component, can reinforce or interrupt the ICE-NAO stratospheric pathway.

Given that our understanding of Arctic-midlatitude teleconnections must account for the combined influences of such linkages across regions and time scales, it is no surprise that we have yet to identify a definitive set of mechanisms. Implications of such scale interactions and how they relate to viewpoints presented in previous studies are further discussed in section 4.

4 Discussion

This study quantifies the robustness of atmospheric teleconnections between the Arctic and midlatitudes, documenting their high level of intermittency in the observational record. In a bootstrapping test, the full stratospheric pathway emerges in only 16% of the sample populations derived from the observations (Fig. 5). The existence of intermittency is likely why studies using various analytical approaches and time periods find teleconnections that differ in pattern, timing, robustness and apparent mechanisms (*Overland et al.*, 2016; *Francis*, 2017; *Cohen et al.*, 2018b; *Overland and Wang*, 2018; *Cohen et al.*, 2020). In this section we discuss some of the factors that may contribute to the intermittency. Of course, anything that influences polar vortex strength is a potential source of intermittency (including internal variability, anthropogenic forcing, tropical variability, etc.), but we focus the discussion on factors that are most directly related to our CEN results.

To be more concrete, the intermittency of the stratospheric pathway stems from the fact that it can be reinforced or interrupted by other processes. For example, reinforcement can come from tropospheric pathways also detected by the CEN algorithm (see Fig. S1a and S1b):

1) $\downarrow \mathrm{ICE}_{\mathrm{Oct}} \Rightarrow \uparrow \mathrm{THF}_{\mathrm{Nov}} \Rightarrow \uparrow \mathrm{URALS}_{\mathrm{Jan}} \Rightarrow \uparrow \mathrm{URALS}_{\mathrm{Feb}} \Rightarrow \downarrow \mathrm{NAO}_{\mathrm{Mar}}$

2) $\downarrow \mathrm{ICE}_{\mathrm{Jan}} \Rightarrow \uparrow \mathrm{URALS}_{\mathrm{Feb}} \Rightarrow \downarrow \mathrm{NAO}_{\mathrm{Mar}}$

3) $\downarrow \mathrm{ICE}_{\mathrm{Nov}} \Rightarrow \downarrow \mathrm{NAO}_{\mathrm{Jan}}$

4) $\downarrow \mathrm{ICE}_{\mathrm{Jan}} \Rightarrow \downarrow \mathrm{NAO}_{\mathrm{Mar}}$

All these tropospheric and stratospheric pathways lead from the reduction of sea ice to a negative NAO, although they differ slightly in timing. The existence of the tropospheric pathway is supported by sea ice and surface heating perturbation experiments, where negative NAO/AO responses are simulated even when the stratospheric pathway is suppressed (*Wu and Smith*, 2016) or not well represented (*Sun et al.*, 2015). However, the NAO/AO response is stronger when the stratospheric pathway is active than when it emerges through the tropospheric pathway alone (*Nakamura et al.*, 2016; *Zhang et al.*, 2018a,b).

Another example of a factor that may contribute to intermittency is the El Niño Southern Oscillation (ENSO). El Niño winters are associated with a deepened Aleutian low, which enhances upward propagating waves, weakens the polar vortex, and favours negative NAO conditions (*Domeisen et al.*, 2019). As such, the stratospheric pathway may be reinforced if an El Niño develops following a low autumn ice season (both are associated with a weakened polar vortex, e.g., winter 1986/87 or 2009/10, Fig. 8); if a La Niña develops instead, the stratospheric pathway may be weakened (e.g., winter 2007/08 or 2010/11, Fig. 8). The relationship between wintertime ENSO and the NAO is rather weak (*Brönnimann*, 2007; *Domeisen et al.*, 2019), consistent with Fig. 8, which shows high and low Nino3.4 values in both the lower (negative NAO) and upper (positive NAO) quadrants of the scatter plot. Given that we find no systematic phasing of ENSO with Barents-Kara sea ice variability during the reanalysis period, it is likely that ENSO contributes to intermittency in the ICE-NAO pathway.

In terms of reinforcing the stratospheric pathway, blocking over the Urals region seems to play a particularly important, but not fully understood, role. Enhanced Urals sea level pressure is closely linked to the Scandinavian pattern in Euro-Atlantic climate variability and is related, but not directly equivalent, to the occurrence of atmospheric blocking. The Urals linkage appears in the monthly CEN ($\downarrow \mathrm{ICE}_{\mathrm{Oct}} \Rightarrow \uparrow \mathrm{URALS}_{\mathrm{Dec}} \Rightarrow \uparrow \mathrm{V^*T^*}_{\mathrm{Dec/Jan}}$ in Fig. 3a). The latter segment from Urals sea level pressure to poleward eddy heat flux is fairly systematic (appears in 74% of the bootstrap samples in Fig. 5) and is grounded in the idea that tropospheric precursors over the Urals lead polar vortex weakening (*Cohen and Jones*, 2011; *Cohen et al.*, 2014a). However, the first segment from Barents-Kara sea ice to Urals blocking is more intermittent (appears in 50% of the bootstrap samples), and whether it is in fact a causal linkage has been questioned by a recent modelling study using ensemble nudging experiments (*Peings*, 2019). Interestingly, not only Barents-Kara sea ice

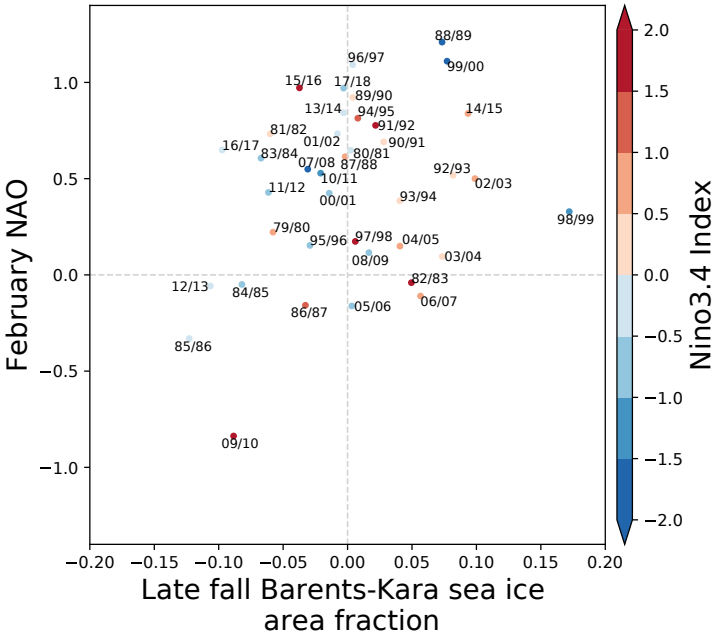

Figure 8: Scatter plots between February NAO and late fall (mean of October and November) Barents-Kara sea ice index for the reanalysis period. Shading indicates the DJF Nino3.4 index. Red (blue) denotes El Niño (La Niña) events.

(Fig. 5e in *King et al.* (2016)) but also ENSO (Figs 5e and 5f in *King et al.* (2018)) has been linked to the Scandinavian pattern, which suggests another avenue for ENSO to contribute to intermittency.

The ICE-URALS relationship highlights the complexity of interactions between atmospheric internal variability and Barents-Kara sea ice over a range of time scales. On synoptic scales, the pentad CEN (Fig. 7) shows linkages from reduced sea ice to enhanced Urals sea level pressure, but also linkages in the opposite direction ($\uparrow$ URALS $\Rightarrow\uparrow$ IR $\Rightarrow\downarrow$ ICE), with Urals sea level pressure altering ice cover via changes in poleward moisture transport that have been tied to synoptic moist intrusions (*Woods et al.*, 2013; *Luo et al.*, 2016; *Gong and Luo*, 2017; *Lee et al.*, 2017). This chain of linkages can act as a positive feedback on sea ice perturbations, but also provides a pathway by which blocking variability (internal to the atmosphere) may interrupt the expected troposphere-stratosphere coupling in response to autumn sea ice (for example, imagine a case where atmospheric conditions inhibit Urals blocking after a low-ice autumn). Furthermore, enhanced Urals blocking and moist intrusions can lead to highly transient perturbations in turbulent heat flux over the Barents-Kara Seas. Initially, turbulent heat loss from the ocean is suppressed near the sea ice edge where moist intrusions act to weaken temperature and moisture contrasts between the atmosphere and ocean (*Woods et al.*, 2013; *Gong and Luo*, 2017). But the heat flux anomaly can become positive (enhanced heat loss from the ocean) after the sea ice melts back in response to the moist intrusion, one to two weeks later (*Woods and Caballero*, 2016; *Lee et al.*, 2017). On longer (monthly to seasonal) time scales, there is evidence that atmospheric variability is the main driver of heat flux variability over the Barents-Kara Seas both in observations and models (*Sorokina et al.*, 2016; *Blackport et al.*, 2019). This perhaps explains why turbulent heat flux does not show up in the monthly CEN (Fig. 3a), but does in the half-monthly CEN (Fig. 3b). Across synoptic to seasonal timescales, it appears that sea ice is best thought of as an intermediary rather than a true boundary forcing, as is implied by prescribed sea ice (e.g., AGCM) experiments.

One outstanding issue involves the mechanisms that have been proposed to explain the $\downarrow \mathrm{ICE}_{\mathrm{Oct}} \Rightarrow\uparrow \mathrm{URALS}_{\mathrm{Dec}}$ linkage, which act on time scales that are inconsistent with the 2-month delay found in observations. For example, reduced sea ice may allow more heating of the atmosphere by the ocean to produce a Rossby wave train with an anomalous high over the Urals region (*Honda et al.*, 2009), but this would be expected to manifest within a matter of days to a week. Alternatively, reduced ice may reduce local baroclinicity, which discourages cyclones from tracking into the Barents-Kara Seas and produces an anomalous high due to the relative absence of low-pressure systems (*Inoue et al.*, 2012). This mechanism could introduce some de-

lay between the ice perturbation and sea level pressure perturbation, but two months persistence of such a pattern is unlikely. Finally, reduced ice may increase atmospheric moisture content, leading to increased Eurasian snow cover, diabatic cooling and anomalously high sea level pressure over the continent (*Liu et al.*, 2012; *Cohen et al.*, 2014a; *Garcia-Serrano and Frankignoul*, 2014). Though this would plausibly lead to persistence on the required time scale, recent observational and modelling studies do not support a role for Eurasian snow in this teleconnection pathway (*Kretschmer et al.*, 2016; *Peings et al.*, 2017; *Henderson et al.*, 2018), and we chose not to include it in our main analyses. Note that these mechanisms may still be responsible for contemporaneous forcing of the winter atmospheric circulation by winter sea ice variability, which has been suggested to be a stronger influence than the forcing by autumn sea ice variability (*Blackport and Screen*, 2019).

Lastly, our experience with the CEN offers some cautionary notes about its application to climate problems. The CEN approach was designed for hypothesis testing - that is, to test causal pathways that are thought or known to exist, either from theory or existing evidence. It should not be used as an exploratory data analysis tool to search for causal pathways because the statistics behind the CEN do not know whether relationships are physically meaningful. One specific problem we encountered is that the algorithm may drop an existing causal linkage if a new variable is added. For example, when we introduce downward longwave radiation into the monthly CEN, its strong correlation with sea ice overrides the $\downarrow \mathrm{ICE}_{\mathrm{Jan}} \Rightarrow \uparrow \mathrm{URALS}_{\mathrm{Feb}}$ linkage (see Fig. S9 compared to Fig. S1a). Since many climate variables are highly correlated, but not necessarily directly related via specific processes, the CEN's ability to identify physically meaningful linkages depends critically on the careful selection of input variables.

5 Concluding remarks

This study uses the Causal Effect Networks (CEN) framework to quantify the robustness of the stratospheric pathway between late autumn Barents-Kara sea ice and the February NAO, documenting its high level of intermittency in the observational record. The pathway has been relatively active over the satellite period, explaining approximately 26% of the interannual variability in the February NAO. However, this result is highly sensitive to which winters are included in the analysis. Results from a bootstrapping test show that the full stratospheric pathway appears in only 16% of the sample populations derived from the observations. The result reflects the strong internal variability of the midlatitude atmosphere and the likelihood that

Arctic-midlatitude teleconnections may require certain background flow conditions. On synoptic time scales, we identify two-way interactions between Barents-Kara sea ice and the midlatitude circulation suggesting a role for atmospheric blocking over the Urals region and moist intrusions, both of which can reduce Barents-Kara sea ice. These synoptic processes can reinforce or interrupt the stratospheric pathway, contributing to intermittency. Finally, we cannot rule out that the causal linkages found on longer time scales may be artefacts of averaging over the synoptic processes, or even the result of entirely different mechanisms (*Smith et al.*, 2017; *Hell et al.*, 2020).

Coupled interactions between sea ice and the midlatitude circulation involve complicated lead-lag feedbacks over a range of time scales. Applying causal inference frameworks such as the CEN can help clarify some of the important physical processes at play, but in the end, models are required to improve our understanding. A complication is that the fidelity of climate models in representing the relevant processes is difficult to ascertain (*King et al.*, 2016; *Smith et al.*, 2017; *Mori et al.*, 2019), especially those processes at fine spatial and temporal scales and their interactions across scales. But ways forward are indicated by this study, along with others (*McCusker et al.*, 2016; *Sun et al.*, 2016; *Peings*, 2019), that provide insight into which linkages are most robust, and which are subject to sampling issues within the relatively short observational record.

Supplementary figures

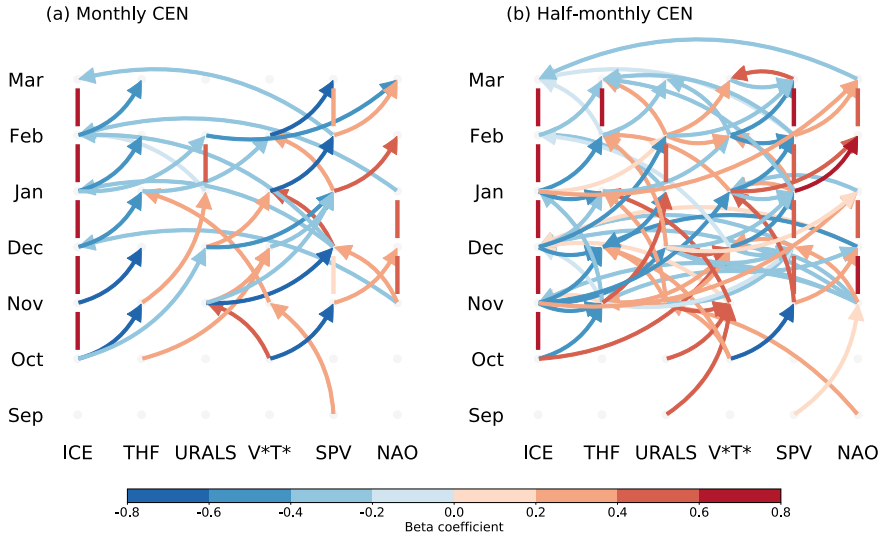

Figure S1: As in Fig. 3, but showing the beta coefficients (colours) of all detected casual linkages. Note that no simultaneous relationships are shown here, including $\uparrow \mathrm{URALS}_{Dec} \Rightarrow \uparrow \mathrm{V^*T^*}_{Dec}$ (coloured horizontal line in Fig. 3a).

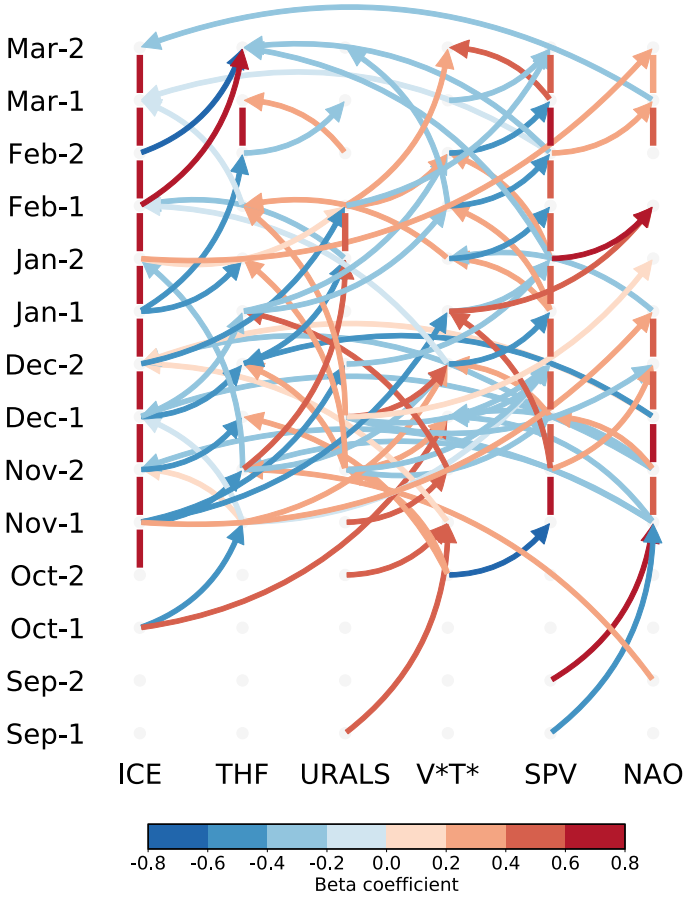

Figure S2: The unaggregated version of the half-monthly CEN, equivalent to Fig. S1b after aggregation.

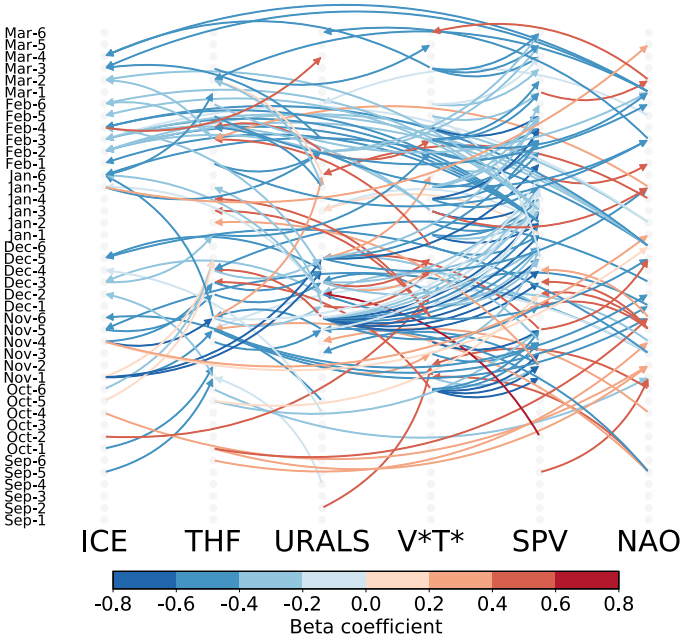

Figure S3: Pentad version of the monthly (Fig. 3a, S1a) and half-monthly (Fig. 3b, S1b) CENs. A 1% significance level is used in the second step (see Data and Methods 2.2). A maximum lag of 12 pentads (i.e., 2 months) is allowed. Autocorrelation is not used to reject causal linkages in the partial correlation tests here.

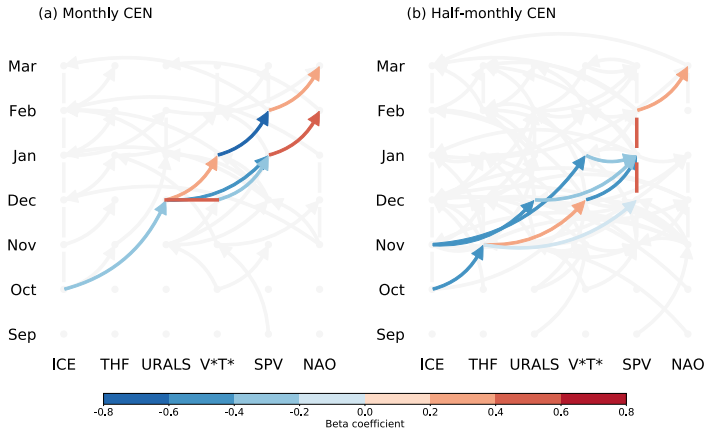

Figure S4: As in Fig. 3, but using AIC with another significance set (5%, 10%, 20%, 30%, 40%, 50%).

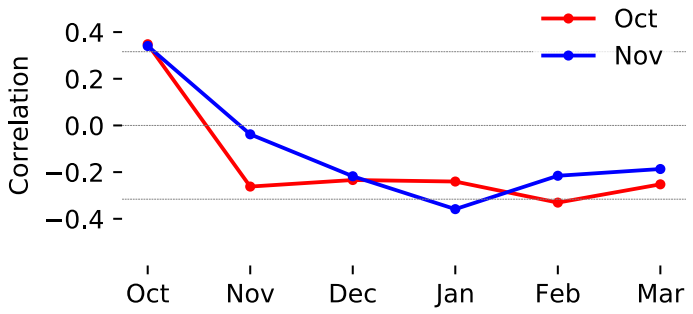

Figure S5: The correlation between October (red) and November (blue) Barents-Kara sea ice indices, and NAO from October to March. Outer grey lines show significant correlations at a 5% level using a two-tailed t-test.

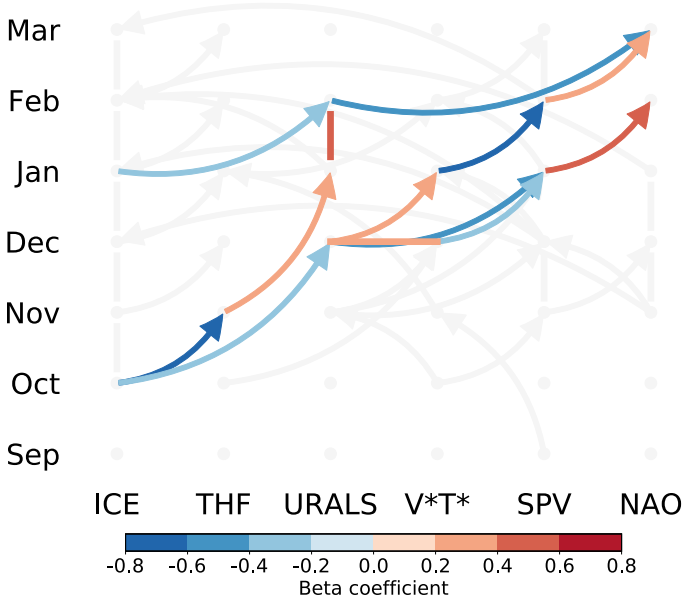

Figure S6: As in Fig. 3a, but highlighting all ICE-NAO strato-spheric and tropospheric pathways.

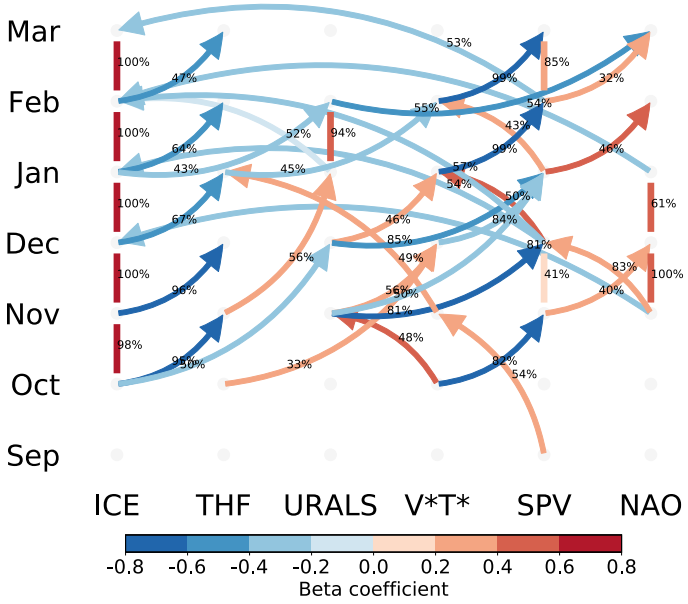

Figure S7: Same as Fig. S1a, but additionally showing the occur-rences rates of all linkages in the bootstrapping test.

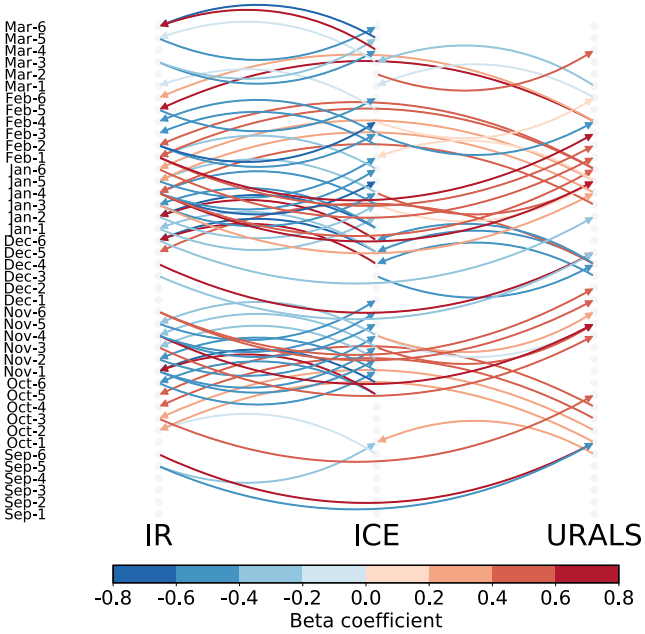

Figure S8: Results of the pentad CEN analysis assessing relation-ships between downward longwave radiation (IR), Barents-Kara sea ice (ICE) and Urals sea level pressure (URALS). A maximum lag of 2 pentads is allowed. Autocorrelation is not calculated. Fig. 7 is aggregated from this figure by sum-ming the number of times each linkage appears in individual months.

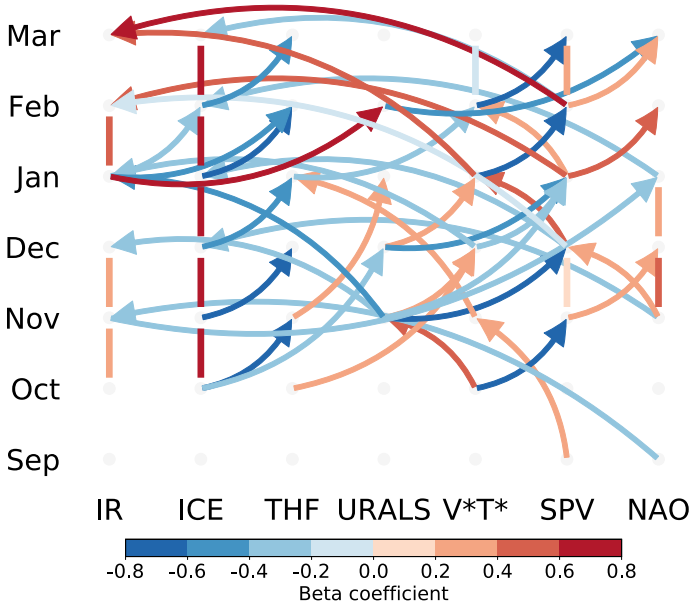

Figure S9: Monthly CEN as in Fig. S1a, but with the addition of downward longwave radiation (IR).

D Paper IV

Control of Barents Sea wintertime cyclone variability by large-scale atmospheric flow

Erica Madonna[1,2], Gabriel Hes[1,2,3], Camille Li[1,2], Clio Michel[1,2], Peter Yu Feng Siew[1,2]
Geophysical Research Letters, **47**, 1-11 (2020)
https://doi.org/10.1029/2020GL090322

Affiliations:
[1] Geophysical Institute, University of Bergen, Bergen, Norway
[2] Bjerknes Centre for Climate Research, Bergen, Norway
[3] Département de Géosciences, École Normale Supérieure, PSL Research University, Paris, France

Abstract

Extratropical cyclones transport heat and moisture into the Arctic, which can promote surface warming and sea ice melt. We investigate wintertime cyclone variability in the Barents Sea region to understand what controls the impacts, frequency and path of cyclones at high latitudes. Large-scale atmospheric conditions are found to be key, with the strongest surface warming from cyclones originating south of 60°N in the North Atlantic and steered northeastwards by the upper-level flow. Atmospheric conditions also control cyclone variability in the Barents proper: months with many cyclones are characterized by an absence of high-latitude blocking and enhanced local baroclinicity, due to the presence of strong upper-level winds and a southwest-northeast tilted jet stream more than changes in sea ice. This study confirms that Arctic cyclones exhibit large interannual variability, and accounting for this variability reveals that trends in Barents cyclone frequency are not robust over the 1979-2018 period.

1 Introduction

Extratropical cyclones play an important role in the global energy budget, redistributing heat and moisture from mid-latitudes to high-latitudes. In the North Atlantic sector, the bulk of the moisture and heat transport into the central Arctic is accomplished by transient eddies *Peixoto and Oort* (1992); *Adams et al.* (2000); *Sorteberg and Walsh* (2008); *Dufour et al.* (2016) such as cyclones. Moisture entering the Arctic can enhance downward infrared radiation and lead to strong surface warming and sea ice melt *Woods et al.* (2013); *Boisvert et al.* (2016); *Messori et al.* (2018), a process that is especially important in winter when insolation is weak. Moreover, winter cyclones can produce intense snowfall that acts as an insulation layer, modifying the melting and growth rates of sea ice *Graham et al.* (2019). Cyclones with strong winds can influence the production and export of sea ice from the Arctic towards mid-latitudes, with the export regions being sensitive to the cyclone's path *Brümmer et al.* (2001); *Rogers et al.* (2005); *Sorteberg and Kvingedal* (2006).

The surface impacts of cyclones entering the Arctic can vary widely from case to case. Already, several studies have shown that seasonal energy transport to the Arctic is dominated by a few specific transport events *Messori and Czaja* (2013); *Moore* (2016), drawing attention to extreme Arctic cyclones *Simmonds and Keay* (2009); *Sepp and Jaagus* (2011); *Rinke et al.* (2017); *Koyama et al.* (2017). For example, the passage of a single extreme cyclone is thought to be responsible for the unusual warmth of the entire 2015/2016 winter season *Moore* (2016); *Boisvert et al.* (2016); *Kim et al.* (2017). Extreme Arctic cyclones are often defined in terms of pressure or depth, but moisture content is likely as important, if not more, for surface impacts. Because the uptake and transport of moisture depend on a storm's formation and propagation environments (e.g., *Sodemann et al.*, 2008; *Aemisegger and Papritz*, 2018), discriminating between cyclones based on their origin and tracks should allow us to better evaluate their contribution to high-latitude climate variability.

The dynamics of storm tracks in mid-latitude regions is well established, but there is some uncertainty about which environmental conditions are most important for controlling the development and path of cyclones at high latitudes. The common understanding is that cyclones are generated and grow in regions of enhanced baroclinicity in the presence of strong horizontal and vertical temperature gradients *Hoskins and Valdes* (1990); *Chang et al.* (2002); *Shaw et al.* (2016) and move on average eastward and poleward *Klein* (1958); *Tamarin and Kaspi* (2016), steered by the large-scale flow. Some studies suggest that the large-scale flow also controls high-latitude cyclones through variability in the North Atlantic/Arctic Oscillation *Graversen* (2006); *Sim-*

monds et al. (2008) or the occurrence of blocking over the Ural Mountains *Luo et al.* (2017). Other studies suggest that local conditions, such as the location of the sea ice edge are a more important influence on the track of cyclones *Deser et al.* (2000); *Inoue et al.* (2012). For example, *Inoue et al.* (2012) proposed that the retreat of Barents Sea ice weakens the local sea surface temperature gradient and thus the surface baroclincity. Consequently, cyclones tend not to travel east into the Barents Sea, but rather turn north, resulting in a poleward shift of the storm track.

The Barents Sea is an ideal testbed for studying the effects of the large-scale flow versus local conditions on high-latitude cyclones. Situated at the end of the North Atlantic storm track *Chang et al.* (2002); *Shaw et al.* (2016), the Barents Sea is one of the main corridors for cyclones entering the Arctic, in particular during winter (e.g., *Adams et al.*, 2000; *Simmonds et al.*, 2008; *Sorteberg and Walsh*, 2008). It is also the region with the largest wintertime sea ice variability *Parkinson et al.* (1999); *Parkinson and Cavalieri* (2008) and has experienced the strongest winter sea ice decline during the past decades *Vihma* (2014); *Onarheim et al.* (2018); *Stroeve and Notz* (2018).

This study investigates wintertime cyclone variability in the Barents Sea, exploring the impacts of cyclones from different genesis regions as well as the roles of large-scale versus local conditions in determining cyclones tracks. A novel aspect of this study is that we document generalized relationships between the temperature and moisture signature of cyclones, their strength, and where they travel in their journey poleward. We also consider longer term trends, accounting for cyclone origin and path, to provide a complementary view of regional differences in Arctic cyclones.

2 Data and Methods

We use the European Centre for Medium-Range Weather Forecasts reanalysis ERA-Interim *Dee et al.* (2011) from 1979 to 2018 with 6-hourly time resolution and interpolated onto a $0.5 \times 0.5^{\circ}$ spatial grid. Daily/monthly averages are generated as needed from the 6-hourly fields. Daily anomalies of 2-meter temperature and moisture (vertically integrated from 1000 to 100 hPa) are obtained by removing the monthly seasonal cycle and any linear trend from the total fields. We focus on winter (December, January and February, DJF), the season with the strongest North Atlantic cyclone activity, and on the Barents Sea region, defined as 20-70°E longitude and 70-80°N latitude (see box in Fig. 1).

2.1 PV-blocking

Atmospheric blocking is a persistent quasi-stationary high-pressure system that obstructs the westerly flow. Blocking extends through the whole troposphere and is characterized by low (or negative) potential vorticity (PV) values consistent with the anticyclonic circulation. In this study, blocking is detected using the approach of *Schwierz et al.* (2004), which identifies negative potential vorticity anomalies (-1.3 pvu, vertically averaged between 500 and 150 hPa) that persist for at least five consecutive days. This approach is particularly suitable for higher latitudes (polewards of 75°) as it can be applied to any area, and does not require information from specific latitudinal bands to identify blocks (cf. geopotential height reversal, e.g. *Scherrer et al.*, 2006). After identifying blocking from the 6-hourly data, monthly fields obtained by averaging the number of blocked time steps at each grid point *Sprenger et al.* (2017). A blocking climatology can be found in the supplementary material (Fig. S1). To calculate the blocking time series, we area-average the monthly blocking frequency over the Barents Sea region. Since there are 32 months with zero blocking density in the Barents Sea, no (high) blocking months are defined as the 32 months with zero (most frequent) blocking.

2.2 Cyclone identification

The Melbourne University algorithm detects and tracks maxima in the Laplacian of mean sea level pressure (MSLP) in space and time *Murray and Simmonds* (1991a,b). We apply the algorithm on 6-hourly MSLP using the same parameters as *Uotila et al.* (2009). Only tracks lasting more than two days (9 track points) with genesis during DJF are kept. This excludes most polar lows and polar mesocyclones *Michel et al.* (2018). From these tracks, we generate maps of monthly cyclone track densities (see climatology in Fig. S1). Finally, we area-average the monthly track density over the Barents Sea region to produce a monthly time series of cyclone frequency. Similar to the PV-blocking, we identify the 32 months with highest (lowest) cyclone density, hence frequent (infrequent) presence of cyclones in the Barents Sea. Simply counting the number of tracks entering the Barents Sea yields comparable results (Fig. S2).

2.3 Cyclone categories

We categorize the cyclone tracks based on their origins and paths (Fig. 1, top row):

1. North Atlantic: cyclones entering the Barents Sea from the west with genesis south of 60°N (54 tracks)

2. Nordic: cyclones entering the Barents Sea from the west with genesis north of 60°N (288 tracks)

3. Barents Sea: cyclones with genesis in the Barents Sea (182 tracks)

4. Outside: cyclones travelling from the North Atlantic and crossing 80°N but not entering the Barents Sea (84 tracks)

The first three categories make up 74% of the total cyclone tracks present in the Barents Sea. Of the rest, most enter the Barents Sea from the south (16%), with a few entering from the north (6%) and east (4%). Since cyclones in all categories reach 70°N, we refer to them as Arctic cyclones. For the lag composites, lag 0 is defined for categories 1-3 as the first timestep when the track is in the Barents Sea box, while for category 4 it is the first timestep when the track is north of 80°N. For the trend analysis, the number of tracks is aggregated for each winter, considering tracks starting between 1 December and 28 February.

2.4 Eady growth rate

To detect favourable conditions for cyclone development and growth, we compute the Eady growth rate (EGR). The EGR is a measure of lower-tropospheric baroclinicity *Lindzen and Farrell* (1980); *Hoskins and Valdes* (1990) and it is defined as:

$$EGR = 0.31 \frac{f}{N} \left\| \frac{d\mathbf{u}}{dZ} \right\| \tag{1}$$

with N, the Brunt–Väisälä frequency, defined as:

$$N = \sqrt{\frac{g}{\theta_{700}} \frac{d\theta}{dZ}} \tag{2}$$

where f is the Coriolis parameter, g the gravitational acceleration, θ_{700} the potential temperature at 700 hPa, $d\mathbf{u}/dZ$ the vertical wind shear, and $d\theta/dZ$ the vertical gradient of potential temperature. The vertical gradients are evaluated using 6-hourly wind ($\mathbf{u}$), geopotential height (Z) and potential temperature (θ) at 850 and 500 hPa.

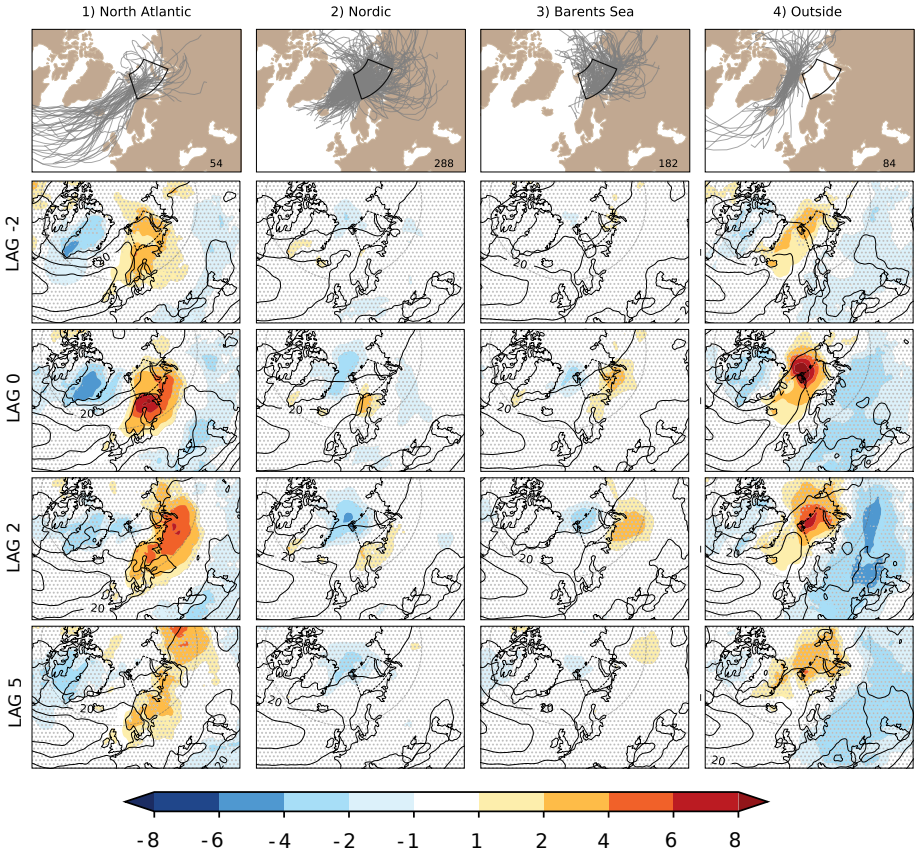

Figure 1: (First row) Cyclone tracks for the four cyclone categories (as defined in Section 2.3: 1) North Atlantic, 2) Nordic, 3) Barents Sea, and 4) Outside. The total number of tracks for each category is shown at the bottom right corner of each panel and the Barents Sea region is marked by the black box. (Four bottom rows) Composites of daily 2-meter temperature anomalies (shading, in °C) and wind speed at 500 hPa (contours, starting at 15 m s^{-1}, 5 m s^{-1} intervals) shown at time lags -2, 0, 2, 5 days. Lag 0 is defined for categories 1-3 as the first timestep when the track is in the Barents Sea box, while for category 4 it is the first timestep when the track is north of 80°N (see Methods). Regions where the 0°C value lies within the 30-70th percentile range are marked with grey dots. The dashed grey circle marks the 60°N parallel.

3. Results

The path travelled by a cyclone is of primary importance for its subsequent temperature impact on the Arctic. Composite analyses show that cyclones originating at lower latitudes (category 1, Fig. 1) are associated with stronger surface warming than cyclones originating at high latitudes (categories 2 and 3). For cyclones from the North Atlantic that reach the Barents Sea (category 1), we observe positive temperature (Fig. 1, up to 8°C) and moisture (Fig. S3, > 2 g kg^{-1}) anomalies at lag zero. The positive temperature anomaly persists for a few days (lag 2) before diminishing (lag 5). This warm anomaly is also present before the arrival of the cyclone in the Barents Sea (lag -2), consistent with the southwest-northeast tilted jet stream (black contours) that advects warm and moist air from mid-latitudes. The warm anomaly at lag -2 is not linked to blocking, as none is detected at this time at high-latitudes (Fig. S4). The temperature and moisture anomalies associated with cyclones with genesis at higher latitudes (category 2, Nordic and category 3, Barents Sea) have smaller magnitude and spatial extent compared to category 1. This is in line with the colder environment in which the cyclones form.

Cyclones forming in the North Atlantic travelling through the Fram Strait (category 4) lead to comparable temperature and moisture anomalies as those entering the Barents Sea (category 1). Here, the jet is strongly tilted as it is the case for category 1, especially at lag -2 and 0, which favours warm air advection. The main difference between categories 1 and 4 is where the warming and moistening maximizes: over Scandinavia and northwest Russia for category 1, over the Barents Sea and Svalbard for category 4. The shift in where the impacts maximize is related to the fact that the warm, moist anomalies are likely situated within the cyclone warm sector (cf. *Wickström et al.*, 2019), while the cold, dry anomalies to the west result from cold air advection on the rear side of the cyclone *Papritz and Grams* (2018).

Since the location of strongest warming depends on the path of a cyclone, the large-scale flow must play a role in determining surface impacts. In the Barents Sea, there is a clear relationship between the presence of cyclones and an atmospheric pattern known as blocking, when a quasi-stationary and persistent high-pressure system diverts the mean westerly flow. A composite of months with high blocking (HB) frequency over the Barents Sea (Fig. 2a) shows a reduction of cyclones locally and an increase in cyclones through the Fram Strait compared to a composite of months with no blocking (NB) in the Barents Sea (Fig. 2b). The mean cyclone track density averaged over the Barents Sea area is 2.3 (3.0) tracks per month for high (no) blocking months (Fig. 2a-b, boxplot). The composites show comparably large

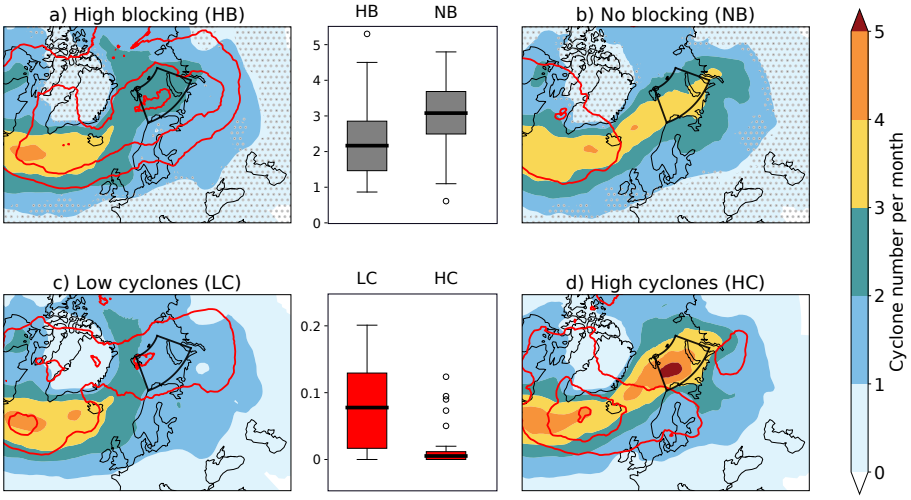

Figure 2: Composites of the number of cyclone tracks per month (shading) and PV-blocking (red contours, as % of time, in 5% intervals) based on a) high (HB) and b) no (NB) blocking frequency and for c) low (LC) and d) high (HC) cyclone density in the Barents Sea. Dots in a) and b) mark regions where the mean composite cyclone density is less than its standard deviation (i.e. signal-to-noise ratio < 1). The box-and-whisker plots show the distributions of cyclones (top, grey) and blocking (bottom, red) frequencies averaged over the Barents Sea region (black box) for the 32 months used in each composite. The black horizontal line shows the median, boxes show the interquartile range (IQR), and whiskers represent the median $\pm$ 1.5 IQR.

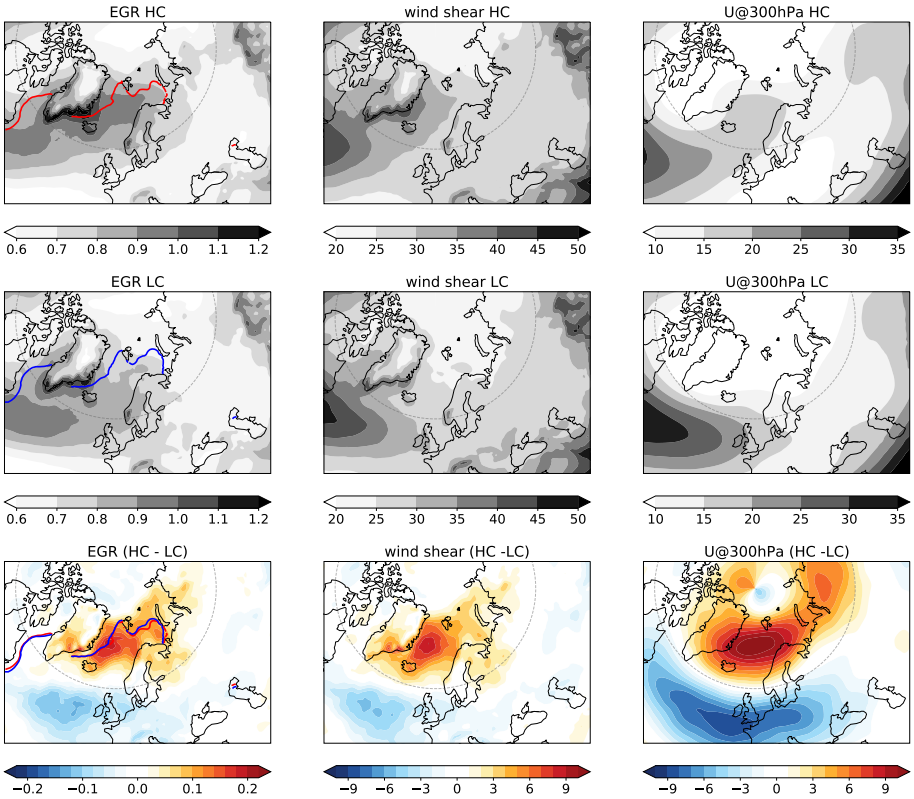

Figure 3: Composites of Eady Growth Rate (EGR, in day^{-1}), wind shear between 500 and 850 hPa (in 10^{-4} s^{-1}) and zonal wind at 300 hPa (U, in m s^{-1}) for high cyclone frequency months (HC, first row), low cyclone frequency months (LC, second row) and their difference (HC - LC, third row). The red (blue) line shows the ice edge (0.15 sea ice area fraction, undetrended data) for the HC (LC) composite. The dashed grey circle marks the 60°N parallel.

month-to-month variability, evident from the overlapping ranges in the HB/NB box-and-whisker plot. Still, the composite means over the considered regions are larger than their standard deviations (dots in Fig. 2a-b indicate signal-to-noise ratio < 1). The link between Barents Sea cyclones and the occurrence of high-latitude blocking is consistent with findings from previous studies that show more cyclones passing through the Fram Strait when there is a high-pressure ridge over Scandinavia *Michel et al.* (2012); *Wickström et al.* (2019).

An inverse analysis produces consistent results: months with a low occurrence of cyclones (LC) in the Barents Sea are associated with blocking over the Barents Sea (Fig. 2c red contours and boxplot) and also more cyclones entering the Arctic through the Fram Strait. In addition, months with a high occurrence of cyclones (HC) in

the Barents Sea show less frequent blocking over the region (Fig. 2d), similar to the NB composite (Fig. 2b). One notable difference is that the HC composite exhibits enhanced cyclone frequency over the whole North Atlantic compared to the NB composite. This suggests that the number of cyclones entering the Barents Sea depends not only on large-scale atmospheric blocking, but also on upstream conditions of the North Atlantic storm track.

Previous studies have linked cyclone variability in the Arctic to changes in baroclinicity *Inoue et al.* (2012); *Koyama et al.* (2017); *Wickström et al.* (2019), with one specific suggestion that sea ice retreat decreases baroclinicity locally and prevents cyclones from the North Atlantic or Nordic Seas from travelling eastwards into the Barents Sea. To test the influence of sea ice on cyclone variability in the Barents Sea region, we examine composites of the Eady growth rate (EGR) and sea ice area for months with high (HC) and low (LC) cyclone frequency in the Barents Sea (i.e. the same months as in Fig. 2c-d). The high-cyclone composite shows higher EGR values over the Barents Sea than the low-cyclone composite (Fig. 3, first column). However, there are almost no differences in the location of the sea ice edge between the two composites (blue and red lines). Moreover, the EGR signals are not confined to the Barents Sea but extend to the Nordic Seas. We see that the differences in the EGR mainly result from differences in the vertical wind shear (second column), which are linked to large-scale flow features such as the extension and tilt of the upper-level jet (third column). Similar conclusions can be drawn by compositing based on blocking frequency (Fig. S5) rather than cyclone frequency. The role of the jet stream in setting favourable conditions for cyclone development is also visible when considering cyclone categories separately. Regions with enhanced EGR are systematically located on the poleward side of the jet stream (Fig. S4) and are observed before the cyclones reach the Arctic (i.e. at lag -2, Fig. S4).

The key elements identified in the composite analysis, including the role of atmospheric blocking, are supported by a case study from the 2015/2016 winter. This winter season saw a major Arctic warming event, with some regions north of Svalbard registering daily temperatures of 30 °C above the wintertime climatology *Boisvert et al.* (2016); *Moore* (2016); *Binder et al.* (2017); *Kim et al.* (2017). From 24 to 27 December, prior to the warming event, several cyclones (Fig. 4, blue shading) enter or are formed in the Barents Sea. On 27 December, a block (red contours) forms north of Iceland and grows, migrating to a position over the Barents Sea by 29 December. The block persists for the next six days and is associated with a high-pressure system at the surface (grey shading). During this time (29 December - 4 January) no cyclones enter the domain, and cyclones travelling from the North Atlantic instead enter the Arctic through Fram Strait, most of them accompanied by a strong upper-level jet

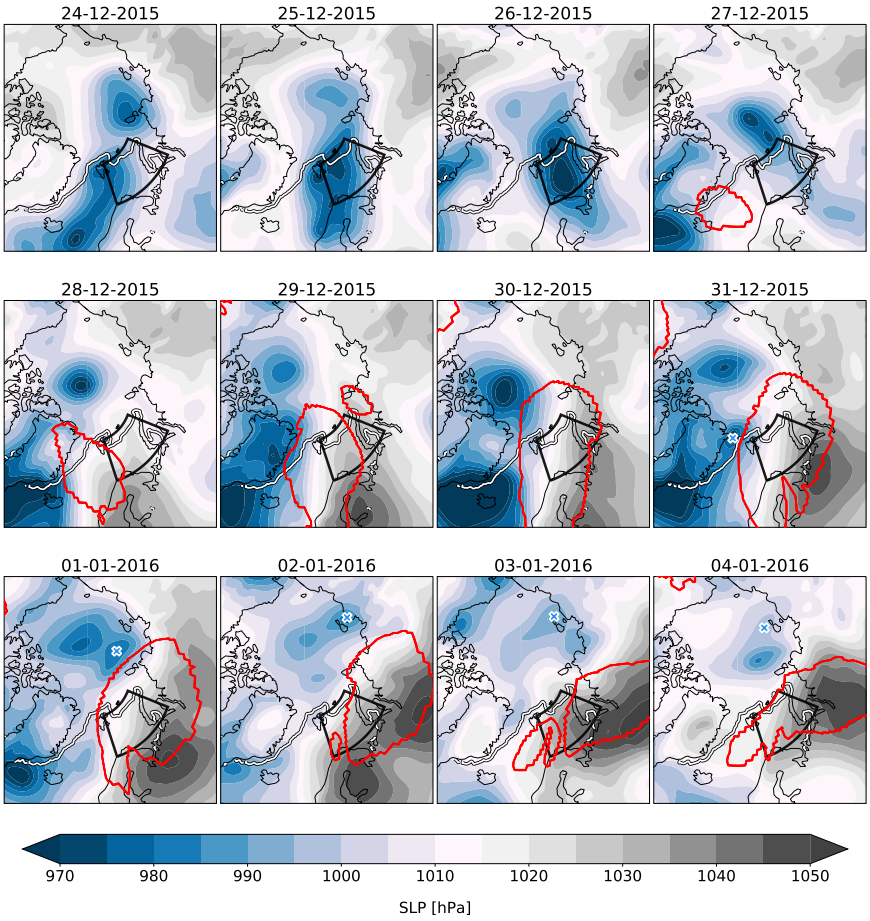

Figure 4: Temporal evolution of mean sea level pressure (MSLP in hPa, shading), sea ice edge (white line showing 0.15 ice area fraction) and blocked area (enclosed by red contours) at 12 UTC from 24 December 2015 to 4 January 2016. The black box delimits the Barents Sea region, while the blue cross marks the cyclone described in *Boisvert et al.* (2016).

(Fig. S6). The cyclone entering the Fram Strait on 31 December, marked by a blue cross in Fig. 4, transported an extremely warm and humid air mass into the Arctic *Boisvert et al.* (2016); *Moore* (2016) and likely contributed to the localised thinning of sea ice over the Barents-Kara Seas region *Boisvert et al.* (2016); *Binder et al.* (2017). Despite the reduction in sea ice thickness, the location of the sea ice edge (white contour), which may influence the low-level baroclinicity, did not change substantially during the 10-day warming event. Regions with high EGR values (purple contours in Fig. S6) mainly coincide with strong upper-level winds.

4. Discussion

We have examined cyclone variability in the Barents Sea and demonstrated links to the large-scale atmospheric conditions. We have also shown that variability in cyclone frequency and baroclinicity in the Barents Sea reflect variability in the upper-level flow more than the sea ice edge. Under global warming scenarios, models studies suggest that the melting of sea ice might impact the atmospheric circulation (e.g. *Butler et al.*, 2010; *Zappa et al.*, 2018). Given the notable retreat of winter sea ice in the Barents Sea over recent decades, it is natural to ask if this region exhibits long term changes in cyclones.

We find no robust trends in cyclone frequency in any of the considered categories (Fig. 5). This result is at odds with recent studies that reported a decrease in cyclone frequency in the southeastern Barents Sea during winter *Rinke et al.* (2017); *Zahn et al.* (2018); *Wickström et al.* (2019). The discrepancy arises in part from differences in the cyclone tracking schemes or datasets used, but mostly from how significance of trends is evaluated. In addition to using a t-test, we also use a Theil-Sen estimator, a method that is insensitive to outliers and more appropriate for short, noisy records. The time series of the number of winter (DJF) cyclones entering the Barents Sea (categories 1-3, Fig. 5) show large interannual variability, with weakly negative but non-significant trends based on both the t-test (using a standard significance level of 0.05) and the Theil-Sen test (uncertainty range includes both positive and negative slopes). Applying a five-winter running mean (red lines) does not reveal any particular cyclic behaviour. Considering categories 1-3 together confirms the general picture of a slight and non-significant decrease in cyclones in the Barents Sea (not shown). These results agree with the studies of *Koyama et al.* (2017), who found no link between changes in cyclone frequency and sea ice loss, and *Vessey et al.* (2020), who found no trend in winter Arctic cyclone frequency and characteristics. The "outside" category shows a positive but non-robust trend in cyclone frequency.

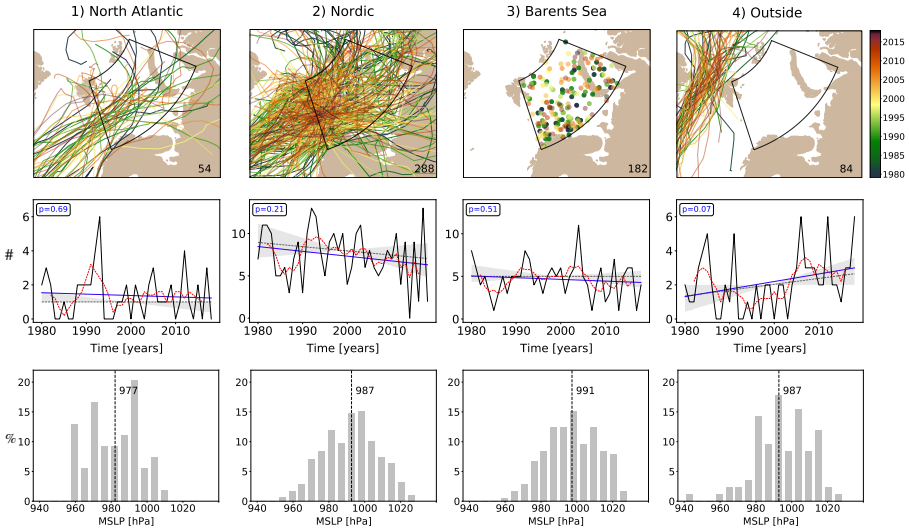

Figure 5: Spatial distribution of cyclone tracks (first row), time series of the number of cyclone tracks (second row) and MSLP at lag 0 (third row) for the four categories as defined in section 2.3 during DJF winter. First row: For cyclones with genesis in the Barents Sea (category 3), cyclogenesis locations are shown instead of cyclone tracks. Both track and genesis locations are colour-coded by year. The total number of tracks in each category is shown at the bottom right corner of each panel. Second row: Linear regression slopes (p-value in the top left corner) are shown in blue. Theil-Sen median slope is shown in grey (dashed line), and the corresponding 95% confidence interval is indicated by the grey shading. A five-winter moving average is shown in red (dashed line). Year labels correspond to the January and February, such that 1980 is the winter season from December 1979 to February 1980. Third row: Histograms of MSLP (normalized frequency in %) at lag 0 for the four categories. Median value (in hPa) is shown by the black dashed line.

In addition to the number of cyclones, the path of cyclones also shows large interannual variability. *Inoue et al.* (2012) suggested that cyclone tracks shift northwards as sea ice retreats. Such a northward (or more generally, poleward) shift is expected under global warming (*Yin*, 2005; *Harvey et al.*, 2014; *Shaw et al.*, 2016; *Tamarin-Brodsky and Kaspi*, 2017), but most of the proposed mechanisms involve changes in the upper-level temperature gradient. Whether such changes are already detectable in the observational period is questionable. We do not observe any clear poleward shift of cyclone tracks with time (Fig. 5, coloured tracks, first row), consistent with the results of *Koyama et al.* (2017). Furthermore, for cyclones with genesis in the Barents Sea (Fig. 5), the spatial distribution shows no systematic shift over the last four decades.

Wickström et al. (2019) suggested that decreasing cyclone frequency in the Barents Sea is linked to changes in the large-scale flow. They documented an increase in the frequency of the Scandinavian pattern, an anticyclonic circulation anomaly over Scandinavia and western Russia. This pattern might be linked to Barents Sea blocking, which we showed to be important for determining the path of cyclones. There is an apparent increase in the blocking time series, but again this trend is not robust over the observational period (Fig. S7). The other pattern of interest in this region is the North Atlantic Oscillation (NAO). As expected, when the NAO is positive the jet stream has a strong southwest-northeast tilt, steering more cyclones towards the high-latitudes (Fig. S8). However, the NAO index and frequency of cyclones is poorly correlated (correlations below 0.4) for all categories, on both seasonal and monthly time scales (Fig. S8).

Cyclones with the strongest surface warming are not necessarily the most extremes. Extreme cyclones are often defined using a MSLP threshold *Rinke et al.* (2017); *Chang et al.* (2012); *Vavrus* (2013). Figure 5 (third row) shows cyclone MSLP at lag 0 for the four Arctic cyclone categories. Each category exhibits large variability in MSLP. The North Atlantic cyclones have lower MSLP values (median of 977 hPa) than the others. Outside cyclones have the same MSLP median (987 hPa) as the Nordic but show much stronger temperature and moisture anomalies (c.f. lag 0 in Fig. 1 and S3). This suggests that not all cyclones producing strong surface warming are extreme in MSLP.

Cyclones are just one of several phenomena that give rise to sea ice variability in the Barents Sea. The impact of cyclones on sea ice depends on their characteristics and spans from surface warming to mechanical ice break-up *Graham et al.* (2019). Other factors influencing wintertime sea ice variability are the inflow of warm Atlantic water into the Barents Sea driven by local wind forcing (e.g. *Årthun et al.*, 2012; *Smedsrud et al.*, 2013; *Alexeev et al.*, 2017; *Akperov et al.*, 2020), as well as the pre-

conditions at the end of the melting season. Also, marine cold air outbreaks *Papritz* (2020) and high-latitude blocking *Pfahl and Wernli* (2012); *Gong and Luo* (2017); *Papritz* (2020) influence Arctic temperatures.

5. Conclusions

In this study, we investigate Arctic cyclones to understand what influences variability in their frequency, path and impacts. Surface warming associated with Arctic cyclones depends not only on their strength (Fig. 5) but most importantly on their origin and the path they take towards the Arctic (Fig. 1). The path of Arctic cyclones is controlled by the large-scale flow, just as for mid-latitude cyclones. The upper-level jet is more important than sea ice for enhancing baroclinicity and creating favourable conditions for cyclone growth (Fig. 3). Cyclones travel north through the Fram Strait when there is blocking over the Barents Sea (Figs. 2 and 4). Interannual variability is large for all Arctic cyclone categories and no robust trends in frequency are observed (Fig. 5). While a single extreme cyclone can affect sea ice cover, the link on seasonal and longer timescales is more complicated and might change with global warming as the sea ice thins and easily breaks up and drifts.

Supplementary figures

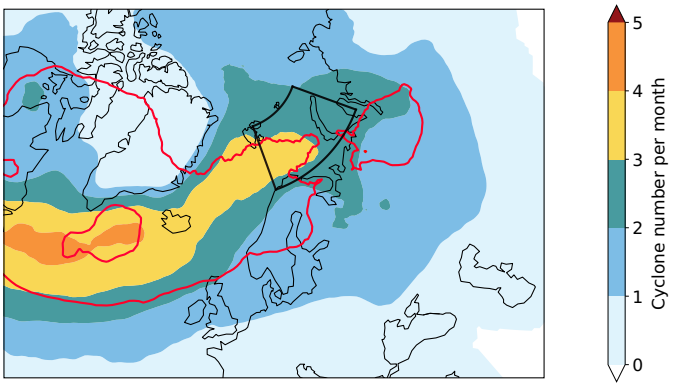

Figure S1. Wintertime (DJF) climatologies of cyclone density (shading, unit: cyclone number per month) and PV-blocking frequency (red contours, interval: 5% of the time). The black box denotes the Barents Sea region (20-70°N longitude and 70-80°E latitude). In winter in the Barents Sea, there are on average 2 to 4 cyclones per month and the PV-blocking has a frequency of about 5%. The highest cyclone density and blocking frequency are located on the western side of the Barents Sea.

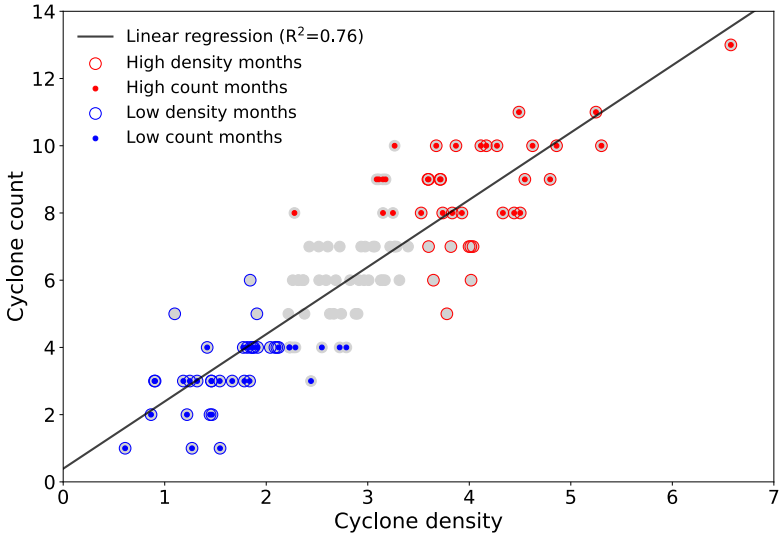

Figure S2. Scatterplot of monthly count of cyclones entering or forming in the Barents sea (unit: number of cyclones per month) versus cyclone density averaged over the Barents Sea region (70-80°N/20-70°E). The two time series are strongly correlated (R^2=0.76). The majority of the months (24/25 out of 32) with high/low cyclone density (red/blue circles) correspond to the months with high/low cyclone counts (red/blue dots). High and low categories include 32 months, 32 being the number of months with no blocking in the Barents Sea (see details in Method). We do not expect a perfect agreement between the two times series as the cyclone count is a time series of integers, while the cyclone density is not.

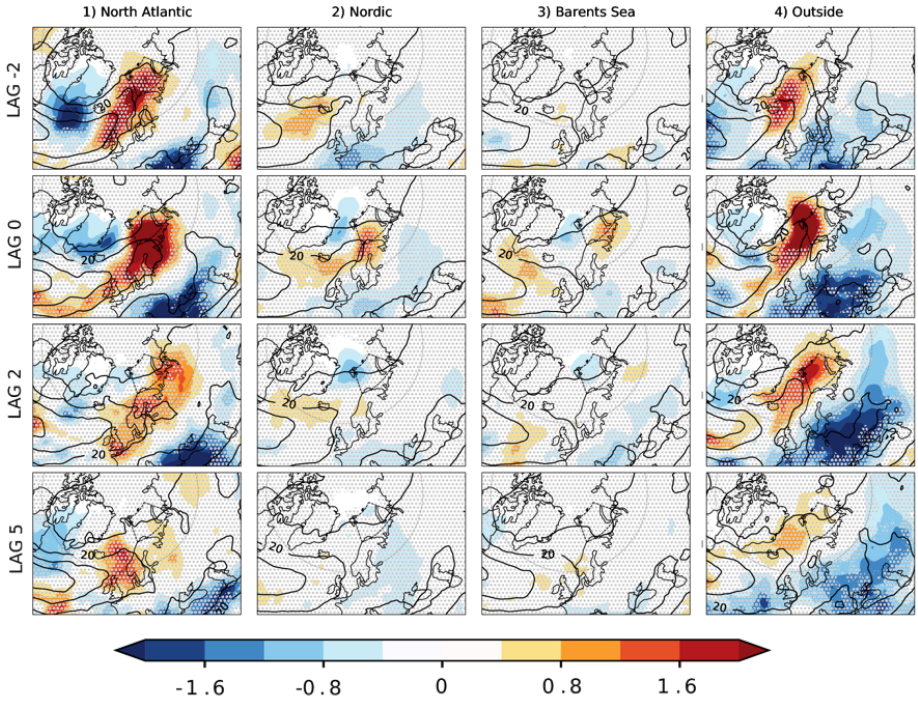

Figure S3. Composite of daily wind speed at 500 hPa (black contours, starting at 15 $m\,s^{-1}$, 5 $m\ s^{-1}$ intervals) and specific humidity anomalies (shading, in $g\,kg^{-1}$) shown at time lags -2, 0, 2, 5 days for the four cyclones categories (as defined in Section 2.3): 1) North Atlantic, 2) Nordic, 3) Barents Sea, and 4) Outside. The grey circle denotes the 60°N parallel.

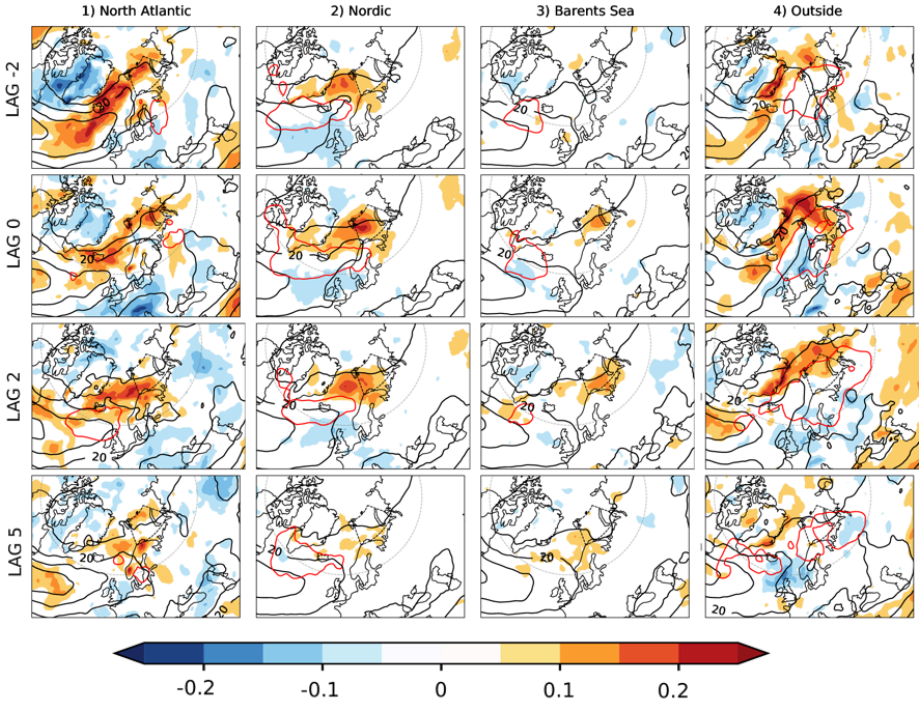

Figure S4. Composites of daily wind speed at 500 hPa (black contours, starting at 15 $\mathrm{m\,s^{-1}}$, 5 $\mathrm{m\ s^{-1}}$ intervals), blocking frequency (red contours starting at 10% of the time, in 10% intervals) and Eady Growth Rate anomalies (shading, in 1/day), shown at time lags -2, 0, 2, 5 days for the four cyclones categories. The grey circle denotes the 60°N parallel.

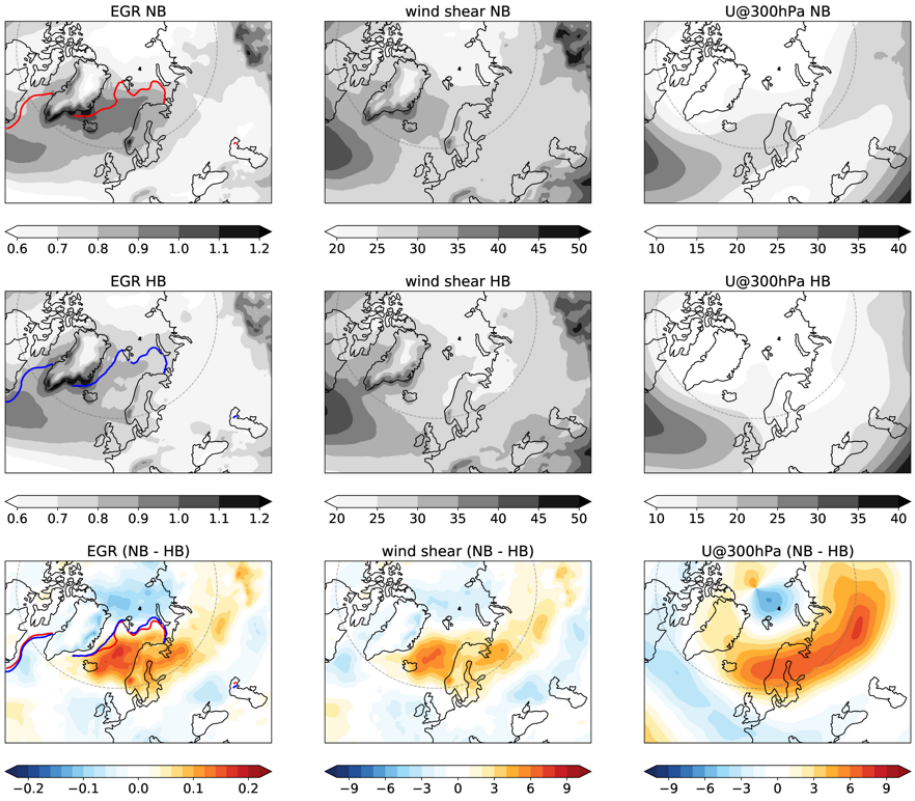

Figure S5. Composites of Eady Growth Rate (EGR, in day^{-1}), wind shear between 500 and 850 hPa (10^{-4} s^{-1}) and zonal wind at 300 hPa (U, in m s^{-1}), as Figure 4 in the manuscript, but for no blocking months (NB), high blocking months (HB) and their difference (NB - HB, third row). The red (blue) line shows the ice edge (0.15 ice area fraction) for the NB (HB) composite. The grey circle denotes the 60°N parallel.

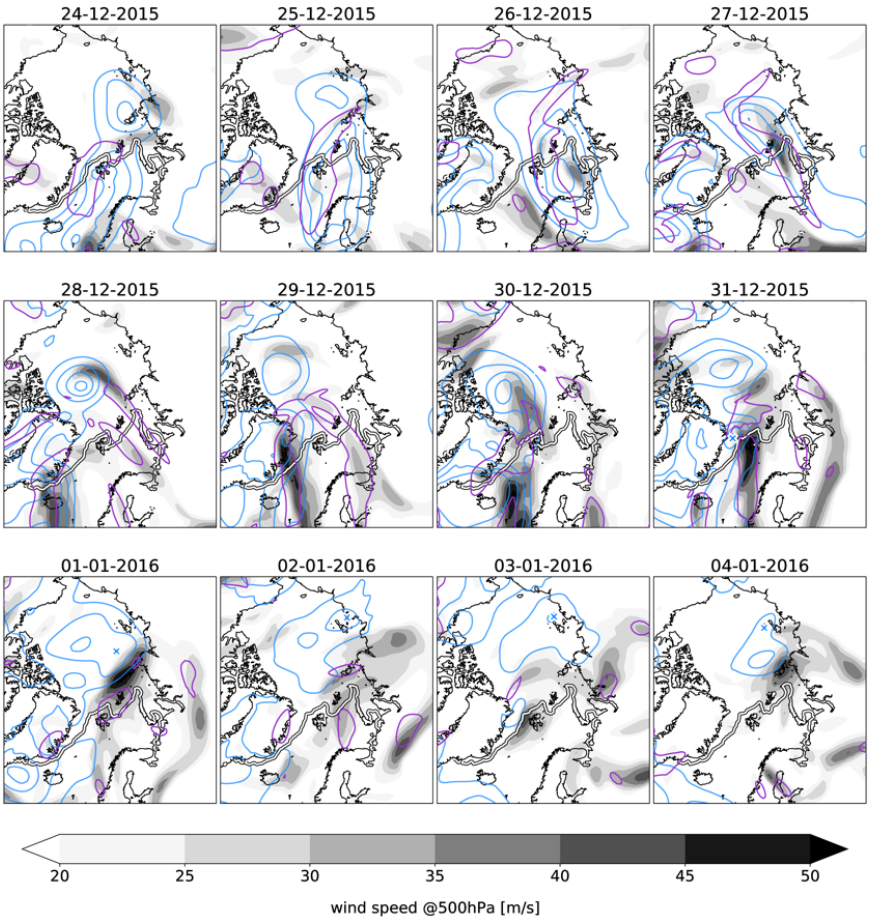

Figure S6. Temporal evolution of the upper-level wind (shading, wind speed at 500 hPa, in $m\,s^{-1}$), sea ice edge (white line showing 0.15 ice area fraction), high Eady Growth Rate values (> 1.3 day^{-1},enclosed by purple contours) and mean sea level pressure (MSLP, blue contours, 10 hPa intervals, shown only for values below 1000 hPa) at 12 UTC from 24 December 2015 to 4 January 2016.

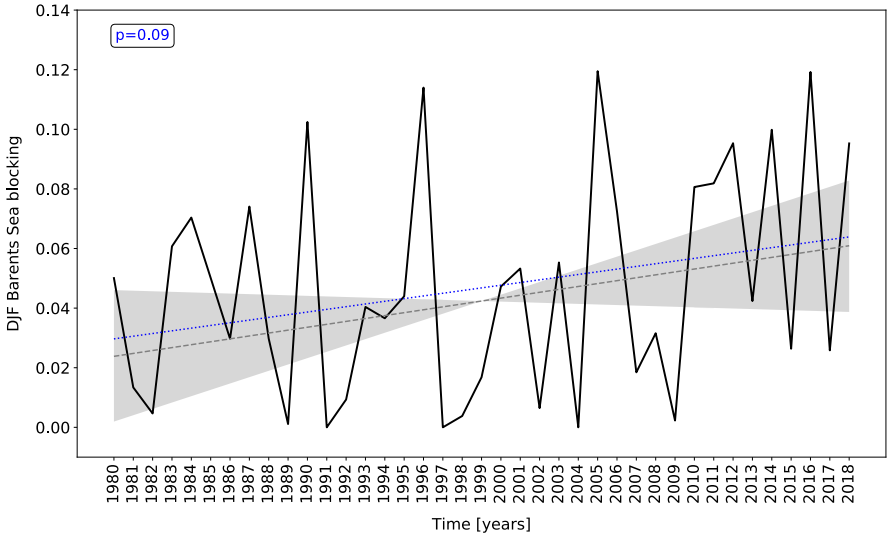

Figure S7. Winter (DJF) time series of Barents Sea blocking. The linear regression slope (p-value in the top left corner) is shown in blue. Theil-Sen median slope is shown in grey (dashed line), and the corresponding 95% confidence interval is indicated by the grey shading. The blocking frequency is obtained by taking the monthly mean of the 6-hourly binary blocking masks and area-averaging them over the Barents Sea box. No robust trends are observed in the Barents Sea (positive and negative slopes are possible). We do not consider the number of blocking events nor their duration, but just the frequency of the blocked area.

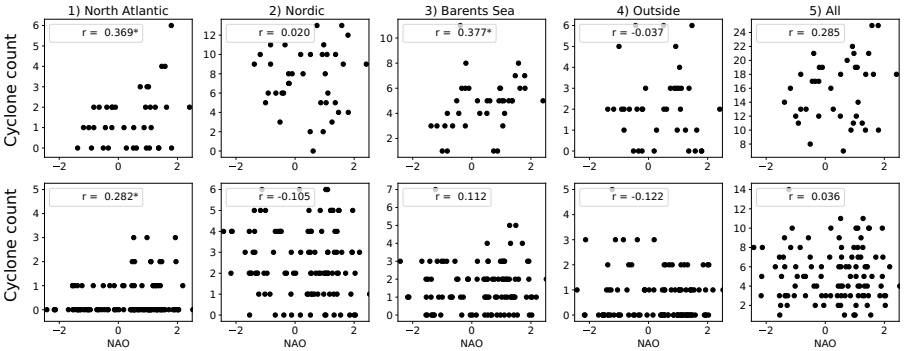

Figure S8. Relationship between the NAO index and the number of cyclones for the 4 different categories and their sum for (top row) winter (DJF) and (bottom row) monthly (December, January and February) means. Correlation coefficients (r) are shown in each panel and the "*" denotes values that are statistically significant at the 0.05 level. The NAO index was downloaded from `https://climatedataguide.ucar.edu/climate-data/hurrell-north-atlantic-oscillation-nao-index-pc-based`.

Bibliography

Adams, J. M., N. A. Bond, and J. E. Overland (2000), Regional variability of the Arctic heat budget in fall and winter, *Journal of Climate*, *13*(19), 3500–3510.

Aemisegger, F., and L. Papritz (2018), A climatology of strong large-scale ocean evaporation events. Part I: Identification, global distribution, and associated climate conditions, *Journal of Climate*, *31*(18), 7287–7312.

Akperov, M., V. A. Semenov, I. I. Mokhov, W. Dorn, and A. Rinke (2020), Impact of Atlantic water inflow on winter cyclone activity in the Barents Sea: Insights from coupled regional climate model simulations, *Environmental Research Letters*, *15*(2), 024,009.

Alexander, M. A., U. S. Bhatt, J. E. Walsh, M. S. Timlin, J. S. Miller, and J. D. Scott (2004), The atmospheric response to realistic arctic sea ice anomalies in an agcm during winter, *Journal of climate*, *17*(5), 890–905.

Alexeev, V. A., J. E. Walsh, V. V. Ivanov, V. A. Semenov, and A. V. Smirnov (2017), Warming in the Nordic Seas, North Atlantic storms and thinning Arctic sea ice, *Environmental research letters*, *12*(8), 084,011.

Årthun, M., T. Eldevik, L. Smedsrud, Ø. Skagseth, and R. Ingvaldsen (2012), Quantifying the influence of Atlantic heat on Barents Sea ice variability and retreat, *Journal of Climate*, *25*(13), 4736–4743.

Baldwin, M. P., and T. J. Dunkerton (1999), Propagation of the arctic oscillation from the stratosphere to the troposphere, *Journal of Geophysical Research: Atmospheres*, *104*(D24), 30,937–30,946.

Barnes, E. A. (2013), Revisiting the evidence linking arctic amplification to extreme weather in midlatitudes, *Geophysical research letters*, *40*(17), 4734–4739.

Barnes, E. A., and L. M. Polvani (2015), Cmip5 projections of arctic amplification, of the north american/north atlantic circulation, and of their relationship, *Journal of Climate*, *28*(13), 5254–5271.

Barnes, E. A., and J. A. Screen (2015), The impact of arctic warming on the midlatitude jet-stream: Can it? has it? will it?, *Wiley Interdisciplinary Reviews: Climate Change*, *6*(3), 277–286.

Binder, H., M. Boettcher, C. M. Grams, H. Joos, S. Pfahl, and H. Wernli (2017), Exceptional air mass transport and dynamical drivers of an extreme wintertime Arctic warm event, *Geophysical Research Letters*, *44*(23), 12,028–12,036, doi: 10.1002/2017GL075841.

Bintanja, R., R. Graversen, and W. Hazeleger (2011), Arctic winter warming amplified by the thermal inversion and consequent low infrared cooling to space, *Nature Geoscience*, *4*(11), 758–761.

Blackport, R., and P. J. Kushner (2017), Isolating the atmospheric circulation response to arctic sea ice loss in the coupled climate system, *Journal of Climate*, *30*(6), 2163–2185.

Blackport, R., and J. A. Screen (2019), Influence of arctic sea ice loss in autumn compared to that in winter on the atmospheric circulation, *Geophysical Research Letters*, *46*(4), 2213–2221.

Blackport, R., and J. A. Screen (2020), Insignificant effect of arctic amplification on the amplitude of midlatitude atmospheric waves, *Science advances*, *6*(8), eaay2880.

Blackport, R., and J. A. Screen (2021), Observed statistical connections overestimate the causal effects of arctic sea ice changes on midlatitude winter climate, *Journal of Climate*, *34*(8), 3021–3038.

Blackport, R., J. A. Screen, K. van der Wiel, and R. Bintanja (2019), Minimal influence of reduced arctic sea ice on coincident cold winters in mid-latitudes, *Nature Climate Change*, *9*(9), 697–704.

Boisvert, L. N., T. Markus, C. L. Parkinson, and T. Vihma (2012), Moisture fluxes derived from eos aqua satellite data for the north water polynya over 2003–2009, *Journal of Geophysical Research: Atmospheres*, *117*(D6).

Boisvert, L. N., A. A. Petty, and J. C. Stroeve (2016), The impact of the extreme winter 2015/16 arctic cyclone on the barents–kara seas, *Monthly Weather Review*, *144*(11), 4279–4287.

Boland, E. J., T. J. Bracegirdle, and E. F. Shuckburgh (2017), Assessment of sea ice-atmosphere links in cmip5 models, *Climate Dynamics*, *49*(1), 683–702.

Brönnimann, S. (2007), Impact of el niño–southern oscillation on european climate, *Reviews of Geophysics*, *45*(3).

Brümmer, B., G. Müller, B. Affeld, R. Gerdes, M. Karcher, and F. Kauker (2001), Cyclones over Fram Strait: impact on sea ice and variability, *Polar research*, *20*(2), 147–152.

Butler, A. H., D. W. Thompson, and R. Heikes (2010), The steady-state atmospheric circulation response to climate change–like thermal forcings in a simple general circulation model, *Journal of Climate*, *23*(13), 3474–3496.

Cash, B. A., R. Barimalala, J. L. Kinter, E. L. Altshuler, M. J. Fennessy, J. V. Manganello, F. Molteni, P. Towers, and F. Vitart (2017), Sampling variability and the changing enso–monsoon relationship, *Climate Dynamics*, *48*(11), 4071–4079.

Cassano, E. N., J. J. Cassano, M. E. Higgins, and M. C. Serreze (2014), Atmospheric impacts of an arctic sea ice minimum as seen in the community atmosphere model, *International Journal of Climatology*, *34*(3), 766–779.

Cavalieri, D. J., and C. L. Parkinson (2012), Arctic sea ice variability and trends, 1979-2010, *The Cryosphere*, *6*(4), 881.

Chang, E. K., S. Lee, and K. L. Swanson (2002), Storm track dynamics, *Journal of Climate*, *15*(16), 2163–2183.

Chang, E. K., Y. Guo, and X. Xia (2012), CMIP5 multimodel ensemble projection of storm track change under global warming, *Journal of Geophysical Research: Atmospheres*, *117*(D23).

Charney, J. G., and P. G. Drazin (1961), Propagation of planetary-scale disturbances from the lower into the upper atmosphere, *Journal of Geophysical Research*, *66*(1), 83–109.

Chen, H. W., F. Zhang, and R. B. Alley (2016), The robustness of midlatitude weather pattern changes due to arctic sea ice loss, *Journal of Climate*, *29*(21), 7831–7849.

Chen, X., D. Luo, S. B. Feldstein, and S. Lee (2018), Impact of winter ural blocking on arctic sea ice: short-time variability, *Journal of Climate*, *31*(6), 2267–2282.

Cohen, J., and J. Jones (2011), Tropospheric precursors and stratospheric warmings, *Journal of climate*, *24*(24), 6562–6572.

Cohen, J., J. A. Screen, J. C. Furtado, M. Barlow, D. Whittleston, D. Coumou, J. Francis, K. Dethloff, D. Entekhabi, J. Overland, et al. (2014), Recent arctic amplification and extreme mid-latitude weather, *Nature geoscience*, *7*(9), 627–637.

Cohen, J., J. C. Furtado, J. Jones, M. Barlow, D. Whittleston, and D. Entekhabi (2014a), Linking siberian snow cover to precursors of stratospheric variability, *Journal of Climate*, *27*(14), 5422–5432.

Cohen, J., K. Pfeiffer, and J. A. Francis (2018a), Warm arctic episodes linked with increased frequency of extreme winter weather in the united states, *Nature communications*, *9*(1), 1–12.

Cohen, J., X. Zhang, J. Francis, T. Jung, R. Kwok, J. Overland, T. Ballinger, R. Blackport, U. Bhatt, H. Chen, et al. (2018b), Arctic change and possible influence on mid-latitude climate and weather: a us clivar white paper, *US CLIVAR reports*.

Cohen, J., X. Zhang, J. Francis, T. Jung, R. Kwok, J. Overland, T. J. Ballinger, U. S. Bhatt, H. W. Chen, D. Coumou, S. Feldstein, H. Gu, D. Handorf, G. Henderson, M. Ionita, M. Kretschmer, F. Laliberte, S. Lee, H. W. Linderholm, W. Maslowski, Y. Peings, K. Pfeiffer, I. Rigor, T. Semmler, J. Stroeve, P. C. Taylor, S. Vavrus, T. Vihma, S. Wang, M. Wendisch, Y. Wu, and J. Yoon (2020), Divergent consensuses on Arctic amplification influence on midlatitude severe winter weather, *Nature Climate Change*, *10*(1), 20–29, doi:10.1038/s41558-019-0662-y.

Cohen, J. L., J. C. Furtado, M. A. Barlow, V. A. Alexeev, and J. E. Cherry (2012), Arctic warming, increasing snow cover and widespread boreal winter cooling, *Environmental Research Letters*, *7*(1), 014,007.

Collow, T. W., W. Wang, and A. Kumar (2018), Simulations of eurasian winter temperature trends in coupled and uncoupled cfsv2, *Advances in Atmospheric Sciences*, *35*(1), 14–26.

Compo, G. P., J. S. Whitaker, P. D. Sardeshmukh, N. Matsui, R. J. Allan, X. Yin, B. E. Gleason, R. S. Vose, G. Rutledge, P. Bessemoulin, et al. (2011), The twentieth century reanalysis project, *Quarterly Journal of the Royal Meteorological Society*, *137*(654), 1–28.

Dai, A., and M. Song (2020), Little influence of arctic amplification on mid-latitude climate, *Nature Climate Change*, *10*(3), 231–237.

De, B., and Y. Wu (2019), Robustness of the stratospheric pathway in linking the barents-kara sea sea ice variability to the mid-latitude circulation in cmip5 models, *Climate dynamics*, *53*(1), 193–207.

De, B., Y. Wu, and L. M. Polvani (2020), Non-additivity of the midlatitude circulation response to regional arctic temperature anomalies: The role of the stratosphere, *Geophysical Research Letters*, *47*(16), e2020GL088,057.

Dee, D. P., S. Uppala, A. Simmons, P. Berrisford, P. Poli, S. Kobayashi, U. Andrae, M. Balmaseda, G. Balsamo, d. P. Bauer, et al. (2011), The era-interim reanalysis: Configuration and performance of the data assimilation system, *Quarterly Journal of the royal meteorological society*, *137*(656), 553–597.

Deser, C., J. E. Walsh, and M. S. Timlin (2000), Arctic sea ice variability in the context of recent atmospheric circulation trends, *Journal of Climate*, *13*(3), 617–633.

Deser, C., G. Magnusdottir, R. Saravanan, and A. Phillips (2004), The effects of north atlantic sst and sea ice anomalies on the winter circulation in ccm3. part ii: Direct and indirect components of the response, *Journal of Climate*, *17*(5), 877–889.

Deser, C., R. A. Tomas, and S. Peng (2007), The transient atmospheric circulation response to north atlantic sst and sea ice anomalies, *Journal of Climate*, *20*(18), 4751–4767.

Deser, C., R. Tomas, M. Alexander, and D. Lawrence (2010), The seasonal atmospheric response to projected arctic sea ice loss in the late twenty-first century, *Journal of Climate*, *23*(2), 333–351.

Deser, C., A. Phillips, V. Bourdette, and H. Teng (2012), Uncertainty in climate change projections: the role of internal variability, *Climate dynamics*, *38*(3), 527–546.

Deser, C., R. A. Tomas, and L. Sun (2015), The role of ocean–atmosphere coupling in the zonal-mean atmospheric response to arctic sea ice loss, *Journal of Climate*, *28*(6), 2168–2186.

Deser, C., I. R. Simpson, A. S. Phillips, and K. A. McKinnon (2018), How well do we know enso's climate impacts over north america, and how do we evaluate models accordingly?, *Journal of Climate*, *31*(13), 4991–5014.

Deser, C., F. Lehner, K. Rodgers, T. Ault, T. Delworth, P. DiNezio, A. Fiore, C. Frankignoul, J. Fyfe, D. Horton, et al. (2020), Insights from earth system model initial-condition large ensembles and future prospects, *Nature Climate Change*, *10*(4), 277–286.

Domeisen, D. I., C. I. Garfinkel, and A. H. Butler (2019), The teleconnection of el niño southern oscillation to the stratosphere, *Reviews of Geophysics*, *57*(1), 5–47.

Dufour, A., O. Zolina, and S. K. Gulev (2016), Atmospheric moisture transport to the Arctic: Assessment of reanalyses and analysis of transport components, *Journal of Climate*, *29*(14), 5061–5081.

Dunstone, N., D. Smith, A. Scaife, L. Hermanson, R. Eade, N. Robinson, M. Andrews, and J. Knight (2016), Skilful predictions of the winter north atlantic oscillation one year ahead, *Nature Geoscience*, *9*(11), 809–814.

Ebert-Uphoff, I., and Y. Deng (2012), Causal discovery for climate research using graphical models, *Journal of Climate*, *25*(17), 5648–5665.

Eyring, V., S. Bony, G. A. Meehl, C. A. Senior, B. Stevens, R. J. Stouffer, and K. E. Taylor (2016), Overview of the coupled model intercomparison project phase 6 (cmip6) experimental design and organization, *Geoscientific Model Development*, *9*(5), 1937–1958.

Fang, Z., and J. M. Wallace (1994), Arctic sea ice variability on a timescale of weeks and its relation to atmospheric forcing, *Journal of Climate*, *7*(12), 1897–1914.

Feldl, N., and G. H. Roe (2013), The nonlinear and nonlocal nature of climate feedbacks, *Journal of Climate*, *26*(21), 8289–8304.

Francis, J. A. (2017), Why are arctic linkages to extreme weather still up in the air?, *Bulletin of the American Meteorological Society*, *98*(12), 2551–2557.

Francis, J. A., and S. J. Vavrus (2012), Evidence linking arctic amplification to extreme weather in mid-latitudes, *Geophysical Research Letters*, *39*(6).

Francis, J. A., and S. J. Vavrus (2015), Evidence for a wavier jet stream in response to rapid arctic warming, *Environmental Research Letters*, *10*(1), 014,005.

Frierson, D. M. (2007), The dynamics of idealized convection schemes and their effect on the zonally averaged tropical circulation, *Journal of the Atmospheric Sciences*, *64*(6), 1959–1976.

Frierson, D. M., I. M. Held, and P. Zurita-Gotor (2006), A gray-radiation aquaplanet moist gcm. part i: Static stability and eddy scale, *Journal of the atmospheric sciences*, *63*(10), 2548–2566.

Fyfe, J. C. (2019), Midlatitudes unaffected by sea ice loss, *Nature Climate Change*, *9*(9), 649–650.

Garcia-Serrano, J., and C. Frankignoul (2014), Retraction: High predictability of the winter euro–atlantic climate from cryospheric variability.

García-Serrano, J., C. Frankignoul, G. Gastineau, and A. De La Càmara (2015), On the predictability of the winter euro-atlantic climate: lagged influence of autumn arctic sea ice, *Journal of Climate*, *28*(13), 5195–5216.

García-Serrano, J., C. Frankignoul, M. King, A. Arribas, Y. Gao, V. Guemas, D. Matei, R. Msadek, W. Park, and E. Sanchez-Gomez (2017), Multi-model assessment of linkages between eastern arctic sea-ice variability and the euro-atlantic atmospheric circulation in current climate, *Climate Dynamics*, *49*(7), 2407–2429.

Garfinkel, C. I., D. L. Hartmann, and F. Sassi (2010), Tropospheric precursors of anomalous northern hemisphere stratospheric polar vortices, *Journal of Climate*, *23*(12), 3282–3299.

Gong, T., and D. Luo (2017), Ural blocking as an amplifier of the arctic sea ice decline in winter, *Journal of Climate*, *30*(7), 2639–2654.

Gong, T., S. Feldstein, and S. Lee (2017), The role of downward infrared radiation in the recent arctic winter warming trend, *Journal of Climate*, *30*(13), 4937–4949.

Goosse, H., J. E. Kay, K. C. Armour, A. Bodas-Salcedo, H. Chepfer, D. Docquier, A. Jonko, P. J. Kushner, O. Lecomte, F. Massonnet, et al. (2018), Quantifying climate feedbacks in polar regions, *Nature communications*, *9*(1), 1–13.

Graham, R. M., P. Itkin, A. Meyer, A. Sundfjord, G. Spreen, L. H. Smedsrud, G. E. Liston, B. Cheng, L. Cohen, D. Divine, et al. (2019), Winter storms accelerate the demise of sea ice in the Atlantic sector of the arctic ocean, *Scientific reports*, *9*(1), 1–16.

Graversen, R. G. (2006), Do changes in the midlatitude circulation have any impact on the Arctic surface air temperature trend?, *Journal of Climate*, *19*(20), 5422–5438.

Graversen, R. G., T. Mauritsen, M. Tjernström, E. Källén, and G. Svensson (2008), Vertical structure of recent arctic warming, *Nature*, *451*(7174), 53–56.

Graversen, R. G., P. L. Langen, and T. Mauritsen (2014), Polar amplification in ccsm4: Contributions from the lapse rate and surface albedo feedbacks, *Journal of Climate*, *27*(12), 4433–4450.

Hall, R. J., A. A. Scaife, E. Hanna, J. M. Jones, and R. Erdélyi (2017), Simple statistical probabilistic forecasts of the winter nao, *Weather and Forecasting*, *32*(4), 1585–1601.

Hartmann, D. L. (2015), *Global physical climatology*, vol. 103, Newnes.

Harvey, B., L. Shaffrey, and T. Woollings (2014), Equator-to-pole temperature differences and the extra-tropical storm track responses of the CMIP5 climate models, *Climate Dynamics*, *43*(5-6), 1171–1182.

Hassanzadeh, P., Z. Kuang, and B. F. Farrell (2014), Responses of midlatitude blocks and wave amplitude to changes in the meridional temperature gradient in an idealized dry gcm, *Geophysical Research Letters*, *41*(14), 5223–5232.

Hay, S., P. J. Kushner, R. Blackport, and K. E. McCusker (2018), On the relative robustness of the climate response to high-latitude and low-latitude warming, *Geophysical Research Letters*, *45*(12), 6232–6241.

He, S., X. Xu, T. Furevik, and Y. Gao (2020), Eurasian cooling linked to the vertical distribution of arctic warming, *Geophysical Research Letters*, *47*(10), e2020GL087,212.

Held, I. M. (2005), The gap between simulation and understanding in climate modeling, *Bulletin of the American Meteorological Society*, *86*(11), 1609–1614.

Hell, M. C., T. Schneider, and C. Li (2020), Atmospheric circulation response to short-term arctic warming in an idealized model, *Journal of the Atmospheric Sciences*, *77*(2), 531–549.

Henderson, G. R., Y. Peings, J. C. Furtado, and P. J. Kushner (2018), Snow–atmosphere coupling in the northern hemisphere, *Nature Climate Change*, *8*(11), 954–963.

Hersbach, H., B. Bell, P. Berrisford, S. Hirahara, A. Horányi, J. Muñoz-Sabater, J. Nicolas, C. Peubey, R. Radu, D. Schepers, et al. (2020), The era5 global reanalysis, *Quarterly Journal of the Royal Meteorological Society*, *146*(730), 1999–2049.

Hesterberg, T. C. (2015), What teachers should know about the bootstrap: Resampling in the undergraduate statistics curriculum, *The American Statistician*, *69*(4), 371–386.

Holland, M. M., and C. M. Bitz (2003), Polar amplification of climate change in coupled models, *Climate Dynamics*, *21*(3-4), 221–232.

Honda, M., J. Inoue, and S. Yamane (2009), Influence of low arctic sea-ice minima on anomalously cold eurasian winters, *Geophysical Research Letters*, *36*(8).

Hopsch, S., J. Cohen, and K. Dethloff (2012), Analysis of a link between fall arctic sea ice concentration and atmospheric patterns in the following winter, *Tellus A: Dynamic Meteorology and Oceanography*, *64*(1), 18,624.

Hoshi, K., J. Ukita, M. Honda, K. Iwamoto, T. Nakamura, K. Yamazaki, K. Dethloff, R. Jaiser, and D. Handorf (2017), Poleward eddy heat flux anomalies associated with recent arctic sea ice loss, *Geophysical Research Letters*, *44*(1), 446–454.

Hoshi, K., J. Ukita, M. Honda, T. Nakamura, K. Yamazaki, Y. Miyoshi, and R. Jaiser (2019), Weak stratospheric polar vortex events modulated by the arctic sea-ice loss, *Journal of Geophysical Research: Atmospheres*, *124*(2), 858–869.

Hoskins, B., and T. Woollings (2015), Persistent extratropical regimes and climate extremes, *Current Climate Change Reports*, *1*(3), 115–124.

Hoskins, B. J., and D. J. Karoly (1981), The Steady Linear Response of a Spherical Atmosphere to Thermal and Orographic Forcing, *Journal of the Atmospheric Sciences*, *38*(6), 1179–1196, doi:10.1175/1520-0469(1981)038⟨1179:TSLROA⟩2.0.CO;2.

Hoskins, B. J., and P. J. Valdes (1990), On the existence of storm-tracks, *Journal of the Atmospheric Sciences*, *47*(15), 1854–1864.

Hurrell, J. W. (1995), Decadal trends in the north atlantic oscillation: Regional temperatures and precipitation, *Science*, *269*(5224), 676–679.

Inoue, J., M. E. Hori, and K. Takaya (2012), The role of barents sea ice in the wintertime cyclone track and emergence of a warm-arctic cold-siberian anomaly, *Journal of Climate*, *25*(7), 2561–2568.

Jaiser, R., K. Dethloff, and D. Handorf (2013), Stratospheric response to arctic sea ice retreat and associated planetary wave propagation changes, *Tellus A: Dynamic Meteorology and Oceanography*, *65*(1), 19,375.

Jaiser, R., T. Nakamura, D. Handorf, K. Dethloff, J. Ukita, and K. Yamazaki (2016), Atmospheric winter response to arctic sea ice changes in reanalysis data and model simulations, *Journal of Geophysical Research: Atmospheres*, *121*(13), 7564–7577.

Karpechko, A. Y., P. Hitchcock, D. H. Peters, and A. Schneidereit (2017), Predictability of downward propagation of major sudden stratospheric warmings, *Quarterly Journal of the Royal Meteorological Society*, *143*(704), 1459–1470.

Kay, J. E., C. Deser, A. Phillips, A. Mai, C. Hannay, G. Strand, J. M. Arblaster, S. Bates, G. Danabasoglu, J. Edwards, et al. (2015), The community earth system model (cesm) large ensemble project: A community resource for studying climate change in the presence of internal climate variability, *Bulletin of the American Meteorological Society*, *96*(8), 1333–1349.

Kelleher, M., and J. Screen (2018), Atmospheric precursors of and response to anomalous arctic sea ice in cmip5 models, *Advances in Atmospheric Sciences*, *35*(1), 27–37.

Kim, B.-M., S.-W. Son, S.-K. Min, J.-H. Jeong, S.-J. Kim, X. Zhang, T. Shim, and J.-H. Yoon (2014), Weakening of the stratospheric polar vortex by arctic sea-ice loss, *Nature communications*, *5*, 4646.

Kim, B.-M., J.-Y. Hong, S.-Y. Jun, X. Zhang, H. Kwon, S.-J. Kim, J.-H. Kim, S.-W. Kim, and H.-K. Kim (2017), Major cause of unprecedented arctic warming in january 2016: Critical role of an atlantic windstorm, *Scientific reports*, *7*, 40,051.

Kim, H.-M., and B.-M. Kim (2017), Relative contributions of atmospheric energy transport and sea ice loss to the recent warm arctic winter, *Journal of Climate*, *30*(18), 7441–7450.

King, M. P., M. Hell, and N. Keenlyside (2016), Investigation of the atmospheric mechanisms related to the autumn sea ice and winter circulation link in the northern hemisphere, *Climate dynamics*, *46*(3-4), 1185–1195.

King, M. P., I. Herceg-Bulić, I. Bladé, J. García-Serrano, N. Keenlyside, F. Kucharski, C. Li, and S. Sobolowski (2018), Importance of late fall enso teleconnection in the euro-atlantic sector, *Bulletin of the American Meteorological Society*, *99*(7), 1337–1343.

Klein, W. H. (1958), The frequency of cyclones and anticyclones in relation to the mean circulation, *Journal of Meteorology*, *15*(1), 98–102.

Koenigk, T., M. Caian, G. Nikulin, and S. Schimanke (2016), Regional arctic sea ice variations as predictor for winter climate conditions, *Climate Dynamics*, *46*(1-2), 317–337.

Koenigk, T., Y. Gao, G. Gastineau, N. Keenlyside, T. Nakamura, F. Ogawa, Y. Orsolini, V. Semenov, L. Suo, T. Tian, et al. (2019), Impact of arctic sea ice variations on winter temperature anomalies in northern hemispheric land areas, *Climate Dynamics*, *52*(5), 3111–3137.

Kolstad, E., and J. Screen (2019), Nonstationary relationship between autumn arctic sea ice and the winter north atlantic oscillation, *Geophysical Research Letters*, *46*(13), 7583–7591.

Kopec, B. G., X. Feng, F. A. Michel, and E. S. Posmentier (2016), Influence of sea ice on arctic precipitation, *Proceedings of the National Academy of Sciences*, *113*(1), 46–51.

Koyama, T., J. Stroeve, J. Cassano, and A. Crawford (2017), Sea ice loss and Arctic cyclone activity from 1979 to 2014, *Journal of Climate*, *30*(12), 4735–4754.

Kretschmer, M., D. Coumou, J. F. Donges, and J. Runge (2016), Using causal effect networks to analyze different arctic drivers of midlatitude winter circulation, *Journal of Climate*, *29*(11), 4069–4081.

Kretschmer, M., J. Cohen, V. Matthias, J. Runge, and D. Coumou (2018), The different stratospheric influence on cold-extremes in eurasia and north america, *npj Climate and Atmospheric Science*, *1*(1), 1–10.

Kretschmer, M., G. Zappa, and T. G. Shepherd (2020), The role of barents–kara sea ice loss in projected polar vortex changes, *Weather and Climate Dynamics*, *1*(2), 715–730.

Kug, J.-S., J.-H. Jeong, Y.-S. Jang, B.-M. Kim, C. K. Folland, S.-K. Min, and S.-W. Son (2015), Two distinct influences of arctic warming on cold winters over north america and east asia, *Nature Geoscience*, *8*(10), 759.

Kvamstø, N. G., P. Skeie, and D. B. Stephenson (2004), Impact of labrador sea-ice extent on the north atlantic oscillation, *International Journal of Climatology: A Journal of the Royal Meteorological Society*, *24*(5), 603–612.

Kwok, R., G. Cunningham, M. Wensnahan, I. Rigor, H. Zwally, and D. Yi (2009), Thinning and volume loss of the arctic ocean sea ice cover: 2003–2008, *Journal of Geophysical Research: Oceans*, *114*(C7).

Labe, Z., Y. Peings, and G. Magnusdottir (2019), The effect of qbo phase on the atmospheric response to projected arctic sea ice loss in early winter, *Geophysical Research Letters*, *46*(13), 7663–7671.

Labe, Z., Y. Peings, and G. Magnusdottir (2020), Warm arctic, cold siberia pattern: Role of full arctic amplification versus sea ice loss alone, *Geophysical Research Letters*, *47*(17), e2020GL088,583.

Lee, S. (2012), Testing of the tropically excited arctic warming mechanism (team) with traditional el niño and la niña, *Journal of Climate*, *25*(12), 4015–4022.

Lee, S. (2014), A theory for polar amplification from a general circulation perspective, *Asia-Pacific Journal of Atmospheric Sciences*, *50*(1), 31–43, doi:10.1007/s13143-014-0024-7.

Lee, S., T. Gong, N. Johnson, S. B. Feldstein, and D. Pollard (2011), On the possible link between tropical convection and the northern hemisphere arctic surface air temperature change between 1958 and 2001, *Journal of Climate*, *24*(16), 4350–4367.

Lee, S., T. Gong, S. B. Feldstein, J. A. Screen, and I. Simmonds (2017), Revisiting the cause of the 1989–2009 arctic surface warming using the surface energy budget: downward infrared radiation dominates the surface fluxes, *Geophysical research letters*, *44*(20), 10–654.

Li, C., and J. J. Wettstein (2012), Thermally driven and eddy-driven jet variability in reanalysis, *Journal of Climate*, *25*(5), 1587–1596.

Li, F., Y. J. Orsolini, H. Wang, Y. Gao, and S. He (2018), Atlantic multidecadal oscillation modulates the impacts of arctic sea ice decline, *Geophysical Research Letters*, *45*(5), 2497–2506.

Liang, Y.-c., Y.-O. Kwon, C. Frankignoul, G. Danabasoglu, S. Yeager, A. Cherchi, Y. Gao, G. Gastineau, R. Ghosh, D. Matei, et al. (2020), Quantification of the arctic sea ice-driven atmospheric circulation variability in coordinated large ensemble simulations, *Geophysical research letters*, *47*(1), e2019GL085,397.

Lindzen, R. S., and B. Farrell (1980), A simple approximate result for the maximum growth rate of baroclinic instabilities, *Journal of the Atmospheric Sciences*, *37*(7), 1648–1654, doi:10.1175/1520-0469(1980)037⟨1648:ASARFT⟩2.0.CO;2.

Liptak, J., and C. Strong (2014), The winter atmospheric response to sea ice anomalies in the barents sea, *Journal of Climate*, *27*(2), 914–924.

Liu, J., J. A. Curry, H. Wang, M. Song, and R. M. Horton (2012), Impact of declining arctic sea ice on winter snowfall, *Proceedings of the National Academy of Sciences*, *109*(11), 4074–4079.

Lorenz, D. J., and D. L. Hartmann (2003), Eddy–zonal flow feedback in the northern hemisphere winter, *Journal of climate*, *16*(8), 1212–1227.

Luo, B., D. Luo, L. Wu, L. Zhong, and I. Simmonds (2017), Atmospheric circulation patterns which promote winter arctic sea ice decline, *Environmental Research Letters*, *12*(5), 054,017.

Luo, D., Y. Xiao, Y. Diao, A. Dai, C. L. Franzke, and I. Simmonds (2016), Impact of ural blocking on winter warm arctic–cold eurasian anomalies. part ii: The link to the north atlantic oscillation, *Journal of Climate*, *29*(11), 3949–3971.

Magnusdottir, G., C. Deser, and R. Saravanan (2004), The effects of north atlantic sst and sea ice anomalies on the winter circulation in ccm3. part i: Main features and storm track characteristics of the response, *Journal of Climate*, *17*(5), 857–876.

Maher, P., E. P. Gerber, B. Medeiros, T. M. Merlis, S. Sherwood, A. Sheshadri, A. H. Sobel, G. K. Vallis, A. Voigt, and P. Zurita-Gotor (2019), Model hierarchies for understanding atmospheric circulation, *Reviews of Geophysics*, *57*(2), 250–280.

Markus, T., J. C. Stroeve, and J. Miller (2009), Recent changes in arctic sea ice melt onset, freezeup, and melt season length, *Journal of Geophysical Research: Oceans*, *114*(C12).

McCusker, K. E., J. C. Fyfe, and M. Sigmond (2016), Twenty-five winters of unexpected eurasian cooling unlikely due to arctic sea-ice loss, *Nature Geoscience*, *9*(11), 838.

McKenna, C. M., T. J. Bracegirdle, E. F. Shuckburgh, P. H. Haynes, and M. M. Joshi (2018), Arctic sea ice loss in different regions leads to contrasting northern hemisphere impacts, *Geophysical Research Letters*, *45*(2), 945–954.

McKinnon, K. A., and C. Deser (2018), Internal variability and regional climate trends in an observational large ensemble, *Journal of Climate*, *31*(17), 6783–6802.

Messori, G., and A. Czaja (2013), On the sporadic nature of meridional heat transport by transient eddies, *Quarterly Journal of the Royal Meteorological Society*, *139*(673), 999–1008.

Messori, G., C. Woods, and R. Caballero (2018), On the drivers of wintertime temperature extremes in the high Arctic, *Journal of Climate*, *31*(4), 1597–1618.

Michel, C., G. Rivière, L. Terray, and B. Joly (2012), The dynamical link between surface cyclones, upper-tropospheric Rossby wave breaking and the life cycle of the Scandinavian blocking, *Geophysical Research Letters*, *39*(L10806), doi:10.1029/2012GL051682.

Michel, C., A. Terpstra, and T. Spengler (2018), Polar mesoscale cyclone climatology for the Nordic Seas based on ERA-Interim, *Journal of Climate*, *31*, 2511–2532.

Michel, C., C. Li, I. R. Simpson, I. Bethke, M. P. King, and S. Sobolowski (2020), The change in the enso teleconnection under a low global warming scenario and the uncertainty due to internal variability, *Journal of Climate*, *33*(11), 4871–4889.

Moon, T. A., I. Overeem, M. Druckenmiller, M. Holland, H. Huntington, G. Kling, A. L. Lovecraft, G. Miller, T. Scambos, C. Schädel, et al. (2019), The expanding footprint of rapid arctic change, *Earth's Future*, *7*(3), 212–218.

Moore, G. (2016), The December 2015 North Pole warming event and the increasing occurrence of such events, *Scientific Reports*, *6*, 39,084.

Mori, M., M. Watanabe, H. Shiogama, J. Inoue, and M. Kimoto (2014), Robust arctic sea-ice influence on the frequent eurasian cold winters in past decades, *Nature Geoscience*, *7*(12), 869.

Mori, M., Y. Kosaka, M. Watanabe, H. Nakamura, and M. Kimoto (2019), A reconciled estimate of the influence of arctic sea-ice loss on recent eurasian cooling, *Nature Climate Change*, *9*(2), 123.

Murray, R. J., and I. Simmonds (1991a), A numerical scheme for tracking cyclone centres from digital data. Part I: development and operation of the scheme, *Aust. Met. Mag.*, *39*, 155–166.

Murray, R. J., and I. Simmonds (1991b), A numerical scheme for tracking cyclone centres from digital data. Part II: application to January and July general circulation model simulations, *Aust. Met. Mag.*, *39*, 167–180.

Nakamura, T., K. Yamazaki, K. Iwamoto, M. Honda, Y. Miyoshi, Y. Ogawa, and J. Ukita (2015), A negative phase shift of the winter ao/nao due to the recent arctic sea-ice reduction in late autumn, *Journal of Geophysical Research: Atmospheres*, *120*(8), 3209–3227.

Nakamura, T., K. Yamazaki, K. Iwamoto, M. Honda, Y. Miyoshi, Y. Ogawa, Y. Tomikawa, and J. Ukita (2016), The stratospheric pathway for arctic impacts on midlatitude climate, *Geophysical Research Letters*, *43*(7), 3494–3501.

Nishii, K., H. Nakamura, and T. Miyasaka (2009), Modulations in the planetary wave field induced by upward-propagating rossby wave packets prior to stratospheric sudden warming events: A case-study, *Quarterly Journal of the Royal Meteorological Society: A journal of the atmospheric sciences, applied meteorology and physical oceanography*, *135*(638), 39–52.

Notz, D., and S. Community (2020), Arctic Sea Ice in CMIP6, *Geophysical Research Letters*, *47*(10), 1–11, doi:10.1029/2019GL086749.

Notz, D., and J. Stroeve (2016), Observed arctic sea-ice loss directly follows anthropogenic co2 emission, *Science*, *354*(6313), 747–750.

Nummelin, A., C. Li, and P. J. Hezel (2017), Connecting ocean heat transport changes from the midlatitudes to the arctic ocean, *Geophysical Research Letters*, *44*(4), 1899–1908.

Ogawa, F., N. Keenlyside, Y. Gao, T. Koenigk, S. Yang, L. Suo, T. Wang, G. Gastineau, T. Nakamura, H. N. Cheung, et al. (2018), Evaluating impacts of recent arctic sea ice loss on the northern hemisphere winter climate change, *Geophysical Research Letters*, *45*(7), 3255–3263.

O'Gorman, P. A., and T. Schneider (2008), The Hydrological Cycle over a Wide Range of Climates Simulated with an Idealized GCM, *Journal of Climate*, *21*(15), 3815–3832, doi:10.1175/2007JCLI2065.1.

Onarheim, I. H., and M. Årthun (2017), Toward an ice-free barents sea, *Geophysical Research Letters*, *44*(16), 8387–8395.

Onarheim, I. H., T. Eldevik, L. H. Smedsrud, and J. C. Stroeve (2018), Seasonal and regional manifestation of Arctic sea ice loss, *Journal of Climate*, *31*(12), 4917–4932.

Orsolini, Y. J., R. Senan, R. E. Benestad, and A. Melsom (2012), Autumn atmospheric response to the 2007 low arctic sea ice extent in coupled ocean–atmosphere hindcasts, *Climate dynamics*, *38*(11-12), 2437–2448.

Outten, S., and I. Esau (2012), A link between arctic sea ice and recent cooling trends over eurasia, *Climatic Change*, *110*(3), 1069–1075.

Overland, J. E., and M. Wang (2018), Arctic-midlatitude weather linkages in north america, *Polar Science*, *16*, 1–9.

Overland, J. E., K. Dethloff, J. A. Francis, R. J. Hall, E. Hanna, S.-J. Kim, J. A. Screen, T. G. Shepherd, and T. Vihma (2016), Nonlinear response of mid-latitude weather to the changing arctic, *Nature Climate Change*, *6*(11), 992.

Papritz, L. (2020), Arctic lower-tropospheric warm and cold extremes: Horizontal and vertical transport, diabatic processes, and linkage to synoptic circulation features, *Journal of Climate*, *33*(3), 993–1016.

Papritz, L., and C. M. Grams (2018), Linking low-frequency large-scale circulation patterns to cold air outbreak formation in the northeastern North Atlantic, *Geophysical Research Letters*, *45*(5), 2542–2553.

Park, D.-S. R., S. Lee, and S. B. Feldstein (2015a), Attribution of the recent winter sea ice decline over the atlantic sector of the arctic ocean, *Journal of climate*, *28*(10), 4027–4033.

Park, H.-S., S. Lee, S.-W. Son, S. B. Feldstein, and Y. Kosaka (2015b), The impact of poleward moisture and sensible heat flux on arctic winter sea ice variability, *Journal of Climate*, *28*(13), 5030–5040.

Parkinson, C. L., and D. J. Cavalieri (2008), Arctic sea ice variability and trends, 1979–2006, *Journal of Geophysical Research: Oceans*, *113*(C7).

Parkinson, C. L., D. J. Cavalieri, P. Gloersen, H. J. Zwally, and J. C. Comiso (1999), Arctic sea ice extents, areas, and trends, 1978–1996, *Journal of Geophysical Research: Oceans*, *104*(C9), 20,837–20,856.

Pedersen, R. A., I. Cvijanovic, P. L. Langen, and B. M. Vinther (2016), The impact of regional arctic sea ice loss on atmospheric circulation and the nao, *Journal of Climate*, *29*(2), 889–902.

Peings, Y. (2019), Ural blocking as a driver of early-winter stratospheric warmings, *Geophysical Research Letters*, *46*(10), 5460–5468.

Peings, Y., and G. Magnusdottir (2014), Response of the wintertime northern hemisphere atmospheric circulation to current and projected arctic sea ice decline: A numerical study with cam5, *Journal of Climate*, *27*(1), 244–264.

Peings, Y., H. Douville, J. Colin, D. S. Martin, and G. Magnusdottir (2017), Snow–(n) ao teleconnection and its modulation by the quasi-biennial oscillation, *Journal of Climate*, *30*(24), 10,211–10,235.

Peixoto, J. P., and A. H. Oort (1992), *Physics of climate*, 520 pp., New York, NY (United States); American Institute of Physics.

Petoukhov, V., and V. A. Semenov (2010), A link between reduced barents-kara sea ice and cold winter extremes over northern continents, *Journal of Geophysical Research: Atmospheres*, *115*(D21).

Pfahl, S., and H. Wernli (2012), Quantifying the relevance of atmospheric blocking for co-located temperature extremes in the Northern Hemisphere on (sub-) daily time scales, *Geophysical Research Letters*, *39*(12).

Pithan, F., and T. Mauritsen (2014), Arctic amplification dominated by temperature feedbacks in contemporary climate models, *Nature Geoscience*, *7*(3), 181–184, doi: 10.1038/ngeo2071.

Plumb, R. A. (1985), On the three-dimensional propagation of stationary waves, *Journal of the Atmospheric Sciences*, *42*(3), 217–229.

Polvani, L., A. Clement, B. Medeiros, J. Benedict, and I. Simpson (2017), When less is more: Opening the door to simpler climate models, eos, 98, *Eos, Transactions American Geophysical Union*, *99*(3), 15–16.

Polvani, L. M., and D. W. Waugh (2004), Upward wave activity flux as a precursor to extreme stratospheric events and subsequent anomalous surface weather regimes, *Journal of climate*, *17*(18), 3548–3554.

Porter, D. F., J. J. Cassano, and M. C. Serreze (2012), Local and large-scale atmospheric responses to reduced arctic sea ice and ocean warming in the wrf model, *Journal of Geophysical Research: Atmospheres*, *117*(D11).

Ringgaard, I. M., S. Yang, E. Kaas, and J. H. Christensen (2020), Barents-kara sea ice and european winters in ec-earth, *Climate Dynamics*, pp. 1–16.

Rinke, A., M. Maturilli, R. M. Graham, H. Matthes, D. Handorf, L. Cohen, S. R. Hudson, and J. C. Moore (2017), Extreme cyclone events in the Arctic: Wintertime variability and trends, *Environmental Research Letters*, *12*, 094,006, doi: 10.1088/1748-9326/aa7def.

Rogers, J. C., L. Yang, and L. Li (2005), The role of Fram Strait winter cyclones on sea ice flux and on Spitsbergen air temperatures, *Geophysical Research Letters*, *32*(L06709), doi:10.1029/2004GL022262.

Ruggieri, P., F. Kucharski, R. Buizza, and M. Ambaum (2017), The transient atmospheric response to a reduction of sea-ice cover in the barents and kara seas, *Quarterly Journal of the Royal Meteorological Society*, *143*(704), 1632–1640.

Runge, J., V. Petoukhov, and J. Kurths (2014), Quantifying the strength and delay of climatic interactions: The ambiguities of cross correlation and a novel measure based on graphical models, *Journal of Climate*, *27*(2), 720–739.

Runge, J., V. Petoukhov, J. F. Donges, J. Hlinka, N. Jajcay, M. Vejmelka, D. Hartman, N. Marwan, M. Paluš, and J. Kurths (2015), Identifying causal gateways and mediators in complex spatio-temporal systems, *Nature communications*, *6*(1), 1–10.

Runge, J., S. Bathiany, E. Bollt, G. Camps-Valls, D. Coumou, E. Deyle, C. Glymour, M. Kretschmer, M. D. Mahecha, J. Muñoz-Marí, et al. (2019a), Inferring causation from time series in earth system sciences, *Nature communications*, *10*(1), 1–13.

Runge, J., P. Nowack, M. Kretschmer, S. Flaxman, and D. Sejdinovic (2019b), Detecting and quantifying causal associations in large nonlinear time series datasets, *Science Advances*, *5*(11), eaau4996.

Scaife, A., A. Arribas, E. Blockley, A. Brookshaw, R. Clark, N. Dunstone, R. Eade, D. Fereday, C. Folland, M. Gordon, et al. (2014), Skillful long-range prediction of european and north american winters, *Geophysical Research Letters*, *41*(7), 2514–2519.

Scaife, A. A., and D. Smith (2018), A signal-to-noise paradox in climate science, *npj Climate and Atmospheric Science*, *1*(1), 1–8.

Scherrer, S. C., M. Croci-Maspoli, C. Schwierz, and C. Appenzeller (2006), Two-dimensional indices of atmospheric blocking and their statistical relationship with winter climate patterns in the euro-atlantic region, *International Journal of Climatology*, *26*, 233–249.

Schwierz, C., M. Croci-Maspoli, and H. Davies (2004), Perspicacious indicators of atmospheric blocking, *Geophysical Research Letters*, *31*(L06125), doi:10.1029/2003GL019341.

Screen, J. A. (2014), Arctic amplification decreases temperature variance in northern mid-to high-latitudes, *Nature Climate Change*, *4*(7), 577–582.

Screen, J. A. (2017a), Climate science: Far-flung effects of arctic warming, *Nature Geoscience*, *10*(4), 253.

Screen, J. A. (2017b), The missing northern european winter cooling response to arctic sea ice loss, *Nature communications*, *8*(1), 1–9.

Screen, J. A. (2017c), Simulated atmospheric response to regional and pan-arctic sea ice loss, *Journal of Climate*, *30*(11), 3945–3962.

Screen, J. A., and J. A. Francis (2016), Contribution of sea-ice loss to arctic amplification is regulated by pacific ocean decadal variability, *Nature Climate Change*, *6*(9), 856–860.

Screen, J. A., and I. Simmonds (2010), The central role of diminishing sea ice in recent Arctic temperature amplification, *Nature*, *464*(7293), 1334–1337, doi:10.1038/nature09051.

Screen, J. A., and I. Simmonds (2013), Exploring links between arctic amplification and mid-latitude weather, *Geophysical Research Letters*, *40*(5), 959–964.

Screen, J. A., I. Simmonds, C. Deser, and R. Tomas (2013), The atmospheric response to three decades of observed arctic sea ice loss, *Journal of climate*, *26*(4), 1230–1248.

Screen, J. A., C. Deser, I. Simmonds, and R. Tomas (2014), Atmospheric impacts of arctic sea-ice loss, 1979–2009: Separating forced change from atmospheric internal variability, *Climate dynamics*, *43*(1-2), 333–344.

Screen, J. A., C. Deser, and L. Sun (2015), Reduced risk of north american cold extremes due to continued arctic sea ice loss, *Bulletin of the American Meteorological Society*, *96*(9), 1489–1503.

Screen, J. A., C. Deser, D. M. Smith, X. Zhang, R. Blackport, P. J. Kushner, T. Oudar, K. E. McCusker, and L. Sun (2018), Consistency and discrepancy in the atmospheric response to arctic sea-ice loss across climate models, *Nature Geoscience*, *11*(3), 155–163.

Seierstad, I. A., and J. Bader (2009), Impact of a projected future arctic sea ice reduction on extratropical storminess and the nao, *Climate dynamics*, *33*(7-8), 937.

Semenov, V. A., and M. Latif (2015), Nonlinear winter atmospheric circulation response to arctic sea ice concentration anomalies for different periods during 1966–2012, *Environmental Research Letters*, *10*(5), 054,020.

Sepp, M., and J. Jaagus (2011), Changes in the activity and tracks of Arctic cyclones, *Climatic Change*, *105*(3-4), 577–595, doi:10.1007/s10584-010-9893-7.

Serreze, M., A. Barrett, J. Stroeve, D. Kindig, and M. Holland (2009), The emergence of surface-based arctic amplification, *The Cryosphere*, *3*(1), 11–19.

Serreze, M. C., and J. A. Francis (2006), The arctic amplification debate, *Climatic change*, *76*(3), 241–264.

Serreze, M. C., and J. Stroeve (2015), Arctic sea ice trends, variability and implications for seasonal ice forecasting, *Philosophical Transactions of the Royal Society A: Mathematical, Physical and Engineering Sciences*, *373*(2045), 20140,159.

Shaw, T., M. Baldwin, E. Barnes, R. Caballero, C. Garfinkel, Y.-T. Hwang, C. Li, P. O'Gorman, G. Rivière, I. Simpson, and A. Voigt (2016), Storm track processes and the opposing influences of climate change, *Nature Geoscience*, *9*(9), 656–664.

Shepherd, T. G. (2016), Effects of a warming arctic, *Science*, *353*(6303), 989–990.

Siew, P. Y. F., C. Li, S. P. Sobolowski, and M. P. King (2020), Intermittency of arctic–mid-latitude teleconnections: stratospheric pathway between autumn sea ice and the winter north atlantic oscillation, *Weather and Climate Dynamics*, *1*(1), 261–275.

Simmonds, I., and K. Keay (2009), Extraordinary September Arctic sea ice reductions and their relationships with storm behavior over 1979–2008, *Geophysical Research Letters*, *36*(19).

Simmonds, I., C. Burke, and K. Keay (2008), Arctic climate change as manifest in cyclone behavior, *Journal of Climate*, *21*(22), 5777–5796.

Simon, A., C. Frankignoul, G. Gastineau, and Y.-O. Kwon (2020), An observational estimate of the direct response of the cold-season atmospheric circulation to the arctic sea ice loss, *Journal of Climate*, *33*(9), 3863–3882.

Singarayer, J. S., J. L. Bamber, and P. J. Valdes (2006), Twenty-first-century climate impacts from a declining arctic sea ice cover, *Journal of Climate*, *19*(7), 1109–1125.

Smedsrud, L. H., I. Esau, R. B. Ingvaldsen, T. Eldevik, P. M. Haugan, C. Li, V. S. Lien, A. Olsen, A. M. Omar, O. H. Otterå, et al. (2013), The role of the barents sea in the arctic climate system, *Reviews of Geophysics*, *51*(3), 415–449.

Smith, D. M., N. J. Dunstone, A. A. Scaife, E. K. Fiedler, D. Copsey, and S. C. Hardiman (2017), Atmospheric response to arctic and antarctic sea ice: The importance of ocean–atmosphere coupling and the background state, *Journal of Climate*, *30*(12), 4547–4565.

Smith, D. M., J. A. Screen, C. Deser, J. Cohen, J. C. Fyfe, J. García-Serrano, T. Jung, V. Kattsov, D. Matei, R. Msadek, et al. (2019), The polar amplification model intercomparison project (pamip) contribution to cmip6: investigating the causes and consequences of polar amplification, *Geoscientific Model Development*, *12*, 1139–1164.

Smith, K. L., C. G. Fletcher, and P. J. Kushner (2010), The role of linear interference in the annular mode response to extratropical surface forcing, *Journal of Climate*, *23*(22), 6036–6050.

Sodemann, H., C. Schwierz, and H. Wernli (2008), Interannual variability of Greenland winter precipitation sources: Lagrangian moisture diagnostic and North Atlantic Oscillation influence, *Journal of Geophysical Research: Atmospheres*, *113*(D3).

Sorokina, S. A., C. Li, J. J. Wettstein, and N. G. Kvamstø (2016), Observed atmospheric coupling between barents sea ice and the warm-arctic cold-siberian anomaly pattern, *Journal of Climate*, *29*(2), 495–511.

Sorteberg, A., and B. Kvingedal (2006), Atmospheric forcing on the Barents Sea winter ice extent, *Journal of Climate*, *19*, 4772–4784, doi:10.1175/JCLI3885.1.

Sorteberg, A., and J. E. Walsh (2008), Seasonal cyclone variability at 70°N and its impact on moisture transport into the Arctic, *Tellus*, *60A*(3), 570–586.

Sprenger, M., G. Fragkoulidis, H. Binder, M. Croci-Maspoli, P. Graf, C. M. Grams, P. Knippertz, E. Madonna, S. Schemm, B. Škerlak, et al. (2017), Global climatologies of Eulerian and Lagrangian flow features based on ERA-Interim, *Bulletin of the American Meteorological Society*, *98*(8), 1739–1748.

Strey, S. T., W. L. Chapman, and J. E. Walsh (2010), The 2007 sea ice minimum: Impacts on the northern hemisphere atmosphere in late autumn and early winter, *Journal of Geophysical Research: Atmospheres*, *115*(D23).

Stroeve, J., and D. Notz (2018), Changing state of Arctic sea ice across all seasons, *Environmental Research Letters*, *13*(10), 103,001.

Stroeve, J., T. Markus, L. Boisvert, J. Miller, and A. Barrett (2014), Changes in arctic melt season and implications for sea ice loss, *Geophysical Research Letters*, *41*(4), 1216–1225.

Stroeve, J. C., V. Kattsov, A. Barrett, M. Serreze, T. Pavlova, M. Holland, and W. N. Meier (2012), Trends in Arctic sea ice extent from CMIP5, CMIP3 and observations, *Geophysical Research Letters*, *39*(16), n/a–n/a, doi:10.1029/2012GL052676.

Strong, C., G. Magnusdottir, and H. Stern (2009), Observed feedback between winter sea ice and the north atlantic oscillation, *Journal of Climate*, *22*(22), 6021–6032.

Stuecker, M. F., C. M. Bitz, K. C. Armour, C. Proistosescu, S. M. Kang, S.-P. Xie, D. Kim, S. McGregor, W. Zhang, S. Zhao, et al. (2018), Polar amplification dominated by local forcing and feedbacks, *Nature Climate Change*, *8*(12), 1076–1081.

Sun, L., C. Deser, and R. A. Tomas (2015), Mechanisms of stratospheric and tropospheric circulation response to projected arctic sea ice loss, *Journal of Climate*, *28*(19), 7824–7845.

Sun, L., J. Perlwitz, and M. Hoerling (2016), What caused the recent "warm arctic, cold continents" trend pattern in winter temperatures?, *Geophysical Research Letters*, *43*(10), 5345–5352.

Tamarin, T., and Y. Kaspi (2016), The poleward motion of extratropical cyclones from a potential vorticity tendency analysis, *Journal of the Atmospheric Sciences*, *73*(4), 1687–1707.

Tamarin, T., and Y. Kaspi (2017), The poleward shift of storm tracks under global warming: A lagrangian perspective, *Geophysical Research Letters*, *44*(20), 10–666.

Tamarin-Brodsky, T., and Y. Kaspi (2017), Enhanced poleward propagation of storms under climate change, *Nature Geoscience*, *10*(12), 908–913.

Tang, Q., X. Zhang, X. Yang, and J. A. Francis (2013), Cold winter extremes in northern continents linked to arctic sea ice loss, *Environmental research letters*, *8*(1), 014,036.

Taylor, K. E., R. J. Stouffer, and G. A. Meehl (2012), An overview of cmip5 and the experiment design, *Bulletin of the American meteorological Society*, *93*(4), 485–498.

Taylor, P. C., M. Cai, A. Hu, J. Meehl, W. Washington, and G. J. Zhang (2013), A decomposition of feedback contributions to polar warming amplification, *Journal of Climate*, *26*(18), 7023–7043.

Taylor, P. C., B. M. Hegyi, R. C. Boeke, and L. N. Boisvert (2018), On the increasing importance of air-sea exchanges in a thawing arctic: A review, *Atmosphere*, *9*(2), 41.

Thompson, D. W., and J. M. Wallace (1998), The arctic oscillation signature in the wintertime geopotential height and temperature fields, *Geophysical research letters*, *25*(9), 1297–1300.

Thomson, S. I., and G. K. Vallis (2018), Atmospheric Response to SST Anomalies. Part I: Background-State Dependence, Teleconnections, and Local Effects in Winter, *Journal of the Atmospheric Sciences*, *75*(12), 4107–4124, doi:10.1175/JAS-D-17-0297.1.

Ting, M. (1991), The stationary wave response to a midlatitude sst anomaly in an idealized gcm, *Journal of Atmospheric Sciences*, *48*(10), 1249–1275.

Ting, M., and I. M. Held (1990), The stationary wave response to a tropical sst anomaly in an idealized gcm, *Journal of Atmospheric Sciences*, *47*(21), 2546–2566.

Tomas, R. A., C. Deser, and L. Sun (2016), The role of ocean heat transport in the global climate response to projected arctic sea ice loss, *Journal of Climate*, *29*(19), 6841–6859.

Tsubouchi, T., K. Våge, B. Hansen, K. M. H. Larsen, S. Østerhus, C. Johnson, S. Jónsson, and H. Valdimarsson (2021), Increased ocean heat transport into the nordic seas and arctic ocean over the period 1993–2016, *Nature Climate Change*, *11*(1), 21–26.

Uotila, P., A. B. Pezza, J. J. Cassano, K. Keay, and A. H. Lynch (2009), A comparison of low pressure system statistics derived from a high-resolution NWP output and three reanalysis products over the Southern Ocean, *Journal of Geophysical Research*, *114*, D17,105, doi:10.1029/2008JD011583.

Vallis, G. K., G. Colyer, R. Geen, E. Gerber, M. Jucker, P. Maher, A. Paterson, M. Pietschnig, J. Penn, and S. I. Thomson (2018), Isca, v1. 0: A framework for the global modelling of the atmospheres of earth and other planets at varying levels of complexity, *Geoscientific Model Development*, *11*(3), 843–859.

Vavrus, S. (2004), The impact of cloud feedbacks on arctic climate under greenhouse forcing, *Journal of Climate*, *17*(3), 603–615.

Vavrus, S. J. (2013), Extreme arctic cyclones in CMIP5 historical simulations, *Geophysical Research Letters*, *40*(23), 6208–6212.

Vavrus, S. J. (2018), The influence of arctic amplification on mid-latitude weather and climate, *Current Climate Change Reports*, *4*(3), 238–249.

Vessey, A. F., K. I. Hodges, L. C. Shaffrey, and J. J. Day (2020), An inter-comparison of Arctic synoptic scale storms between four global reanalysis datasets, *Climate Dynamics*, *54*, 2777–2795, doi:10.1007/s00382-020-05142-419.

Vihma, T. (2014), Effects of Arctic sea ice decline on weather and climate: A review, *Surveys in Geophysics*, *35*(5), 1175–1214.

Voigt, A., M. Biasutti, J. Scheff, J. Bader, S. Bordoni, F. Codron, R. D. Dixon, J. Jonas, S. M. Kang, N. P. Klingaman, et al. (2016), The tropical rain belts with an annual cycle and a continent model intercomparison project: Tracmip, *Journal of Advances in Modeling Earth Systems*, *8*(4), 1868–1891.

Wallace, J. M. (2000), North atlantic oscillatiodannular mode: two paradigms—one phenomenon, *Quarterly Journal of the Royal Meteorological Society*, *126*(564), 791–805.

Wallace, J. M., I. M. Held, D. W. Thompson, K. E. Trenberth, and J. E. Walsh (2014), Global warming and winter weather, *Science*, *343*(6172), 729–730.

Walsh, J. E. (2014), Intensified warming of the arctic: Causes and impacts on middle latitudes, *Global and Planetary Change*, *117*, 52–63.

Wang, L., M. Ting, and P. Kushner (2017), A robust empirical seasonal prediction of winter nao and surface climate, *Scientific reports*, *7*(1), 279.

Warner, J., J. Screen, and A. Scaife (2020), Links between barents-kara sea ice and the extratropical atmospheric circulation explained by internal variability and tropical forcing, *Geophysical Research Letters*, *47*(1), e2019GL085,679.

Wickström, S., M. Jonassen, T. Vihma, and P. Uotila (2019), Trends in cyclones in the high-latitude North Atlantic during 1979–2016, *Quarterly Journal of the Royal Meteorological Society*, pp. 1–18, doi:https://doi.org/10.1002/qj.3707.

Winton, M. (2006), Amplified Arctic climate change: What does surface albedo feedback have to do with it?, *Geophysical Research Letters*, *33*(3), L03,701, doi:10.1029/2005GL025244.

Woods, C., and R. Caballero (2016), The role of moist intrusions in winter arctic warming and sea ice decline, *Journal of Climate*, *29*(12), 4473–4485.

Woods, C., R. Caballero, and G. Svensson (2013), Large-scale circulation associated with moisture intrusions into the arctic during winter, *Geophysical Research Letters*, *40*(17), 4717–4721.

Wu, Q., and X. Zhang (2010), Observed forcing-feedback processes between northern hemisphere atmospheric circulation and arctic sea ice coverage, *Journal of Geophysical Research: Atmospheres*, *115*(D14).

Wu, Y., and K. L. Smith (2016), Response of northern hemisphere midlatitude circulation to arctic amplification in a simple atmospheric general circulation model, *Journal of Climate*, *29*(6), 2041–2058.

Yang, S., and J. H. Christensen (2012), Arctic sea ice reduction and european cold winters in cmip5 climate change experiments, *Geophysical Research Letters*, *39*(20).

Yang, W., and G. Magnusdottir (2017), Springtime extreme moisture transport into the Arctic and its impact on sea ice concentration, *Journal of Geophysical Research: Atmospheres*, *122*(10), 5316–5329, doi:10.1002/2016JD026324.

Yang, X.-Y., X. Yuan, and M. Ting (2016), Dynamical link between the barents–kara sea ice and the arctic oscillation, *Journal of Climate*, *29*(14), 5103–5122.

Yin, J. H. (2005), A consistent poleward shift of the storm tracks in simulations of 21st century climate, *Geophysical Research Letters*, *32*(18).

Zahn, M., M. Akperov, A. Rinke, F. Feser, and I. I. Mokhov (2018), Trends of cyclone characteristics in the Arctic and their patterns from different reanalysis data, *Journal of Geophysical Research: Atmospheres*, *123*(5), 2737–2751.

Zappa, G., F. Pithan, and T. G. Shepherd (2018), Multimodel evidence for an atmospheric circulation response to arctic sea ice loss in the cmip5 future projections, *Geophysical Research Letters*, *45*(2), 1011–1019.

Zhang, P., Y. Wu, and K. L. Smith (2018a), Prolonged effect of the stratospheric pathway in linking barents-kara sea sea ice variability to the midlatitude circulation in a simplified model, *Climate Dynamics*, *50*(1-2), 527–539.

Zhang, P., Y. Wu, I. R. Simpson, K. L. Smith, X. Zhang, B. De, and P. Callaghan (2018b), A stratospheric pathway linking a colder siberia to barents-kara sea sea ice loss, *Science advances*, *4*(7), eaat6025.

Zhang, X., J. He, J. Zhang, I. Polyakov, R. Gerdes, J. Inoue, and P. Wu (2013), Enhanced poleward moisture transport and amplified northern high-latitude wetting trend, *Nature Climate Change*, *3*(1), 47–51, doi:10.1038/nclimate1631.

Zhong, L., L. Hua, and D. Luo (2018), Local and external moisture sources for the arctic warming over the barents–kara seas, *Journal of Climate*, *31*(5), 1963–1982.

Graphic design: Communication Division, UiB / Print: Skipnes Kommunikasjon AS

uib.no

ISBN: 9788230856710 (print)
9788230843628 (PDF)